

PDF hosted at the Radboud Repository of the Radboud University Nijmegen

The following full text is a publisher's version.

For additional information about this publication click this link.

<http://hdl.handle.net/2066/60695>

Please be advised that this information was generated on 2017-12-06 and may be subject to change.

**Conductance and diffusion of a SiGe
two-dimensional hole gas in magnetic field**

Cover:

Balls on a billiard-table: an example of a two-dimensional system out of daily-life experience.

ISBN 90-9017991-7

Conductance and diffusion of a SiGe two-dimensional hole gas in magnetic field

een wetenschappelijke proeve op het gebied
van de Natuurwetenschappen, Wiskunde en Informatica

Proefschrift

ter verkrijging van de graad van doctor
aan de Katholieke Universiteit Nijmegen,
op gezag van de Rector Magnificus Prof. Dr. C.W.P.M.Blom,
volgens besluit van het College van Decanen
in het openbaar te verdedigen op
maandag 28 juni 2004
des namiddags om 1.30 uur precies

door

Cecilia Possanzini

geboren op 3 december 1971
te Rome (Italië)

Promotor: Prof. Dr. Ir. J. C. Maan

Manuscriptcommissie: Prof. Dr. R. Fletcher
(Queen's University, Kingston, Ontario, Canada)

Dr. R. van der Heijden
(Eindhoven University of Technology)

Dr. A. de Visser
(University of Amsterdam)

A mamma e papà

*Vedi, in questi silenzi in cui le cose
s'abbandonano e sembrano vicine
a tradire il loro ultimo segreto,
talora ci aspetta
di scoprire uno sbaglio di Natura
il punto morto del mondo, l'anello che non tiene,
il filo da disbrogliare che finalmente ci metta
nel mezzo di una verità.*

EUGENIO MONTALE

*See, in these silences where things
give over and seem close to betraying
their final secret,
at times we feel we're about
to discover an error in Nature,
the dead point of the world, the link that won't hold,
the thread to untangle that will finally lead
to the midst of truth.*

EUGENIO MONTALE

Acknowledgements

During my Ph.D., I had the fortune to meet many colleagues and friends who supported, helped, cheered me up. I am glad to have the opportunity to thank them here.

I am enormously indebted to Robin Fletcher, who has always been a patient teacher, a strong support and a reference point for the work on thermoelectric power presented in this thesis. I also would like to thank his family, and in particular his wife, Sandra, for their warm hospitality during my stay in Canada. Thank you very much, I will never forget it and I hope you will come by in Nijmegen or in Rome and be my guest!

I also would like to thank Anne de Visser, Dennis de Lang, and Leonid Ponomarenko for sharing their expertise on metal-insular transition with me. Thank you very much for your time and your help! In addition, I would like to thank Prof. Pruisken for discussing the experimental data with us.

Ik wil graag iedereen bedanken in het Laboratorium voor Hoge Magneetvelden van Nijmegen voor hun hulp en gezelligheid. In particular, I owe my gratitude to Stef Olsthoorn, who assisted me daily with the cryogenic work. Beste Stef, reuze bedankt voor de leuke tijd en al je hulp! Hung van Luong was always very patient and willing to solve my frequent software/network troubles. Jos Rook and Lijnis Nelemans physically built the ^3He insert for the experiment described in the last Chapter. Henk Neijenhuisen built the electronics for the “pulsed experiment” and he was able to solve, explain, and foresee any kind of weird problems. Dear Henk, thank you for all your patience, your time, your moral and professional support, and your lekkere koffie everyday after lunch! Ik wil ook graag Adri Michielsen, Ruud Gelzing, John Schermer, en Peter Mulder bedanken voor hun hulp met het opdampen. Tenslotte wil

ik graag Harry Balster bedanken voor het zorgen voor de beschikbaarheid van de magneet-tijd and ijs.

I would like to thank all the AIO/OIO colleagues of the laboratory with whom I shared happiness, frustrations, doubts, and...(last but not least) instruments! Ate, Freddy, Alex, Sjoerd, Eric, Urs, and Marc initiated me to the Dutch “cuisine”: they let me try the first (and the last!) *frikandel* of my life...frietje waterfiets...typisch Nijmeegs!!! Guys, I know you meant good! I forgive you! Alex, Sjoerd, Freddy, Kostya, Igor, Cecile. Maaïke, Robert, Sasa, Robert, Giorgia, Maarten, Hans, Frans, Fabio, Andrea, Ate, Marius, Marc, Vadim, Urs: thank you very much for the cosy evenings we spent together, for the many barbeques, multicultural dinners, and borrels inside and outside the Lab. A special thanks to Sjoerd, who taught and helped me a lot at the beginning of my project, and to Marius, and Kostya who were always very helpful, extremely kind, and full of suggestions. Dear Fabio, we started this adventure together and I wish you all the best for your new life!

Last but not least, I would like to thank Martha and Ine for their kindness and help, and the senior scientists of the Magnet Lab, Peter Christianen, Andrey Geim, Marijn Devillers, Uli Zeitler, Jan van Bentum, Jos Perenboom, and Stef Wiegers for their suggestions, their friendship, and their support.

Ik wil hier ook graag mijn collegas van Philips Medical Systems bedanken voor the gezellige sfeer op werk, and voor hun verplichting in mijn Nederlands te verbeteren (a never ending project!).

During most of my Ph.D., I used to live in a very special place in Nijmegen: Muzenplaats. People living there, the so-called *Muzenplaats community*, made this place very special. Like in a big family, we helped each other with every-day problems, we exchanged recipes, feelings, ideas, books, music, we celebrated birthdays, new years, Christmases, Easters according to different calendars, traditions and countries, and we organized numerous barbeques and parties. I would like to thank the Muzenplaats community and their “adopted members” for being always so warm, funny, kind, and supporting. Special thanks to Iulia, Marius, Alexej, Alla, Igor, Masha, Kostya, Irina, “red Alexej”, Luca, Caroline, Anthony, Wil, Muriel, Florian, Mona, Andy, Felix, Alessandra, Abbas, Henrik, Andrea, Monica, and the little stars Anamaria, Amir, Lisa, and (at that time still in the belly) Simona.

I have been incredibly lucky to meet exceptional friends during these years. Their presence in times of need has been invaluable. My musketeers, Alessandra, Ambra, and Maria, always present, in good and in bad moments, always with the right words at the right moment, and in some moments, when there were not words available, they could come up with astonishing Italian food! Kostya is a genuine friend and an essential support. Luca has been always a very eclectic friend, often offering a different perspective and interesting ideas, he even composed a *sonetto* for me! Annalisa always kept the door open for me for coffee as well as for discussing about everything, from Dutch habits to the band structure of SiGe. Marjolein, thanks for many evenings spent talking about life, for showing me the Dutch way of living while cooking beautiful Italian food with Andrea! Graziana, picciridda, grazie

dell'affetto che mi hai sempre dimostrato anche con la tua Pasta alla Norma da applauso! Wim was always ready with a good strong Italian coffee at University. Andrea, Monica, Robbert and Vasillis were always good friends on whom I could count in any situation.

Nonostante la distanza e gli anni trascorsi lontano da Roma, ho potuto sempre contare sul sostegno e l'affetto dei miei amici di sempre: Danilo, Stefano, Monica, Carla, Federica, Barbara, Raffaele e Francesca. Un grazie speciale per farmi sentire sempre a casa quando sono a Roma, come se non fossi mai andata via.

Un pensiero affettuoso va alla mia famiglia che non mi ha mai fatto mancare affetto, incoraggiamento, e...cibo ! Care nonna Lidia e zia Nella, nonostante viviamo tanto lontane, ho sempre potuto contare sul vostro supporto, spesso telefonico! Cari mamma e papà, grazie per essermi stati sempre vicino nel modo giusto e nei momenti opportuni, per avermi insegnato a vedere sempre il lato migliore delle cose, e per contagiarmi sempre con la vostra allegria quando chiacchieriamo!

Ik wil graag mijn Nederlandse familie bedanken voor hun warme opname. Mamma Mia, papa Theo, Laetitia, en Martijn hebben mij altijd gesteund om mijn proefschrift af te maken, en zij hebben mij altijd verwend met heerlijk eten, lekkere wijn en gezelligheid in hun huis.

In Holland I also found a special person able to give me love, serenity, strength, and the support necessary to complete this thesis besides of my job. Frank, amore mio, I also love every moment of our life together so... *what is the future my happy one? A sea beneath a cloudless sun, A mighty glorious dazzling sea, Stretching into infinity...*

Table of contents

Chapter 1	19
The p-type Si/SiGe heterostructure	19
1.1 The band structure	19
1.2 Classical transport properties	20
1.2.1 Classical magnetoresistance	20
1.2.2 Thermoelectric power and Nernst-Ettingshausen effect.....	21
1.3 Two-dimensional electron system in a magnetic field	21
1.4 Magnetoresistivity of a two-dimensional system	23
1.4.1 Shubnikov-de Haas effect.....	23
1.4.2 The Integer Quantum Hall effect.....	23
1.5 Thermoelectric power.....	25
1.5.1 Thermoelectric power at zero magnetic field	25
1.5.2 Thermoelectric power in magnetic field	27
1.6 References	29
Chapter 2	31
Experimental Techniques	31
2.1 The sample	31
2.2 Sample Design and Electrical connections	33
2.3 Thermopower measurements in metallic and insulating samples.....	34
2.4 Resistivity measurements.....	37
2.5 References	38
Chapter 3	39
Thermopower of a p-type Si/Si_{1-x}Ge_x heterostructure	39
3.1 Introduction.....	39
3.2 Theory	42
3.3 Experimental technique.....	44
3.4 Results and discussion	46
3.4.1 Thermopower data at zero field.....	46
3.4.2 Thermopower in a magnetic field.....	46
3.4.3 Explanation of the temperature behavior of thermopower at zero field	56
3.5 Conclusions.....	60
3.6 References	61

Chapter 4	63
Metal-insulator transitions in a Si/SiGe two-dimensional hole gas in high magnetic fields	63
4.1 The metal insulator transition in 2D.....	63
4.1.1 The metallic and the insulating states in a Si/SiGe two dimensional hole gas.....	63
4.1.2 Two mechanisms for electron localization.....	65
4.1.3 One-parameter scaling theory.....	65
4.1.4 Scaling in the quantum Hall regime: the two parameters theory.....	67
4.1.5 An overview of the experiments and issues in the scaling in quantum Hall regime.....	68
4.2 Scaling of the magnetic field induced metal-insulator transitions.....	69
4.3 References.....	72
Chapter 5	75
Diffusion thermopower of a two-dimensional hole gas in SiGe in a quantum Hall insulating state	75
5.1 Introduction.....	75
5.2 Experimental setup.....	77
5.3 Magnetothermopower measurements.....	78
5.4 The TEP in the insulating state.....	81
5.5 References.....	83
Chapter 6	85
Probing the 2DEG with short non-equilibrium phonon pulses	85
6.1 Introduction.....	85
6.2 Experimental technique.....	87
6.2.1 The sample.....	87
6.2.2 Electronic system for pulse generation and detection.....	89
6.2.3 Cryogenic system.....	92
6.3 Measurements.....	94
6.4 Conclusions.....	97
6.5 References.....	98
Summary	99
Samenvatting	103
List of Publications	107
Curriculum vitae	109

Introduction

The rapid expansion of the high frequency technology commonly employed in everyday life (e.g. in mobile phones or in logic processor chips for PC) requires a tremendous scientific and manufacturing effort in achieving always cheaper, faster and smaller integrated devices. For decades, the worldwide semiconductor market has been dominated by Silicon (Si), which turns out to be a easily available and chemically highly stable material, onto which a unique homogeneous oxide can easily be made. The constant improvement of the growth technique and of the processing technology, with the consequent shrinkage of the dimensions and increase of the package density, allows building logic processor chips with more than 100 million transistors and a clock frequency of more than 2GHz.

The effort in achieving continuously higher frequencies and the wide application of integrated technology in different areas led to the investigation of new materials besides Si, like GaAs/AlGaAs or Si/SiGe heterostructures. Advanced growth techniques have been developed to produce two-dimensional structures, where the carriers are no longer free to move in all directions but are confined in a two-dimensional layer, like balls on a billiard table. The opportunity to control physical properties by changing different layer materials on almost atomic scale provides an enormous scientific attraction. From the point of view of the physics, low dimensional systems have revealed interesting unexpected properties and have led to discoveries such as the quantum Hall effect, weak and strong localization, and charge quantization.

This thesis focuses on the two-dimensional system in Si/SiGe heterostructures, which is experimentally investigated through resistivity and thermoelectric power measurements. By applying an electrical field E , a system of charged carriers reacts by conducting a current J proportional to E , i.e. $E=\rho J$ (with ρ the resistivity), known

as Ohm's law. If, instead of a current, a temperature gradient ∇T is applied, this gradient also induces an electric current which in turn leads to an electric field proportional to the temperature difference through a factor S called *thermoelectric power*, i.e. $E=S\nabla T$ (Seebeck's law).

Resistivity and thermopower measurements provide complementary information about the properties of the two dimensional system. If the driving force is the electric field, the current is limited by the scattering of the carriers caused by static impurities, giving rise to the resistivity ρ . In thermopower, the driving force ∇T gives rise to a current through the phonon-carrier interaction and through the diffusive motion of carriers with different kinetic energy on the hot and on the cold side of the sample. The first contribution to thermopower is called *phonon drag* and arises because ∇T leads to a net flow of phonons from hot to cold, consequently phonon drag is a measure of the interaction between carriers and phonons, normally too small to be detected by resistivity measurements at low temperatures. The second contribution is the *diffusion thermopower* and it gives precious information about the carrier distribution and their intrinsic thermodynamic properties.

In heterostructures where the phonon-carriers interaction is mediated through a piezoelectric potential like in AlGaAs/GaAs, phonon drag dominates until very low temperatures and diffusion is negligible. Si/SiGe heterostructures are expected to be non-piezoelectric and therefore the phonon drag is supposed to be small enough at low temperatures to measure the diffusion contribution. Most of the previous work on heterostructures has been done on piezoelectric active systems where drag dominates down to low temperatures. Therefore diffusion has been difficult to probe. In this thesis, with Si/SiGe systems, we have been able to clearly measure diffusion separately from phonon drag. Diffusion is an interesting physical parameter because it can easily be related to a thermodynamic parameter, the entropy, which is one of the most fundamental properties of any system.

Two-dimensional systems show an interesting transport behavior in high magnetic fields, related to Landau quantization and to carrier localization: the integer quantum Hall effect, observed for the first time by K.von Klitzing in 1980 in Si-MOSFET. If a magnetic field is applied perpendicular to the two-dimensional system, the Lorentz force causes a full quantization of the energy spectrum of the carriers, called *Landau quantization*. As a consequence the electronic density of states is altered to a discrete set of levels (*Landau levels*) equally separated by the cyclotron energy. This energy structure is reflected in the quantum oscillations in resistivity (Shubnikov-de Haas) and in thermopower. In high magnetic fields, the Hall resistance shows exactly quantized plateaus at integer fractions of h/e^2 (where h is the Plank's constant and e the electron charge), independent of any sample characteristics. At the same time the longitudinal resistivity vanishes. The remarkable accuracy of the quantization of the Hall resistance (about 10^{-11} precision reproducible among different samples) has led to a recommended value of the resistance. The

quantum Hall effect is generally explained with the localization-delocalization of the carriers but the remarkable precision is still astonishing.

The system investigated in this thesis is a Si/SiGe two-dimensional hole gas, i.e. missing electrons in the valence band behaving as carriers with a positive charge. This system is known to exhibit peculiar phenomena related to localization of carriers: *i*) a metal insulator transition as a function of carrier density at zero magnetic field, *ii*) a field induced metal-insulator transition between the first two Landau levels, and *iii*) a strongly insulating phase at very high fields, where the carriers are in the low energy tail of the lowest Landau level. The field driven insulating state between two (integer or fractional) Hall states has also been observed in other two-dimensional systems (AlGaAs/GaAs, Si-MOSFET) but its origin has been not understood yet. In this thesis, the transition to the insulating state between the first two Landau levels has been studied with two different experimental techniques, resistivity and thermopower in a wide range of temperatures and for different carrier densities. The thermoelectric power probes the energy distribution of the carriers and therefore it is capable of clarifying whether the insulating state is due to a discontinuity in the density of states or is induced by the disorder.

This thesis is structured as follows. Chapter 1 describes the *p*-type Si/SiGe heterostructure investigated in Chapter 3, 4, and 5 and it gives an introduction to transport measurements in zero and in magnetic field. The mechanisms responsible for thermopower will be explained in detail as well as the quantum oscillations in the resistivity and thermopower at low magnetic fields (Mott theory for diffusion thermopower and the Shubnikov-den Haas oscillations) and higher fields (quantum Hall effect and the effect of Landau levels on thermopower).

Chapter 2 describes the experimental setup used for the measurements in Chapters 3, 4, and 5.

Chapter 3 presents the thermopower measurements at zero fields and low magnetic field for a *p*-type Si/SiGe heterostructure. The diffusion component is well described by the theory, including quantum oscillations at low fields. Surprisingly, the temperature dependence of phonon drag is different than expected from theory and suggests that the carrier-phonon coupling is mediated either by an unscreened deformation potential or by a screened piezoelectric scattering.

Chapter 4 and 5 focus on the resistivity and thermopower measurements in the metal-insulator transition between the first two Landau levels. A scaling analysis shows that the metal insulator transition and the insulating transition at higher field belong to the same universality class, supporting the idea that the two metal-insulator transitions are driven by the same mechanism. In contrast to resistivity, the diffusion thermoelectric power probes the energy distribution of the carriers and it is therefore able to answer the question whether the transition is the result of a discontinuity in the carrier density of states or if it is due to the presence of a disorder-induced mobility gap. The thermopower measurements suggest the latter hypothesis.

The last Chapter is dedicated to the description of the technique for pulsed thermopower experiments. The goal is to probe how local is the electron-phonon

interaction by detecting time-resolved the response of the carriers to short non-equilibrium heat pulses. The Chapter gives a description of the solutions to some cryogenic and electrical problems, points out the issues which still need to solve in order to be able to detect time-resolved the response of the two dimensional system to pulsed heat excitations.

Chapter 1

The p-type Si/SiGe heterostructure

A two-dimensional hole (or electron) gas can exist at the interface between different materials, in systems called “heterostructures” (e.g. GaAs/AlGaAs, Si/SiGe are heterostructures). Because of the two-dimensional nature of these systems, they exhibit new quantum phenomena, such as the quantum Hall effect. In this thesis, we study the p-type Si/SiGe heterostructure.

1.1 The band structure

The sample used in this thesis is a strained, asymmetrically doped p-type Si/Si_{0.88}Ge_{0.12} heterostructure. The carriers are holes (positive electric charge) confined in a triangular potential well. Fig. (1.1) shows a schematic picture of the valence band in a p-type Si/SiGe heterostructure with a confining potential $V(z)$ in the z direction.

Band structure calculations on strained p-type Si/SiGe heterostructures show that the strain and the confinement in the z direction lift the heavy hole band, and therefore remove the degeneracy with the light-hole band at the zone center [1]. For moderate carrier density, the holes occupy only the heavy hole subband ($|M_J| = 3/2$), which is well above the light hole band and therefore is strongly decoupled. In these circumstances, the transport properties of the system are found to be well described by a single band picture.

In such a simplified picture, we can assume that the two-dimensional hole gas consists of carriers with positive charge $+e$ and with an effective mass $m^* = 0.3m_e$, with m_e the free electron mass.

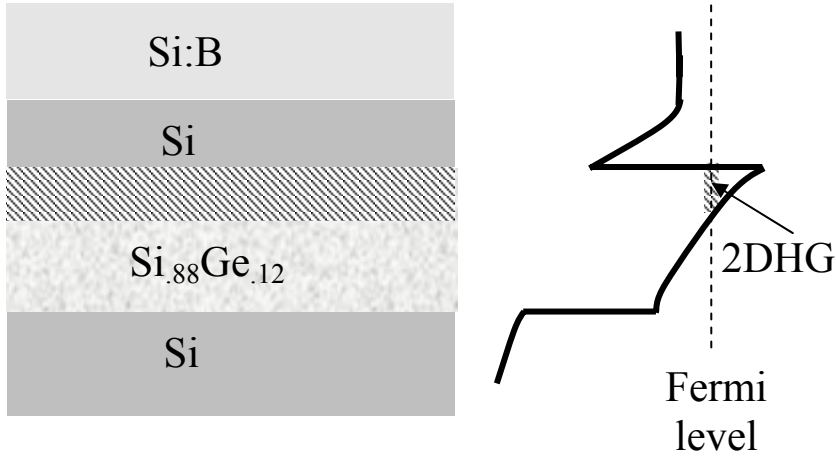


Figure 1.1: Schematic of the valence band in a Si/SiGe heterostructure.

1.2 Classical transport properties

1.2.1 Classical magnetoresistance

By applying an electrical field E , a conductor reacts by conducting a current J proportional to E , i.e. $E=\rho J$ where ρ is the resistivity which depends on the properties of the material. In the presence of a magnetic field perpendicular to the conductor, ρ becomes a tensor where $\rho_{xx}=\rho_{yy}$ and $\rho_{xy}=-\rho_{yx}$. The conductivity tensor σ is defined as the inverse of the resistivity tensor and, in a two-dimensional system, they are related to the elements of the resistivity tensor by:

$$\rho_{xx} = \frac{\sigma_{xx}}{\sigma_{xx}^2 + \sigma_{xy}^2} \quad (1.1a)$$

$$\rho_{xy} = \frac{\sigma_{xy}}{\sigma_{xx}^2 + \sigma_{xy}^2} \quad (1.1b)$$

In zero magnetic field, ρ is given by $\rho = \rho_{xx}(B=0) = 1/(e\mu n)$, where μ and n are the transport mobility and the density of the carriers, respectively.

1.2.2 Thermoelectric power and Nernst-Ettingshausen effect

When a temperature gradient ∇T is applied to a conductor, the electric and the thermal currents J and U are related to the field E and the temperature gradient ∇T by two basic transport equations:

$$\begin{aligned} J &= \sigma E - \varepsilon \nabla T \\ U &= \pi E - \lambda \nabla T \end{aligned} \quad (1.2)$$

where the coefficients are the conductivity tensor σ , the thermoelectric tensor ε , the Peltier tensor π , and the thermal conductivity λ . All the coefficients are scalars at zero magnetic field and become tensors in presence of magnetic field.

Because the TEP is measured with zero total current ($J=0$), it follows (Eq. (1.2)) that $E = \rho \varepsilon \nabla T$, which shows the fundamental relation $S = \rho \varepsilon$ with S the Seebeck coefficient defined by $E = S \nabla T$.

When a magnetic field B is applied in the direction perpendicular to the two-dimensional carrier system, two independent components of the thermopower tensor S are found:

$$\begin{aligned} S_{xx} &= \rho_{xx} \varepsilon_{xx} + \rho_{xy} \varepsilon_{yx} \\ S_{yx} &= \rho_{xx} \varepsilon_{yx} + \rho_{yx} \varepsilon_{xx} \end{aligned}$$

S_{xx} is the *longitudinal thermopower*, or thermopower, and S_{yx} is the *Nernst-Ettingshausen coefficient*, or transverse thermopower. S_{xx} and S_{yx} can be measured by the thermal voltage appearing in the direction of ∇T (S_{xx}) and perpendicular to ∇T (S_{yx}).

1.3 Two-dimensional electron system in a magnetic field

The energy levels of a two-dimensional system in a magnetic field are given by

$$E_{n,s,i} = \hbar \omega_c \left(n + \frac{1}{2} \right) - s g^* \mu_B B + E_i$$

which corresponds to the well known spin-split Landau levels originating from each confined subband E_{is} . ω_c is the cyclotron frequency ($\omega_c = eB/m^*$).

Hence, in a magnetic field B the density of states (DOS) of the two-dimensional system becomes a discrete set of δ -like functions, separated by $\hbar \omega_c$:

$$g(E) = G \sum_{n,s} \delta(E - E_{n,s})$$

The degeneracy of each Landau level for a given magnetic field B is $G=eB/h$.

For a fixed concentration of carrier density p_h , the levels are filled up to the Fermi energy, which becomes dependent on magnetic field. The number of filled Landau levels, called *filling factor*, is defined as $\nu = p_h h / eB$.

In a non-ideal system, the carriers have a finite lifetime τ_q and the DOS has a finite width $\Gamma \sim \hbar / \tau_q$, as a result of lifetime broadening due to impurity scattering or potential fluctuations, as shown in Figure (1.2).

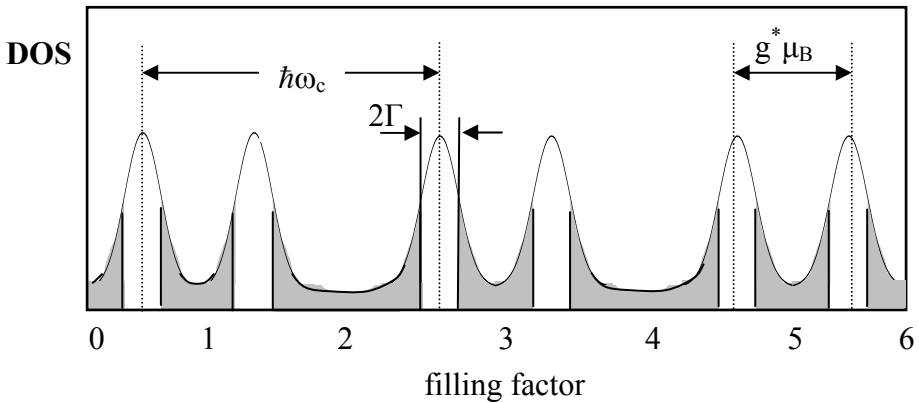


Figure 1.2: Broadened Landau levels in a two-dimensional system.

The behavior of resistivity and thermopower in a magnetic field depends on the ratio between the Landau level splitting ($\hbar\omega_c$) and the Landau level broadening Γ . When $\hbar\omega_c \ll \Gamma$, the system can be described in the classical limit. At intermediate fields ($\hbar\omega_c \geq \Gamma$), Shubnikov-de Haas quantum oscillations become observable in the resistance. In the extreme quantum limit ($\nu < 1$ and $\hbar\omega_c \gg k_B T$ and $\hbar\omega_c \gg \Gamma$), only the lowest Landau level is occupied and new phenomena (which are discussed later) may occur.

1.4 Magnetoresistivity of a two-dimensional system

1.4.1 Shubnikov-de Haas effect

When $k_B T \ll \hbar\omega_c$ and $\hbar\omega_c \leq \Gamma$ (or $\mu_q B \leq 1$, with $\mu_q = e\tau_q/m^*$ the quantum mobility), the Landau levels are not completely separated and the DOS can be approximated as an oscillatory function of the energy. For an isotropic two-dimensional hole system, the oscillatory longitudinal resistivity ρ_{xx} is given by [2,3]

$$\tilde{\rho}_{xx}(B) = 4\bar{\rho}_{xx} \sum_s D(sX) e^{-\frac{\pi s}{\mu_q B}} \cos\left(\frac{s2\pi E_F}{\hbar\omega_c} - s\pi\right) \quad (1.3)$$

where $\tilde{\rho}$ and $\bar{\rho}$ are the oscillatory and non-oscillatory resistivity, respectively, E_F is the Fermi energy, and $D(sX) = (sX)/\sinh(sX)$ is the thermal damping factor for the oscillations with $X = (2\pi k_B^2 T / \hbar\omega_c)$ and s is an integer number indicating the index of the harmonic component.

The oscillatory part describes the Shubnikov-de Haas oscillations; the first term includes the temperature dependence of the Shubnikov-de Haas oscillations, and the second term is an exponential envelope, which decays rapidly with the harmonic index s .

1.4.2 The Integer Quantum Hall effect

When $\hbar\omega_c \gg k_B T$, at magnetic fields where $\mu_q B \gg 1$, the Integer Quantum Hall Effect (IQHE) becomes visible. This effect was observed for the first time by von Klitzing in 1980 [4] in Si-MOSFET, and it is characterized by the appearance of Hall resistivity plateaus at a integer filling factors $\nu = i$, with quantized values h/ie^2 . This value is independent on the characteristics of the sample. At filling factor $\nu = 1$, the Hall resistance is equal to 25813Ω , measured with an accuracy of 10^{-11} , and it is independent on the sample. The quantization of the Hall resistance is so precise that it is used as the recommended value of the resistance standard nowadays, since no standard resistor gives better accuracy than the measured 10^{-11} quantized values.

In a real system, impurities and crystal defects lead to potential fluctuations, which localize states at the tails of the Landau levels. These tail states do not contribute to the conductivity of the two-dimensional system, which forms the basis of the explanation of the IQHE. Because of the broadening of the Landau levels and the existence of insulating states at the tails, the Fermi energy changes smoothly by

increasing the magnetic field, whereas in a δ -shaped DOS, it would jump from one Landau level to the next one. A crucial point in the explanation of the IQHE is that only the extended states can carry current at $T=0$. If the magnetic field increases continuously, the localized states are filled up without any change in the occupation of the extended states, and therefore ρ_{xx} will be zero (or minimum at finite low temperature) and the Hall resistivity ρ_{xy} will remain constant ($\rho_{xy}=h/e^2\nu$). Only when the Fermi level passes through extended states in the center of a Landau level, ρ_{xx} becomes appreciable and the Hall resistance makes a transition from one plateau to the next.

Alternatively, also edge states are invoked as an explanation of the IQHE. Carriers close to the physical edge of the sample will be reflected by the edge of the device resulting in a net drift velocity that becomes higher the closer the carrier gets to the edge. These “edge states” behave as a one-dimensional conducting channel. In the frame of this thesis, we will restrict to the description of the behavior of the two-dimensional system in terms of localized and extended states. The two models can be reconciled by considering the sample edges as the ultimate potential fluctuation present even in ideal samples, and thus the edge state as the ultimate extended state.

To illustrate the behavior described above, we show in Fig.(1.3) typical magnetoresistivity curves of the Si/SiGe heterostructure. At high magnetic fields (low filling factors) ρ_{xy} shows plateaus at integer filling factor $\nu=i$ with values $\rho_{xy}=h/ie^2$, and at the same time the longitudinal resistivity ρ_{xx} tends to zero. At lower fields the Shubnikov-de Haas oscillations are visible.

An evident feature in Fig. (1.3) is the predominance of odd filling factor for Si/SiGe heterostructures. It is commonly accepted that this peculiar behavior is due to the large value of the g -factor in this system [5]. In fact, the large value of the g -factor ($g^*>2$) induces a Zeeman splitting $\Delta E_s=g^*\mu_B B$ comparable with the Landau level spacing $\hbar\omega_c$ (see Fig. (1.2)). Therefore the state in the Landau level n_L and spin up $(n_L)_\uparrow$ and the state in the next Landau level and spin down $(n_L+1)_\downarrow$ are almost degenerate and not resolved even at very low temperatures. A more detailed analysis of Si/SiGe in magnetic field is the central issue of this thesis and it is reported in Chapters 3-5.

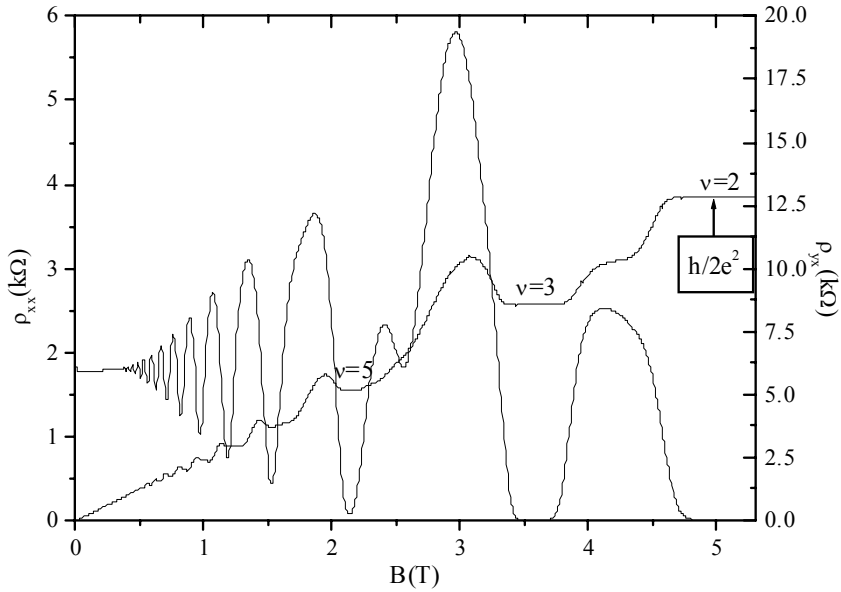


Figure 1.3: The resistivity (ρ_{xx}) and the Hall resistance (ρ_{yx}) as a function of magnetic field in the Si/SiGe heterostructure used in Chapters 3-5.

1.5 Thermoelectric power

1.5.1 Thermoelectric power at zero magnetic field

A temperature gradient ∇T applied across a conductor induces a thermally driven electric current j_{th} . If there is no net current flowing in the system, j_{th} has to be compensated by an electrical current j_e due to an electrical field E . The ratio between the electrical field and the temperature gradient is the *thermoelectric power* S , i.e. $E=S\nabla T$. Since both the thermal and the compensation current are proportional to the impurity relaxation time momentum τ_{imp} , the thermopower results to be independent of τ_{imp} . In this respect, the thermoelectric power is very different from resistivity, which is almost completely dominated by impurities at low temperatures. Thermopower provides information on thermodynamic properties of the carriers and

on the carrier-phonon scattering, which is almost negligible in resistivity measurements at low temperatures.

The thermoelectric power is the result of two different mechanisms: *diffusion* (S^d), due to the diffusive motion of carriers in a temperature gradient, and *phonon drag* (S^g), due to the momentum transfer from phonons to carriers. In the limit of weak coupling between carriers and phonons, these two contributions are additive and the total thermopower is given by $S = S^d + S^g$.

In zero magnetic field, in the limit of weak interaction between the phonon of the three-dimensional substrate and the two-dimensional hole gas, the diffusion contribution to thermopower S^d is given by the ‘‘Mott formula’’

$$S^d = \frac{\pi^2 k_B T}{3|e|} \left. \frac{\partial \ln \sigma}{\partial E} \right|_{E_F} \quad (1.4)$$

where k_B is the Boltzmann constant. If $p = (\partial \ln \tau_t / \partial \ln E)_{E_F}$ is the energy dependence of the relaxation time, then

$$S^d = \frac{\pi^2 k_B T}{3|e|E_F} (1 + p) \quad (1.5)$$

S^d is linear in temperature and consists of two additive contributions: the average entropy per unit of charge and the term proportional to p , related to scattering. The value and the sign of the scattering parameter p depends on the dominant scattering mechanism for diffusion. S^d is negative if $p < -1$.

The phonon drag contribution S^g to thermopower is due to hole-phonon scattering. The momentum transferred from phonons to carriers induces a thermal current $j_{th} = -e \nabla T$. By following the simple idea of the compensation between thermal and electrical current, it can be shown that at low temperatures and low densities, when the phonon scattering is limited by boundary scattering in the substrate, the phonon drag is given by [16]

$$S^g = \frac{\Lambda v}{\mu_{ph} T} \quad (1.6)$$

where Λ is phonon mean free path and μ_{ph} is the phonon-scattering limited electron mobility.

A more formal theory of phonon drag was developed by Cantrell and Butcher [6]. In this model the phonons are considered bulk phonons traveling in a 3D substrate, whereas the electrons are confined in the confining potential. The model assumes that the main scattering mechanism for phonons is boundary scattering, which determines the phonon mean free path Λ . Originally, the electron-phonon coupling was considered to be only due to unscreened deformation potential. Afterwards, Smith and Butcher [7] evaluated the influence of both deformation and piezoelectric potential coupling in the model. The calculations gave a good agreement with experimental data in systems, like Si-MOSFETs, characterized by

the presence of only deformation potential coupling [8], and in piezoelectric structures like GaAs/AlGaAs [9].

In a two-dimensional hole gas, assuming that the carriers with wave vector $k=(k_x, k_y)$ are quasi-elastically scattered by the three-dimensional acoustic phonons with wave vector $Q=(q, q_z)$, where q is the component in the plane of the two-dimensional system and q_z is perpendicular to it, the phonon drag for a 2DHG is given by [8]

$$S^g = \frac{(2m^*)^{3/2} g_v \Lambda}{16(2\pi)^3 k_B T^2 n_e e \rho_m} \sum_i \int_0^\infty \int_{-\infty}^\infty \frac{\Xi_i^2(Q) C_i(Q)}{\epsilon^2(q)} dq dq_z \quad (1.7)$$

where ρ_m is the mass density of silicon, g_v is the valley degeneracy, Λ is the phonon mean free path, and the subscript i refers to phonon polarization. $\Xi(Q)$ denotes the effective acoustic potential scattering. When the energy spectrum of the carriers is isotropic, $\Xi(Q)$ is given by the deformation potential constant Ξ_{DP} . In case the electron-phonon coupling is complicated by the anisotropy of the energy spectrum, like in Si-MOSFET [8], $\Xi(Q)$ contains the deformation potential for both longitudinal and transverse modes. For materials like GaAs, $\Xi(Q)$ accounts for both deformation and piezoelectric coupling: $\Xi^2(Q) = \Xi_{DP}^2 + (eh_{14})^2 A(q, q_z)/Q^2$, where h_{14} is the piezoelectric constant, A is the anisotropy factor which is different for longitudinal and acoustic phonons [10,11]. The factor $C(Q)$ contains the phonon and electron distribution and the momentum transfer from phonons to the electrons [8]. $\epsilon(q)$ is the static dielectric screening function and it is [9] $1 + (Q_s/q)\zeta(q)F_s(q)$ where Q_s is the screening wave vector, $\zeta(q)$ is unity for $q \leq 2k_F$ and $1 - [1 - (2k_F/q)^2]^{1/2}$ for $q > 2k_F$ (k_F is the Fermi wave number) and $F_s(q)$ is the screening form factor that accounts for the finite thickness of the 2DHG [9].

At low temperatures, by allowing several approximation in equation (1.7) and assuming that the mean free path Λ is constant in temperature, it can be shown [8] that for screened deformation potential coupling $S^g \sim T^6$ and that for screened piezoelectric potential coupling $S^g \sim T^4$. Experimental data agree with the calculated temperature dependence in Si-MOSFET [8] and in AlGaAs/GaAs heterostructures [9, 12]

1.5.2 Thermoelectric power in magnetic field

As with magnetoresistivity, also for thermoelectric power we distinguish between low and high field behavior.

In high magnetic fields, in the limit of $\mu_{tr} B \gg 1$, where $\mu_{tr} = e\tau/m^*$ is the transport mobility, electronic scattering can be ignored and S_{xx}^d can be simply estimated as the entropy per unit of charge. The entropy, and therefore S_{xx}^d , is expected to be zero

when the Landau levels are completely full and to reach its maximum value when the Fermi energy E_F lies at the center of the Landau level, which is then half filled. In the latter case, the thermopower for a 2DHG is given by [13]:

$$S_{xx,\max}^d = \frac{k_B \ln 2}{|e|v} = \frac{60 \mu\text{V}}{v \text{ K}} \quad (1.8)$$

where v is the Landau level filling factor.

This model predicts that S_{xx} has an oscillatory behavior in phase with the longitudinal resistivity.

At lower magnetic fields, the Landau levels are not resolved and the overlap between them results in a non-oscillatory background in TEP, on which are superimposed the quantum oscillations due to the magnetic quantization of the electrons. In this case, it is possible to calculate the oscillatory and the non-oscillatory part of thermoelectric power [14,15] by extending the Mott formula (equation (1.4)) to the case of a low magnetic field perpendicular to the 2DHG. The two non-oscillatory part components of thermopower (\bar{S}_{ij}^d) are [15]:

$$\bar{S}_{xx}^d = \frac{L_0 e T}{E_F} \left(1 + \frac{p}{1 + \beta^2} \right) \quad (1.9a)$$

$$\bar{S}_{yx}^d = \frac{L_0 e T}{E_F} \left(\frac{p\beta}{1 + \beta^2} \right) \quad (1.9b)$$

where $L_0 = \pi^2 k_B^2 / 3e^2$, $\beta = \omega_c \tau_r = \mu_i B$ with μ_i the transport mobility and p is the exponent of the energy dependence of the relaxation time. We observe that the equations (1.9a) reduce to the zero field relation eq. (1.5) for $\beta=0$.

The quantum oscillations of diffusion thermopower \tilde{S}_{ij}^d can be calculated from the Fourier components of the resistivity oscillations ($\tilde{\rho}_{ij}$) and from the non-oscillatory part of the resistivity ($\bar{\rho}_{ij}$) [15]:

$$\tilde{S}_{xx}^d = \frac{\alpha}{1 + \beta^2} \left(\frac{\tilde{\rho}_{xx}}{\bar{\rho}_{xx}} + \beta^2 \frac{\tilde{\rho}_{xy}}{\bar{\rho}_{xy}} \right) \quad (1.10a)$$

$$\tilde{S}_{yx}^d = \frac{\alpha\beta}{1 + \beta^2} \left(\frac{\tilde{\rho}_{xx}}{\bar{\rho}_{xx}} + \frac{\tilde{\rho}_{xy}}{\bar{\rho}_{xy}} \right) \quad (1.10b)$$

where $\alpha = i(\pi k_B / e)(D'(X)/D(X))$, $X = 2\pi k_B T / \hbar \omega_c$, and $D'(X)$ is the derivative of the damping factor for the resistivity oscillations $D(X)$: $D'(X) = dD(X)/dX$. $D'(X)$ is the damping factor for diffusion oscillations. The presence of the factor $i = \sqrt{-1}$ shows that the oscillations of \tilde{S}_{ij}^d and $\tilde{\rho}_{ij}$ have a phase difference of $\pi/2$. This feature is a peculiarity of thermopower in the diffusive regime at low fields and can be explained

from eq.(1.1), where the TEP is related to the derivative of conductivity respect to the energy. Noting that $D'(X)$ is a negative quantity, if we write $\tilde{\rho}_{xx} \propto \cos((2\pi r f/B) + \varphi_r)$, then $\tilde{S}_{xx}^d \propto \sin((2\pi r f/B) + \varphi_r)$, where f is the frequency of the fundamental component and φ_r a constant phase factor of the r^{th} harmonic.

A complete theory of phonon drag in magnetic fields is not yet available. Semiclassical theory [16] shows that the thermoelectric power S_{ij}^g is a diagonal tensor independent of the magnetic field: the longitudinal thermopower \tilde{S}_{xx}^g should be independent of the magnetic field and the phonon drag Nernst-Ettingshausen component \tilde{S}_{yx}^g should be zero. Any finite S_{yx} is therefore expected to be purely due to diffusion, although experiments in two-dimensional systems show that S_{yx} seems to be dominated by phonon drag as well [15]. There is no theory for phonon drag quantum oscillations in low fields, however experiments show that the oscillations of \tilde{S}_{xx}^g are in phase with the resistivity $\tilde{\rho}_{xx}$ [17].

At low magnetic fields, it is therefore possible to distinguish between phonon drag and diffusion thermopower only by looking at the phase difference between \tilde{S}_{xx}^g and $\tilde{\rho}_{xx}$: a phase difference of $\pi/2$ implies diffusion, whereas no phase difference means that phonon drag is dominant. However, at higher fields, both diffusion and phonon drag oscillations are in phase with the resistivity oscillations and the phase is not a good criterium to distinguish between the two mechanisms anymore.

1.6 References

- [1] C.J.Emeleus *et al.*, Journal of Applied Physics **73**, 3852 (1993).
- [2] T.Ando, J.Phys.Soc.Japan **37**, 233 (1974).
- [3] P.T.Coleridge, R.Stoner, and R.Fletcher, Phys. Rev.B **39**,1120 (1989) and references therein.
- [4] K.von Klitzing, G.Dorda, and M.Pepper, Phys.Rev.Lett.**45**, 494 (1980).
- [5] P.T.Coleridge, A.S.Sachrajda, H.Lafontaine, and Y.Feng, Phys.Rev.B **54**, 14518 (1996).
- [6] D.G.Cantrell and P.N.Butcher, Journ. Phys.C **20**, 1989 (1987); D.G.Cantrell and P.N.Butcher, Journ. Phys.C **20**, 1993 (1987).
- [7] M.J.Smith and P.N.Butcher, Journ.Phys.:Condens. Matter **1**, 4859 (1989).
- [8] R.Fletcher, V.M.Pudalov, Y.Feng, M.Tsaousidou and P.N.Butcher, Phys.Rev.B **56**, 12422 (1997).
- [9] B.Tieke, U.Zeitler, R.Fletcher, S.A.J.Wiegers, A.K.Geim, J.C.Maan, and M.Henini, Phys. Rev. Lett. **76**, 3630 (1996).
- [10] X.Zianni, P.N.Butcher, and M.J.Kearney, Phys.Rev.B **49**, 7520 (1994).
- [11] S.K.Lyo, Phys.Rev.B **38**, 6345 (1988).
- [12] R.Fletcher, M.Tsaousidou, P.T.Coleridge, Z.R.Wasilewski, and Y.Feng, Physica E **12**, 272 (2002).

- [13] B.L.Gallagher and P.N.Butcher, in *Handbook on Semiconductors*, edited by P.T.Landsberg (Elsevier, Amsterdam, 1992), Vol.1, p.817.
- [14] R.Fletcher, P.T.Coleridge, and Y.Feng, *Phys.Rev.B* **52**, 2823 (1995).
- [15] R.Fletcher, V.M.Pudalov, and S.Cao, *Phys.Rev.B* **57**, 7174 (1998).
- [16] A.Miele, R.Fletcher, E.Zaremba, Y.Feng, C.T.Foxon, and J.J.Harris, *Phys.Rev.B* **58**, 13181 (1998).
- [17] M.D'Iorio, R.Stoner, and R.Fletcher, *Solid St.Comm* **65**, 697 (1988).

Chapter 2

Experimental Techniques

2.1 The sample

The sample used in Chapters 3-5 is a strained p -type Si/Si_{0.88}Ge_{0.12} heterostructure grown by ultra high vacuum/chemical vapor deposition (UHV/CVD) system at the Institute of Microelectronical Sciences of the National Research Council in Ottawa, Ontario, Canada. The sample consists of a n -type Si substrate, a 300nm Si buffer layer, a 40nm Si_{0.88}Ge_{0.12} quantum well, followed by a 12nm spacer layer and a 30nm layer of Si doped with Boron on top. The growth sequence and further details are described by the growers of the sample in P.T.Coleridge *et al.* [1].

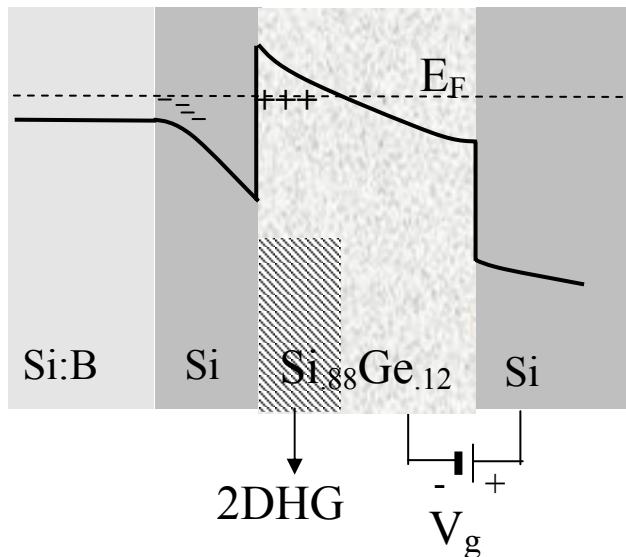


Figure 2.1: Valence band scheme and substrate bias (V_g) in SiGe.

The sample has a hole density around $2.4\text{-}2.7\cdot 10^{15}\text{m}^{-2}$, and at 1K a mobility of around $1.5\text{m}^2/\text{Vs}$ which is strongly dependent on temperature as described in Chapter 3. We observed that different cooling procedures lead to different densities with the same sample: in the data presented in Chapter 4, the density could be changed about 30% in two different cooling runs. In order to change the density in a more controlled way, the sample was backgated, i.e. the bandstructure and therefore the carrier density was changed by applying a potential difference between the Si substrate and the 2DHG, as shown in Figure (2.1).

By applying a substrate bias (V_g), the carriers of the 2DHG were depleted: Figure (2.2) shows the hole density as a function of the external voltage V_g applied for the sample used.

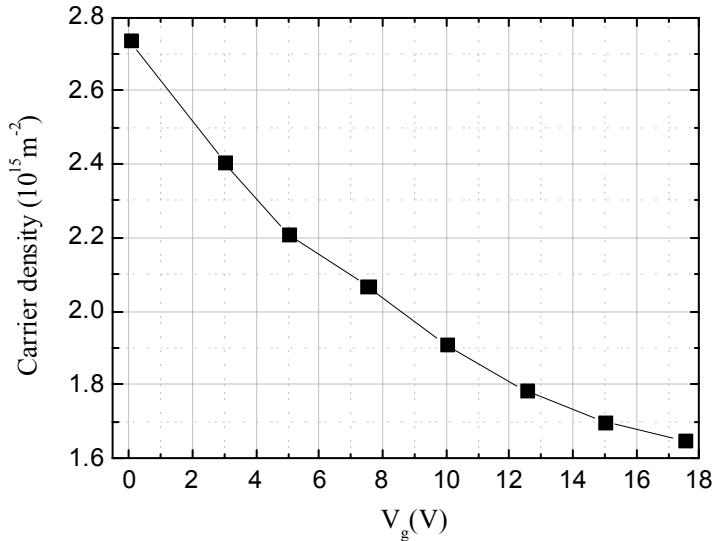


Figure 2.2: Carrier density of the 2DHG measured as a function of the bias voltage V_g .

It was not possible to reach the *critical density* $p_{hc}=1.0\cdot 10^{15}\text{m}^{-2}$ because this would require too high voltages. For densities $p_h < p_{hc}$ the sample is known to become an insulator at zero magnetic field [1]. All the samples used in this thesis exhibit a metallic behavior at $B=0$.

The carrier density was found to drift at temperatures above 4K. For that reason, each set of measurements was taken in the same run, keeping the temperature $T < 4\text{K}$.

Each time the sample was cooled below 4K, the sample density was measured. No shift of density was observed below 4K.

2.2 Sample design and electrical connections

The sample was etched in a 200 μm wide Hall bar with ten Al contacts alloyed (Figure (2.3)). Electrical connections to the sample were done by bonding 10 μm gold wire, successively fixed to the contact pads with EPOTEK, a silver filled epoxy which makes the bonded contacts mechanically stronger and ensures a good electrical contact between the gold wires and the sample. The other end of the gold wires were soldered to 100 μm twisted pairs manganin wires. The manganin was chosen because of its low thermal conductivity, which minimizes the heat transfer to the sample.

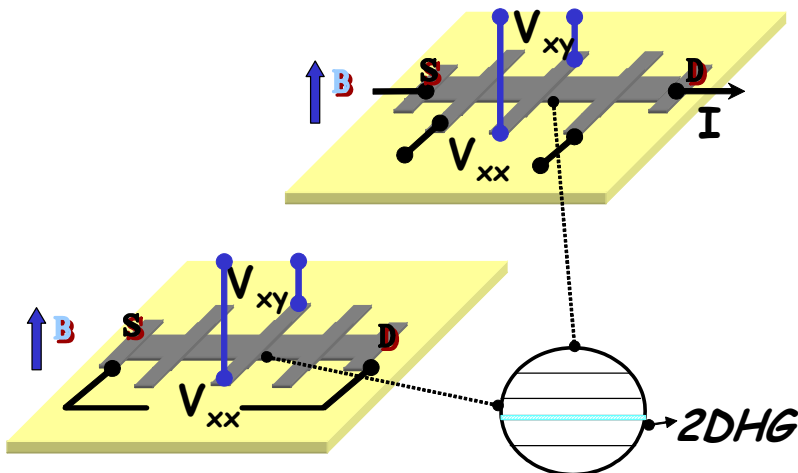


Figure 2.3: Schematic of the Hall bar and contacts in resistivity measurements (above) and thermopower measurements (below)

By applying a current between the source (S) and drain (D) in the geometry shown in Figure (2.3) (top), the voltage drop in the x direction (V_{xx}) gives the resistivity ρ_{xx} , while the voltage V_{xy} measures ρ_{yx} in presence of a magnetic field.

In thermoelectric power measurements, the excitation is given by a temperature gradient ∇T in the longitudinal direction, which thermally creates the measured voltages V_{xx} and V_{xy} , related to the thermopower S_{xx} and the Nerst-Ettingshausen S_{yx} coefficients. While the resistivity depends on the ratio between the voltage contact distance and the width of the mesa, the magnitude of the measured thermopower voltage depends only on the separation between the contacts, since in thermopower no current is flowing through the sample, but a balancing potential distribution is setup across the sample. Therefore the length of the Hall bar has to be maximized (in our samples it was 2.8mm) and the thermopower is preferably measured between source and drain.

2.3 Thermopower measurements in metallic and insulating samples

The thermopower measurements were performed with a ^3He system in a superconducting magnet ($B \leq 8\text{T}$). The sample was mounted *in vacuum* with one end soldered with indium to a cold finger. The indium provides a good thermal contact, allowing a fast dissipation of the heat. In order to establish a temperature gradient, a heater was glued on the “warm” end of the sample with STYCAST epoxy. Figure (2.4) shows a scheme of the sample holder.

The heater is a strain gauge of 350Ω , consisting of a small grid of constantan on a polyamide support and its resistivity is almost temperature and magnetic field independent. The resistance of the heater was measured at low temperatures and therefore the power dissipated on the sample was determined. A second heater was glued with STYCAST on the cold finger to change the base temperature of the sample.

The applied voltage across the heater generates a temperature gradient across the sample and, therefore a thermopower voltage. The temperature was measured with two matched pairs of Philips RuO resistors on the warm and the cold side, with resistances R_H and R_C . The resistors were glued on the back of the sample with a drop of STYCAST, which ensure a good thermal contact with the substrate. Both the resistors have been calibrated in the temperature range of interest by using a Ge thermometer (Lakeshore). In magnetic field, the magnetoresistance of the thermometer was measured and corrected in the data processing. After applying a heating power, the values of the thermometers R_C and $\Delta R = R_C - R_H$ were measured with a resistance bridge. A bridge working at 33Hz was used as a null-detector measuring directly the resistance R_C of the cold thermometer and ΔR , gives a higher

precision of the temperature difference ΔT than a separate measurement of R_H and R_C [2], in particular when the temperature gradient is small.

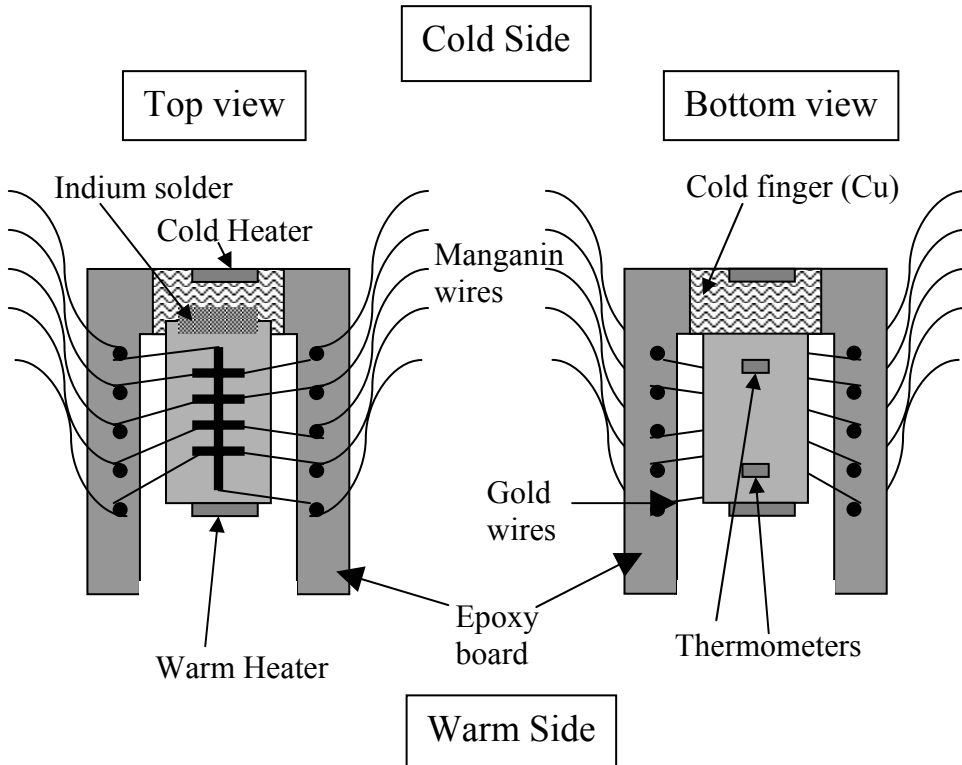


Figure 2.4: Scheme of the thermopower setup.

To verify the thermometry, the thermal conductivity λ of the sample was always calculated from the measurement of the temperature gradient, the temperature, the applied heating power and the dimension of the sample. The results in Figure (2.5) for λ at zero magnetic field and at high magnetic field are identical. Since λ does not depend on the magnetic field, this result shows that the temperature measurement technique is reliable using the appropriate magnetoresistance corrections.

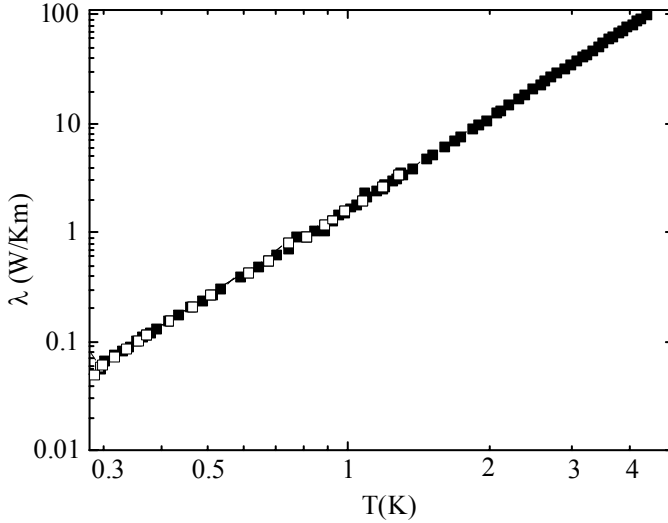


Figure 2.5: Thermal conductivity λ as a function of temperature measured in zero field (■) and in high magnetic field (□).

Thermoelectric power was measured using both AC and DC technique. DC measurements use an analogue EM nanovoltmeter (EM Electronics) or a Keithley 182 nanovoltmeter, both with a resolution of 1nV. Since the signal to noise ratio of the EM nanovoltmeter is poor for input impedance higher than 100k Ω , the analogue EM nanovoltmeter can only be used for measurements of the sample in the metallic state, when the two terminal resistance between the contacts is a few k Ω . For higher sample resistance (which can occur in the metal-insulator transition), the measurements were performed with the nanovoltmeter K182, which has an input impedance in the G Ω range.

An offset in the DC measurements was observed which was dependent on temperature and was related to the bias current of the input of the K182. Normally, the nanovoltmeter input amplifier is biased with a current I_b , which in combination with the resistance of the sample R_s gives rise to a spurious voltage $V_s=R_s I_b$. This voltage is added to the measured TEP voltage and can be the same order of magnitude or bigger than the TEP voltage [3,4]. The bias current I_b depends on the source resistance and, in some nanovoltmeters, it can be as high as 50pA. In the Keithley 182 used for thermopower measurements, $I_b=15$ pA for sources with R_s up

to $1\text{M}\Omega$ and increases to 30pA at higher source impedances. In order to eliminate the spurious voltage, at each temperature the signal was measured with and without temperature gradient, keeping the average temperature constant: the difference between these two values is the TEP signal. This procedure was completely automated and the data were acquired by setting the hot and the cold heaters alternatively on and off, by averaging at least five times and by increasing the number of averages when the TEP voltage was as small as a few nanovolts.

The spurious voltage arising from the input amplifier bias current can be eliminated by measuring the thermopower in AC, providing that the amplifier is AC coupled. Here, the AC phase sensitive Lock-in technique has been used in the TEP field sweeps. The technique relies on the fact that the thermal response of the sample is fast enough to establish a temperature difference when the heater is excited with a signal of few Hertz. The voltage is applied to the heater on the hot side with alternating sign, avoiding voltage pick-up effects in the thermopower detection. The excitation waveform is therefore no sinusoidal [5]. At the same time, the dummy heater on the cold finger is excited with the same signal but 90 degrees shifted [5]. This procedure prevents the sample from cooling down too much during the period that the hot heater is off. However the 90-degree shifted voltage applied to the dummy heater contributes only for minor corrections to the thermopower. Since the thermometers could not follow a few Hertz signal, the temperature was measured in DC conditions before and after each AC magnetic field sweep.

The thermopower voltage measured in AC is always smaller than the one measured in DC. This reduction is due to the detection of only the fundamental Fourier component in the applied excitation, the frequency excitation which cannot be completely followed by the temperature gradient, and the rms-value measured by the Lock-in, which is $\sqrt{2}$ lower than the real signal. The conversion factor between AC and the absolute thermopower has been experimentally determined as a function of temperature by comparing AC and DC TEP measurements at zero field. The factor has almost no dependence on temperature and in our case is 2.8 at 4Hz.

2.4 Resistivity measurements

During the thermoelectric power measurements (Chapter 3 and 5), the resistivity was always measured with the four terminal technique. The measurements as a function of temperature were performed in DC using a battery-powered current source and the Keithley K182 nanovoltmeter. The current was set to 10nA for the sample in the metallic state and 2nA in the insulating state, to prevent heating. The base temperature was changed by using the dummy heater on the cold finger.

In the resistivity measurements described in Chapter 4, the experiments were carried out both in a Bitter magnet ($B \leq 20\text{T}$) using a home-built plastic dilution refrigerator and in a superconducting magnet ($B \leq 8\text{T}$) using a commercial

refrigerator. The sample was mounted on a brass support in thermal contact with the cold finger. The measurements were performed with a standard Lock-in technique with a frequency of 12Hz and a current of 2nA. Preliminary checks verified that the carriers were not heated by the applied excitation current. In the experiment described in Chapter 4, the carrier density changed with different cooling procedures. With this method the density can be changed in a non-controlled way and measured at low temperatures, in our case we could perform the experiment at two different carrier densities: $p_h=1.8\cdot 10^{15}\text{m}^{-2}$ and $2.4\cdot 10^{15}\text{m}^{-2}$.

2.5 References

- [1] P.T.Coleridge, R.L.Williams, Y.Feng, and P.Zawadzki, Phys. Rev. B **56**, R12764 (1997).
- [2] R.Fletcher, Semicond.Sci.Technol. **14**, R1-R15 (1999).
- [3] R.Fletcher, V.M.Pudalov, Y.Feng, M.Tsaousidou and P.N.Butcher, Phys. Rev. B **56**, 12422 (1997).
- [4] R.Fletcher, V.M.Pudalov, A.D.B.Radcliffe and C.Possanzini, Semicond. Sci. Technol. **16**, 386 (2001).
- [5] B.Tieke, *Thermoelectric Power of Two- and Three-Dimensional Metallic Semiconductors in High Magnetic Fields*, Ph.D. Thesis, University of Nijmegen, 1997.

Chapter 3

Thermopower of a p-type Si/Si_{1-x}Ge_x heterostructure

Thermopower measurements in zero and low magnetic fields for a p-type Si/SiGe heterostructure show that both the longitudinal and transverse components of the diffusion thermopower are well described by the Mott approach. The zero field measurements deviate from the expected linear temperature dependence for a degenerate system, probably as a result of the nearby metal-insulator transition. Phonon drag does not show the expected approximate T^6 dependence at low temperatures appropriate for screened, hole-phonon, deformation-potential scattering, but instead an approximate T^4 dependence is observed. The experimental data on drag are in good agreement with numerical calculations by assuming either hole-phonon scattering mediated by an unscreened deformation-potential interaction, or by assuming a screened piezoelectric plus screened deformation-potential coupling. Similar conclusions have been previously drawn from the energy loss rates experiments in SiGe hole systems.

3.1 Introduction

In general the thermopower of two-dimensional (2D) systems is now well understood in terms of phonon drag and diffusion of the carriers. When the system is degenerate, the diffusion component, S^d , has a simple linear temperature dependence at low temperatures, which partly reflects the entropy of the 2D gas, and partly is related to the elastic scattering mechanisms of the electrons [1].

Part of this work is published in Phys. Rev. B, 2004 (in press).

The phonon drag component, S^g , has a stronger temperature dependence with a different power law for different mechanism of electron-phonon (e-p) scattering. Systems with screened, piezoelectric e-p scattering of the carriers, e.g. GaAs based structures, have been shown to give a T^4 dependence of drag [2, 3], whereas those with only screened deformation-potential (DP) scattering show a T^6 dependence [4]. In the former case, S^s dominates S^d down to temperatures of the order of 0.3K. However, in the latter case S^s becomes small as the temperature is reduced below about 1K and this allows the examination of the diffusion component. In previous work [4] the only system without piezoelectric scattering for which the thermopower has been studied in detail is the electron inversion layer in Si-MOSFETs, which did show the expected behavior of both diffusion and drag.

SiGe hole or electron systems are expected to behave in a similar fashion to Si-MOSFETs because of the absence of piezoelectricity. However, there are no data on electron systems, and because previous thermopower work on a hole system was performed at relatively high temperatures (1.5-15K) where it is difficult to distinguish the various hole-phonons (h-p) scattering mechanisms, it was inconclusive [5].

The e-p (or h-p) interaction can also be probed by carrier energy loss. The energy loss rate depends on the carrier-phonon *energy* relaxation time, whereas phonon drag thermopower reflects the carrier-phonon *momentum* relaxation time [6, 7]. Thus the two types of measurement provide different but complementary ways to investigate carrier-phonon scattering. Previous measurements on the energy loss rates in SiGe electron systems agree with expectations and are explained theoretically assuming screened DP e-p coupling [8]. However, similar work on SiGe hole systems gave loss rates inconsistent with this mechanism. Early measurements [9] were analyzed in terms of a screened, piezoelectric h-p coupling, but more recent work [10, 11, 12] leaned towards unscreened DP coupling (these two mechanisms are difficult to distinguish because both give the same power law dependence on T at low temperatures), with a small unscreened piezoelectric term contributing at temperatures $T < 0.5K$. The present thermopower measurements throw new light on this problem. The measured S^g is consistent with results found from energy loss measurements, confirming the same anomalous scattering mechanism.

The diffusion thermopower has a (semi-classical) magnetic-field dependence arising from the Lorentz force on the electrons [1], while phonon drag, like resistivity, has essentially no field dependence [6]. When the spacing of the Landau levels becomes comparable to the level broadening, both drag and diffusion components show an oscillatory behavior. Previous experimental work [13] on a system where drag was completely dominant showed that drag oscillations are in phase with oscillations in the electrical resistivity, but there is, as yet, no quantitative theory. Because most previous work has been done on piezoelectrically active systems where drag has been dominant down to low temperatures, diffusion has been difficult to probe. However, it has been predicted [1, 14] that at relatively low fields diffusion oscillations should be independent of the electron scattering mechanisms

and should exhibit a $\pi/2$ phase shift compared to drag or resistivity oscillations. This effect has only been clearly seen in the 2D electron inversion [15] layer in Si-MOSFETs which exhibits only DP coupling. Despite the presence of drag in the investigated hole system, at sufficiently low temperatures it becomes small enough to investigate the behavior of diffusion in detail and the predicted phase difference is clearly seen.

The Si-SiGe is also known to undergo an apparent metal-insulator transition (MIT) at low densities in zero magnetic field. Although this latter transition is not observable in the present work, our sample is relatively close to the transition on the metallic side and showed a strong temperature dependence of the resistivity as a result [9]. Fig. (3.1) shows the temperature dependence of the zero field resistivity at two different densities ($p_h=1.9 \times 10^{15} \text{m}^{-2}$ and $2.7 \times 10^{15} \text{m}^{-2}$) for $T < 4\text{K}$. The measurements show a strong increase of the resistivity with temperature, which is more pronounced at lower densities.

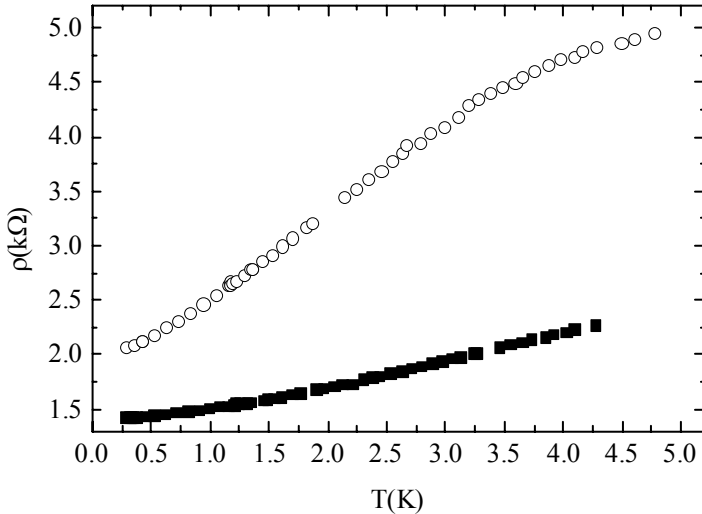


Figure 3.1. The resistivity at zero magnetic field of the p-type Si/SiGe shows a strong dependence of temperature at lower densities. The full square indicates the resistivity for a density $p_h=2.7 \times 10^{15} \text{m}^{-2}$ and the open circles for a lower density $p_h=1.9 \times 10^{15} \text{m}^{-2}$.

In Ref. [9], where the zero field resistivity has been measured over a wider temperature range and at six different densities, the appearance of an insulating state is observed for densities lower than $1.0 \times 10^{15} \text{m}^{-2}$. The resistivity behavior in the metallic state is the result of the competition between the insulating behavior, which develops at lower densities, and the strong conductivity increase that dominates at lower temperatures [9]. It is interesting to determine whether this system shows any other unusual behavior of the zero or low magnetic field thermopower which deviates from the expected linear dependence on temperature.

3.2 Theory

Thermopower of a hole system differs from the one in an electron system mainly because of the positive sign of the electric charge. In the limit of weak coupling between carriers and phonons, the contributions due to diffusion and drag are additive and the total thermopower S is given by $S = S^d + S^g$.

The diffusion component S^d of thermopower for degenerate 2DHGs is given by Mott's expression (Chapter 1)

$$S^d = \frac{\pi^2 k_B T}{3|e|E_F} (1+p) \quad (1.5)$$

The first term in Eq.(1.5) is the entropy per unit of charge of the 2DHG and the second term reflects the scattering mechanisms.

The phonon-drag component S^g of thermopower is given by equation (1.7) (Chapter 1). By assuming Λ independent of T , it can be shown (see Chapter 1) that $S^g \propto T^6$ for screened DP coupling [4] and $S^g \propto T^4$ for screened piezoelectric coupling [2,3]. At low temperatures the screening dielectric function is approximated by the expression $\varepsilon(q) \approx Q_s/q \propto Q_s/T$. Consequently (Eq.(1.7)), when screening effects are neglected (e.g., $\varepsilon(q) = 1$), the temperature dependence of S^g is T^4 for DP coupling and T^2 for piezoelectric coupling.

In a magnetic field, the thermoelectric power is given by a non-oscillatory background (Eqs (1.9) in Chapter 1):

$$\bar{S}_{xx}^d = \frac{L_0 e T}{E_F} \left(1 + \frac{p}{1 + \beta^2} \right) \quad (1.9a)$$

$$\bar{S}_{yx}^d = \frac{L_0 e T}{E_F} \left(\frac{p\beta}{1 + \beta^2} \right) \quad (1.9b)$$

When the Landau level separation $\hbar\omega_c$ exceeds the level broadening $\sim \hbar/\tau_q$, i.e. at $\omega_c\tau_q \sim 1$, (where ω_c is the cyclotron frequency and τ_q is the quantum lifetime) an oscillatory component appears. When the Landau levels are not completely resolved and localized states play no role, the oscillations in S_{ij}^d , say \bar{S}_{ij}^d , can be evaluated using relations based on the Mott approach [1]. The result is given by equations (1.10) (see Chapter 1):

$$\bar{S}_{xx}^d = \frac{\alpha}{1 + \beta^2} \left(\frac{\tilde{\rho}_{xx}}{\bar{\rho}_{xx}} + \beta^2 \frac{\tilde{\rho}_{xy}}{\bar{\rho}_{xy}} \right) \quad (1.10a)$$

$$\bar{S}_{yx}^d = \frac{\alpha\beta}{1 + \beta^2} \left(\frac{\tilde{\rho}_{xx}}{\bar{\rho}_{xx}} + \frac{\tilde{\rho}_{xy}}{\bar{\rho}_{xy}} \right) \quad (1.10b)$$

where $\alpha = i(\pi k_B e)(D'(rX)/D(rX))$ with $D(X)$ being the thermal damping factor for resistivity oscillations ($D(X) = X/\sinh X$ with $X = 2\pi^2 k_B T/\hbar\omega_c$), and $D'(X) = dD(X)/dX$ is the thermal damping factor for diffusion thermopower oscillations. As in Chapter 1, we use the tilde to denote an oscillatory component and a bar to denote the smooth background in all quantities.

Notice that when $\beta = \omega_c\tau_l \geq 1$, the thermopower oscillations are reduced in amplitude by the factor $(1 + \beta^2)$ that appears in the denominators of Eqs. (1.10a) and (1.10b). Because the oscillations only begin to appear when $\omega_c\tau_q \sim 1$, and given that $\tau_l \geq \tau_q$, then the approximate equivalence of τ_l and τ_q that is found in the present system [16] is the most favorable case for producing the largest possible oscillations. This is in contrast to systems where low-angle electron scattering dominates and $\tau_l \gg \tau_q$, e.g. most GaAs heterostructures.

As explained in Chapter 1, there are no theoretical results for the quantum oscillations in S^g in low fields, but experiments where drag was dominant¹³ showed that the oscillations in S_{xx}^g are in phase with those in ρ_{xx} . Thus, in principle it is possible to distinguish which mechanism is responsible for the thermopower oscillations from any phase difference between them and the resistivity oscillations; a phase difference of $\pi/2$ implies diffusion thermopower, and no phase difference means that phonon drag oscillations are dominant. However, at high fields both the diffusion and drag oscillations are in phase with the resistivity oscillations and an unambiguous identification is not possible by this method.

3.3 Experimental technique

As explained in Chapter 2, measurements at two different densities ($p_h = 1.9 \times 10^{15} \text{m}^{-2}$ and $2.7 \times 10^{15} \text{m}^{-2}$) could be performed by applying a substrate bias, but unless specifically noted otherwise, we will present data only for the higher density sample. At 1K, the mobilities were $1.3 \text{m}^2/\text{Vs}$ and $1.5 \text{m}^2/\text{Vs}$ respectively and had a strong temperature dependence [16]. Using an effective mass [16] of $0.3m_e$, the Fermi temperatures are estimated to be 18K and 25K for the two samples. Under normal conditions we would not have anticipated such a strong mobility variation at such low temperatures. This feature has also been observed previously in Si-MOSFETs [17] and in both cases has been ascribed to the effects of a MIT at a somewhat lower density of about $\sim 1.0 \times 10^{15} \text{m}^{-2}$.

Measurements were made in high vacuum in a ^3He cryostat which covered the range 0.3-4.2K. Zero field data were obtained using DC techniques. With thermopower it was necessary to eliminate small temperature-dependent offset voltages in the signal [18]. This was done by measuring the voltage across the sample with and without establishing a temperature gradient, keeping the average temperature of the sample constant. The temperature difference across the sample thermometers varied from about 15mK at 0.3K to 150mK at 4K. The source and drain contacts, separated by 2.8mm, were used for this purpose. For the measurements in magnetic field, a standard ac lock-in technique was used [2] with a detection frequency of 4Hz. The ac signal sensitivity under these conditions was calibrated by using the dc thermopower at zero field. Sweep data were made for both $\pm B$ and the appropriate combinations of data were used to calculate the required coefficients. There was relatively little admixture of the coefficients.

In order to check the thermometry, the thermal conductivity λ of the *n*-type Si substrate was measured as a function of temperature (Fig. (3.2)). It was found that $\lambda = 1.8T^{2.75 \pm 0.02} \text{ W/mK}$ provided an excellent fit over the whole temperature range, 0.27-4.2K, as shown in Fig. (3.2). The deviation of the exponent from the expected T^3 result for boundary scattering may be due to (weak) phonon scattering from impurities. Using the low temperature theoretical limit of λ [2], we estimate the mean free path of the phonons, Λ , in the substrate to be $\sim 1.6 \text{mm}$ at 1K, assuming longitudinal and transverse sound velocities of $v_l = 8861 \text{m/s}$ and $v_t = 5331 \text{m/s}$, respectively.

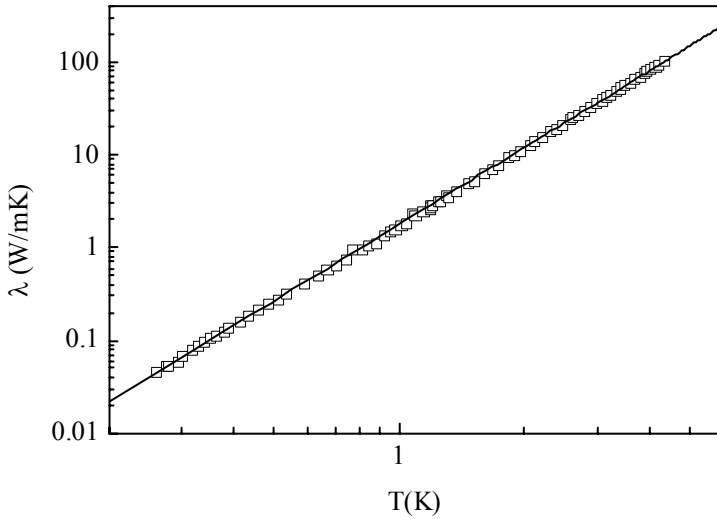


Figure 3.2. Thermal conductivity of the Si substrate as a function of temperature. The line represents the fit of the data with the temperature dependence $T^{2.75}$.

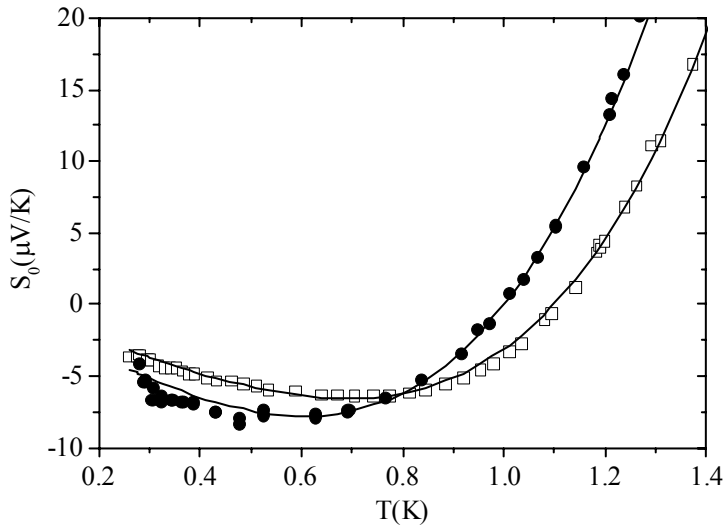


Figure 3.3: The circles are the measured thermopower at $p_h=2.7 \cdot 10^{15} \text{ m}^{-2}$ (open square) and $p_h=1.0 \cdot 10^{15} \text{ m}^{-2}$ (solid circles). The lines correspond to the fit of the TEP for each density according with $S=aT+bT^d$ (see text).

3.4 Results and discussion

3.4.1 Thermopower data at zero field

Thermoelectric power measurements at zero field were performed at two carrier densities: $p_h=1.9\cdot 10^{15}\text{m}^{-2}$ and $p_h=2.7\cdot 10^{15}\text{m}^{-2}$ and they are reported in Fig. (3.3).

Below 1K the thermopower is found to be negative and rapidly increases at higher temperatures. This rapid increase is caused by the strong temperature dependence of the phonon drag contribution. The negative thermopower is explained by the dominating influence of the diffusion contribution, which is negative when the scattering term in Eq. (1.4), proportional to p , becomes larger than the value of the entropy term ($p < -1$ in Eq. (1.4)). The thermopower S was fitted using an expression of the form $S = aT + bT^n$ at low temperatures, with a , b and n parameters to be found. The value of n was found to depend on the temperature range of fit, but it was always near 4 even with the upper temperature limit as high as 1.5K. In addition, in both samples the coefficient a has a relatively small spread of values. The best estimates of the coefficient a for the higher and lower density samples are $a = -13.0\mu\text{V}/\text{K}^2$ and $-18.5\mu\text{V}/\text{K}^2$, respectively. Using Eq. (1.4) and the values of E_F quoted in Section 3.3, we find the scattering parameter $p = -2.15 \pm 0.10$ in both samples. The value of p depends on the electron-impurity scattering mechanisms (e.g., impurity and interface roughness scattering) and has been calculated for GaAs heterostructures and Si-MOSFETs [19], but not yet for SiGe heterostructures. The dependence on p of zero field thermopower (equation (1.4)) arises from the power law temperature dependence of the hole energy relaxation time $\tau_r \approx T^p$. This commonly assumed dependence is usually adequate for a description of transport phenomena. However, it is very well possible that near the MIT the hole energy relaxation time has a different dependence on temperature. Measurements in magnetic field show that p is dependent on temperature (see next Paragraph) and the consequences on the temperature behavior of S^g and S^d are analyzed in Paragraph 3.4.3, where also the possible mechanisms associated to the T^d behavior of S^g are explained.

3.4.2 Thermopower in a magnetic field

Fig. (3.4) and (3.5) show the longitudinal and Hall resistivities, ρ_{xx} and ρ_{yx} , as a function of magnetic field at four different temperatures.

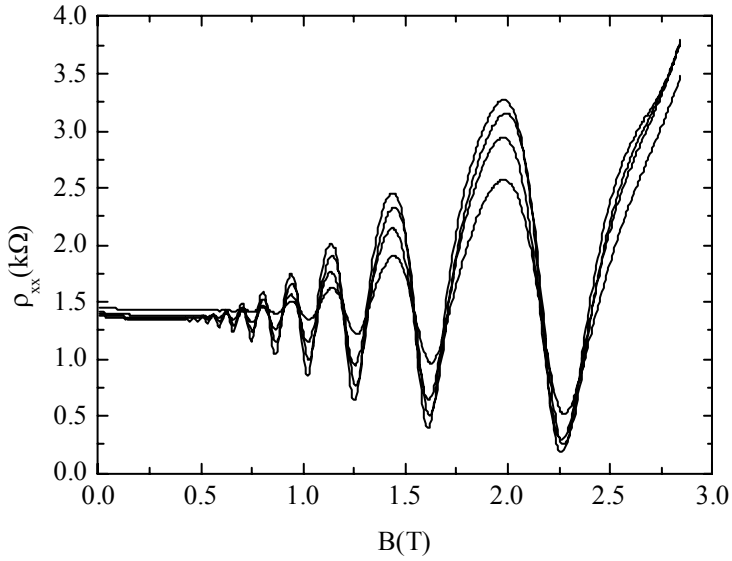


Figure 3.4: Measured longitudinal resistivity at four different temperatures: 0.4K, 0.5K, 0.7K, and 0.9K.

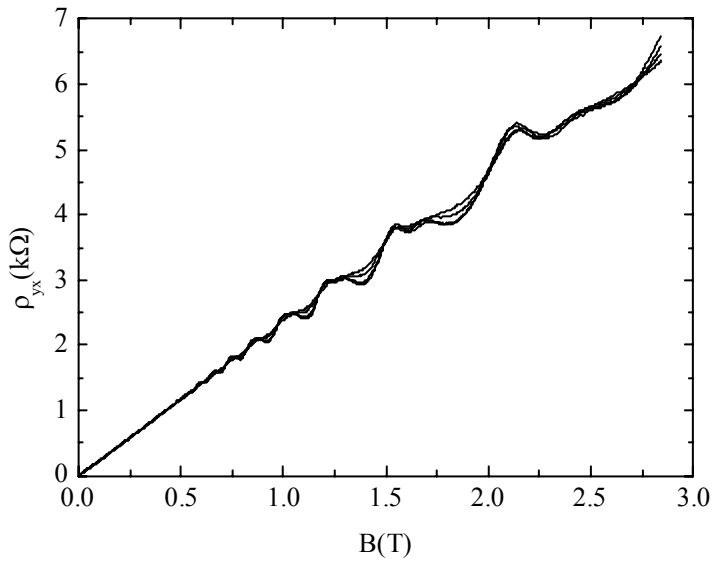


Figure 3.5: Measured Hall resistivity at four different temperatures: 0.4K, 0.5K, 0.7K, and 0.9K.

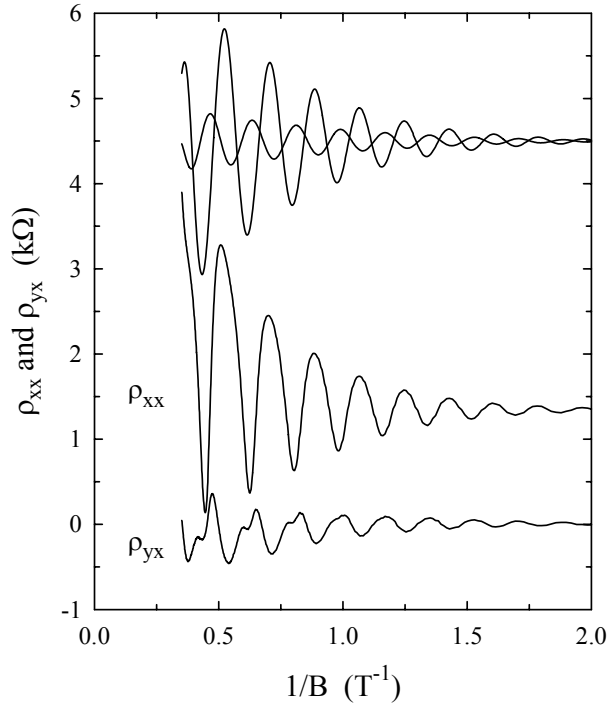


Figure 3.6: Experimental data on ρ_{xx} and ρ_{yx} at 0.41K. The bottom curve is $\bar{\rho}_{yx}$, obtained by subtracting the part linear in B from the measured ρ_{yx} . The next lowest curve is the measured ρ_{xx} , including the non-oscillatory background. The two superimposed curves at the top are the fundamental harmonic components of the two bottom curves, the larger amplitude curve being $\bar{\rho}_{xx}$ and the smaller amplitude curve being $\bar{\rho}_{yx}$. These two curves are offset vertically by $+4.5\text{k}\Omega$. Note the upper two curves are in antiphase at low fields, but there is $\pi/2$ difference at high fields.

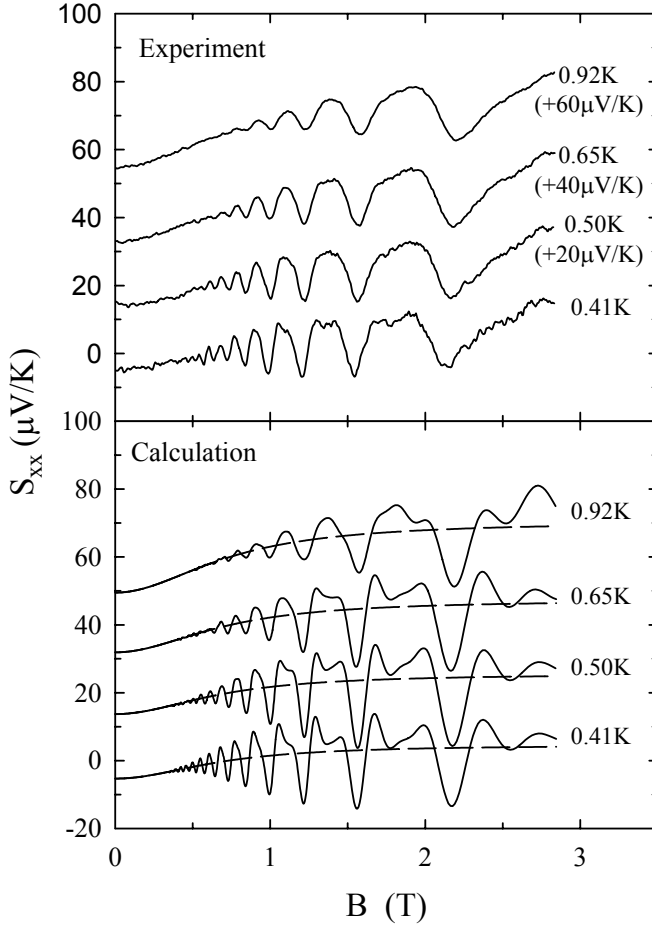


Figure 3.7: Measured longitudinal thermopower, S_{xx} , (upper panel) and calculated diffusion component, S_{xx}^d , (lower panel) as a function of magnetic field at various temperatures. The dashed lines in the lower panel are the semi-classical components, \tilde{S}_{xx}^d . For clarity all but the lowest temperature curves in both panels have been shifted by a vertical offset (as given in brackets in the upper panel).

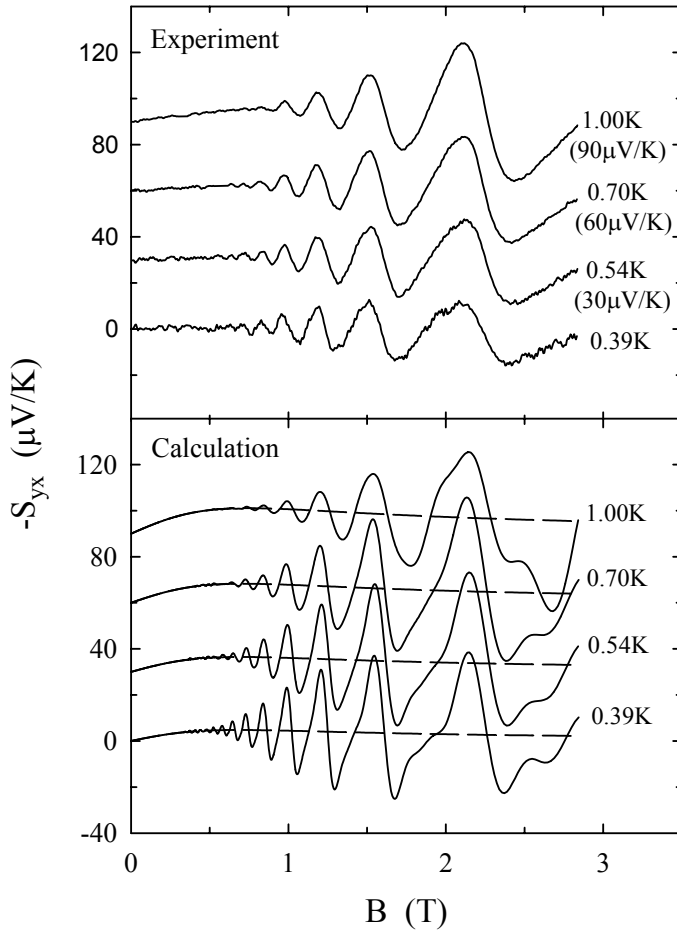


Figure 3.8: Measured Nernst-Ettingshausen coefficient, S_{yx} , (upper panel) and calculated diffusion component, S_{yx}^d , (lower panel) as a function of magnetic field at various temperatures. The dashed lines in the lower panel are the semi-classical components, \tilde{S}_{yx}^d . For clarity all but the lowest temperature curves in both panels have been shifted by a vertical offset (as given in brackets in the upper panel).

Both ρ_{xx} and ρ_{yx} are needed in the analysis of \tilde{S}_{ij}^d (Equations (1.10)), shown in Fig. (3.6). If we examine only the oscillatory components at the fundamental frequency, also shown in Fig. (3.6), the oscillations in ρ_{yx} are found to be accurately π out of phase with those in ρ_{xx} at low fields, but there is a gradual shift in phase above about 1T such that by 3T there is a phase difference approaching $\pi/2$. This behavior has been observed previously in GaAs heterostructures and the phase shift has been ascribed to the appearance of localized states between the Landau levels [20], which primarily affects ρ_{yx} .

The measured longitudinal and transverse thermopower, S_{xx} and S_{yx} , are shown in Figs. (3.7) and (3.8) (upper panels). As we anticipated, the oscillations in S_{ij} at lower fields, which we identify with \tilde{S}_{ij}^d (see below), are superimposed on a changing non-oscillatory background due to $\tilde{S}_{ij}^{d_0}$, implying $\tau_t \sim \tau_q$. Notice that \tilde{S}_{xx}^d changes sign from negative to positive as the field increases showing that at this temperature $p < -1$ in Eq. (1.9a). Close examination of the data also shows that the oscillations in S_{xx} and S_{yx} are in phase with each other, and that both are about $\pi/2$ out of phase with the oscillations in ρ_{xx} , particularly at lower fields. These features are in agreement with Eqs. (1.10a) and (1.10b). The $\pi/2$ phase difference between $\tilde{\rho}_{xx}$ and \tilde{S}_{ij} is particularly clear when one examines only the fundamental oscillatory components of the measured data.

Classical results [6] predict $\bar{S}_{yx}^g = 0$ and \bar{S}_{xx}^g to be independent of field. Thus, in principle, one needs only calculate $\bar{S}_{ij}^d(B)$, using Eqs. (1.9a) and (1.9b) to obtain the semi-classical backgrounds. Previous experience with a similar calculation for Si-MOSFETs [15] has shown that the best value of μ_t to describe \bar{S}_{ij} is not necessarily the same as for the resistivity and here was left as a free parameter. Therefore each data set on \bar{S}_{xx} was fitted to Eq. (1.9a) but with an additive constant to take into account $S^g(T)$. The relevant equation can be written $S = c + d/[1 + (\mu_t B)^2]$ where μ_t , c and d ($d = pL_0 eT/E_F$ where $L_0 = \pi k_B^2/3e^2$) are free parameters with $c + d$ being just the zero field value of S_{xx} .

The results on μ_t from this procedure are shown in Fig. (3.9), and those for p are shown in Fig. (3.10). They are both temperature dependent. Also shown in Fig. (3.9) are data on μ_t taken from the zero-field mobility and these are also temperature dependent. As mentioned above, this latter dependence arises from the MIT in this system at somewhat lower hole density [16] which is known to have a significant effect on the temperature dependence of the resistance (and hence mobility) on the metallic side of the transition to rather high densities. Within the experimental error it is possible that the two sets of data on μ_t coincide as $T \rightarrow 0$, though the relative difference at higher temperatures is becoming larger than we would expect for experimental error. A similar behavior has been previously observed in a Si-MOSFET [15], though in that case the zero field mobility was essentially constant because the sample was well away from the MIT.

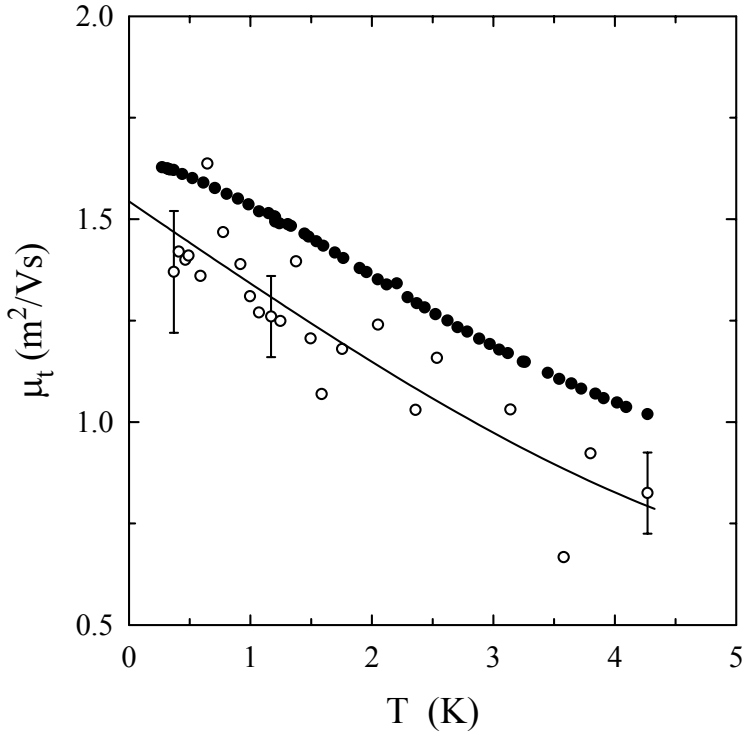


Figure 3.9: The open circles are the transport mobility, μ_t , obtained from the magnetic field dependence of the classical background, \overline{S}_{xx} , as a function of temperature. The closed symbols are also μ_t but obtained from the resistivity at $B = 0$.

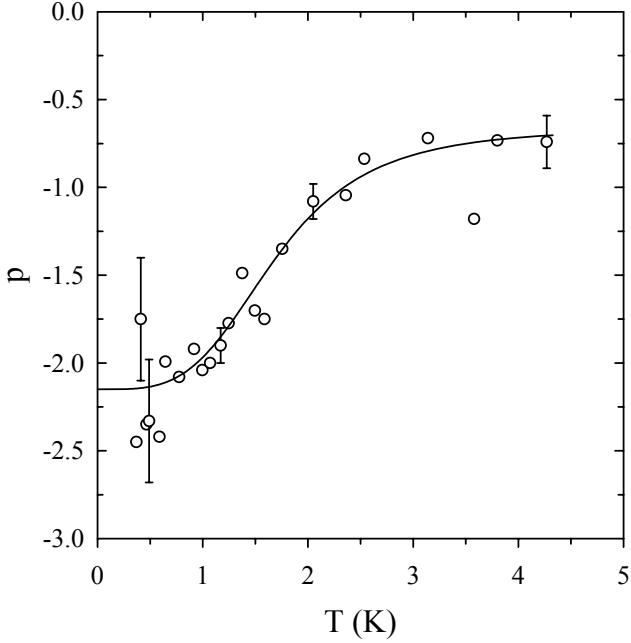


Figure 3.10: The circles are the measured coefficient $p = (\partial \ln \tau / \partial \ln E)_{EF}$ obtained as a fit parameter of the monotonic background of S_{xx} as a function of temperature. The solid line is a phenomenological fit to the experimental data as discussed in the text.

There is no theory for \tilde{S}_{xx}^g , but since S_{xx}^g is small at low temperatures and S_{yx}^g should always be zero, \tilde{S}_{ij}^g is expected to be small. We ignore it in the first instance and compare the measured oscillatory data only with calculations of \tilde{S}_{ij}^d .

The calculation of \tilde{S}_{ij}^d using Eqs. (1.10a) and (1.10b) was done as follows. Data on ρ_{ij} were available at nominally the same temperatures as S_{ij} . After removing most of the non-oscillatory backgrounds, ρ_{xx} and ρ_{yx} were Fourier transformed and the frequency spectra separated into sections, each containing a single harmonic component (retaining 3 harmonics at lower temperatures and 2 at higher temperatures). Taking the inverse Fourier transforms of each section then produced waveforms for the individual harmonics. Using these waveforms and Eqs. (1.10a)

and (1.10b) the harmonic components of \tilde{S}_{ij}^d were calculated. The phase difference of $\pi/2$ was introduced by shifting the value of B at each point by the appropriate amount; therefore $D(X)$ and $D'(X)$ were calculated at somewhat different fields, and in fact usually at somewhat different temperatures because the experimental ρ_{ij} and S_{ij} were usually not at exactly the same temperature. Finally the harmonics were summed and added to \tilde{S}_{ij}^d . The results are shown in Fig. (3.7) and (3.8) (lower panels).

The overall agreement of experiment data on S_{xx} and the calculations for S_{xx}^d is very good, and somewhat less so for S_{yx} and S_{yx}^d . Perhaps not surprisingly the calculated \tilde{S}_{xx}^d accurately fit the experimental data. We recall that fits to \tilde{S}_{xx} were used to evaluate p and μ_t used here (Figs. (3.9), (3.10)), but if we use the values taken from the zero field S^d and resistivity, the calculated \tilde{S}_{ij}^d are not noticeably different. The same features are also observed for the available data on the low density sample (not shown here). The calculations for \tilde{S}_{yx}^d are less convincing. With Si-MOSFETs a large, temperature-dependent, anomalous component was observed for \tilde{S}_{yx} , which does not seem present here, though the magnitude of \tilde{S}_{yx} is not well reproduced by the present calculations.

At low temperatures the phases of the calculated oscillations in both components are in excellent agreement with the experimental oscillations. The phase difference of $\pi/2$ between $\tilde{\rho}_{xx}$ and \tilde{S}_{ij}^d is maintained reasonably accurately over the whole field range, and is particularly clear when one plots only the fundamental oscillatory components of the measured data (Fig. (3.11)). Therefore both \tilde{S}_{xx}^d and \tilde{S}_{yx}^d must be almost purely diffusive at these low temperatures, which justifies *a posteriori* the neglect of \tilde{S}_{ij}^g .

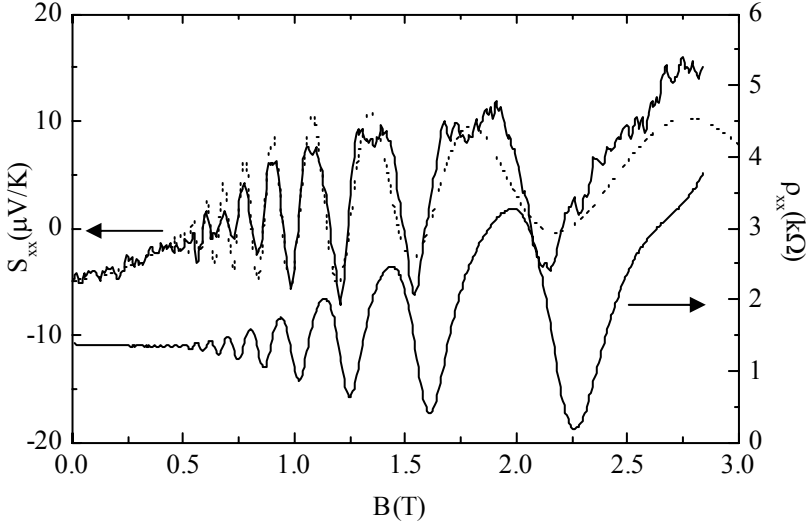


Figure 3.11: Calculated fundamental harmonic component of thermopower is plotted on the top with dashed line superimposed to the measured thermopower (solid line, top curve). The bottom curve is the resistivity at the same temperature (0.4K). The phase difference of $\pi/2$ predicted by Mott theory is maintained over the whole field range.

In both components, the calculations predict too much harmonic content at higher fields and lower temperatures, which might be due to localized states beginning to appear between the Landau levels which would invalidate the model. Such effects are not included in the model and the explanation is consistent with the phase shift noticed in the oscillations in ρ_{yx} at higher fields. The magnitudes of the calculated \tilde{S}_{xx} are in reasonable agreement with the observations up till 3T where the longitudinal resistivity oscillations have an amplitude close to the background value. On the other hand, the calculated magnitudes for \tilde{S}_{yx} tend to be too large, by about a factor of 2 at lower temperatures and higher fields, probably reflecting the appearance of localized states again.

3.4.3 Explanation of the temperature behavior of thermopower at zero field

Measurements in magnetic fields show that in Equation (1.5) the coefficient p is not a constant (as assumed in paragraph 3.2, Fig. (3.3)), but it is temperature dependent above 0.7K (Fig. (3.10)). If p is constant, the diffusion thermopower is expected to be linear (Eq.(1.4)) and the deviation of thermopower from linearity at higher temperatures is therefore mainly due to phonon drag thermopower S^g . In the present situation, the temperature dependence of p has to be taken into account to determine the exact temperature dependence of phonon drag, which is unknown. In fact, at temperatures between 0.7K and 1.5K diffusion and phonon drag are comparable and only a more detailed analysis of the data allows a separation of the two contributions.

The data in Fig. (3.10) show that p becomes independent of T below 0.7K and therefore $S^d \propto T$ in this limit, as assumed in Paragraph 3.2. Lacking a theory of p as a function of T for SiGe heterostructures, we proceeded by fitting to the values of p in Fig.(3.10) the phenomenological expression

$$p = p_0 + \frac{p_1}{(1 + CT^m)} \quad (3.8)$$

with $p_0 + p_1 = -2.15$ at vanishing T as determined previously (Paragraph 3.2) and p_1 , C and m free parameters. The fit with $C = 0.139\text{K}^{-m}$, $m = 3.75$ and $p_1 = -0.66$ (shown in Fig. (3.10)), gave a good description. Using this expression, S^d was calculated from Eq. (1.4) and is plotted in Fig. (3.12). Fig. (3.12) shows that the deviations of S from linearity are actually not caused by the non-linearity of S^d but are in fact due to S^g . By subtracting the calculated values of S^d from the measured S , we obtained S^g over the full temperature range as shown in Fig. (3.13). The observed dependence of S^g is approximately T^4 .

The drag component of both samples from Eq. (1.7) and the standard material parameters for Si were calculated [21]. By assuming only screened DP h-p coupling we find $S^g \propto T^{6.3}$ (this is the nominal T^6 dependence noted in paragraph 3.2) for $0.25 < T < 1.5$ K. The results with $\mathcal{E} = 4.0\text{eV}$ are shown in Figs. (3.12) and (3.13). The calculated S^g is approximately correct at 4.2K, but below 0.5K they are at least two orders of magnitude too low to explain the experimental values. This behavior deviates from that exhibited by a 2D electron gas in a Si-MOSFET where an approximate T^6 dependence was seen for S^g and the calculated magnitude was in good agreement with experiment [4].

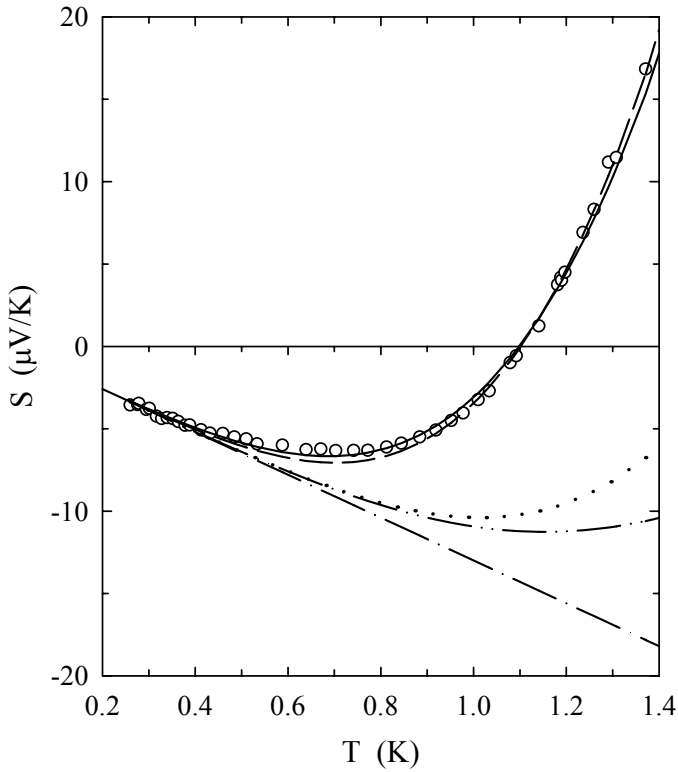


Figure 3.12: The circles are the measured thermopower. The symbol -- gives S^d assuming p is constant at -2.21; -.- gives S^d with p taken from the smooth curve in Figure (3.10). The other curves are $S^d + S^g$ with S^d calculated using the smooth curve in Fig. (3.10) and S^g calculated as follows: unscreened DP coupling; screened DP coupling; ----- screened piezoelectric plus a screened DP coupling.

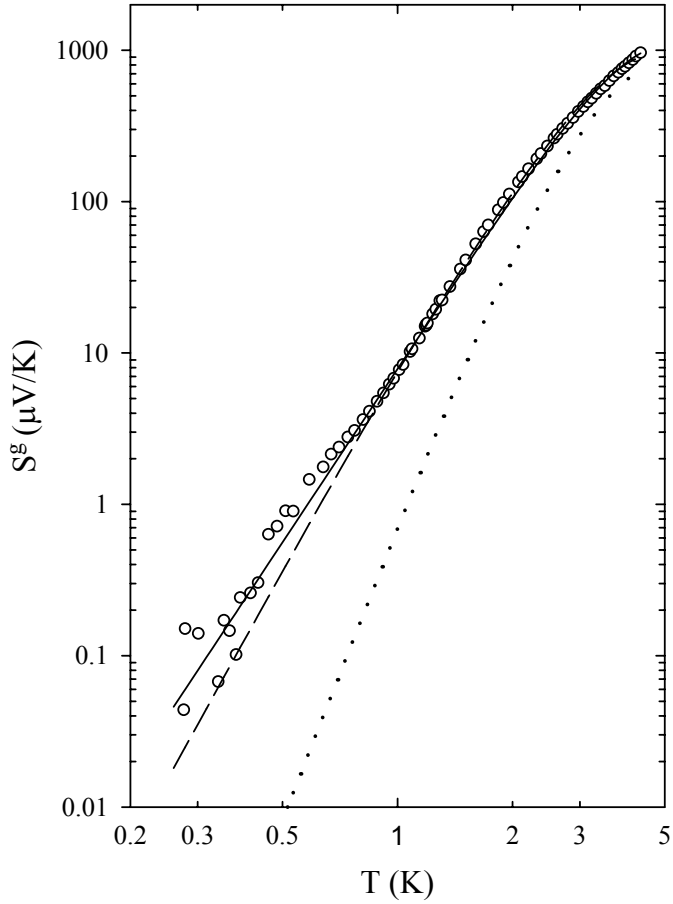


Figure 3.13: The circles symbols are the phonon drag thermopower. The various curves are calculations of S^p : unscreened DP coupling; screened DP coupling; ---- screened piezoelectric plus a screened DP coupling.

There are two mechanisms that would result in $S^g \propto T^4$ (approximately) both of which have previously been invoked to explain the anomalous behavior of the energy-loss rate [9,11,12].

Early data by Xie *et al.* [9] invoked a screened piezoelectric contribution, perhaps arising from the partial ordering of the SiGe alloy (see Ref. 10 for a discussion of this possibility), while others have suggested that the screening of the DP is ineffective in this system [11, 12] which leads to a change in temperature dependence from T^6 to T^4 for S^g (Paragraph 3.2). We examine both of these possibilities in detail.

Using an unscreened DP interaction, with coupling constant of $\mathcal{E}_{DP} = 2.7$ eV chosen to give the best agreement with experiment, detailed calculations of S^g have been made over the whole temperature range. The results are shown in Figs. (3.12) and (3.13) for comparison with experiment. The agreement is excellent over the whole temperature range.

Ansaripour *et al.* [11] have found good agreement with experimental energy-loss rate data using an unscreened DP interaction with a coupling constant of $\mathcal{E}_{DP}=3.0$ eV. Leturcq *et al.*¹² have reported that their energy-loss rate data are best represented by the same mechanism with $\mathcal{E}_{DP} = 2.8$ eV, together with a small unscreened piezoelectric contribution, this latter appearing only below about 0.5 K. In our case this would correspond to a small term $S^g \propto T^2$ at low temperatures. We do not see such an extra term in the present data, though our precision is relatively low below 0.5 K because of the dominance of S^d in this region. Clearly the agreement between phonon-drag and energy-loss rate results is excellent.

We have also carried out theoretical calculations using a screened piezoelectric h-p coupling with a magnitude varied to give a reasonable fit to the low temperature data. The value chosen was $h_{14} = 0.6 \times 10^9$ V/m which is 50% the value of that for GaAs. We have also included a screened DP h-p interaction (with $\mathcal{E}_{DP} = 4.0$ eV) so that the high temperature data could also be reproduced. Again Figs. (3.12) and (3.13) show the results. In general this model also provides very good agreement with the experiments, though perhaps not quite as good as the unscreened DP at low temperatures.

Neither of the above theoretical models is easily understood from a physical point of view. In the latter, the values used for the piezoelectric coupling constant, h_{14} is uncomfortably high [12]. In the former, it is not at all clear why screening should be so ineffective in the SiGe hole system. It is interesting to compare this with Si-MOSFETs. Previous experimental work on Si-MOSFETs at low temperatures has been somewhat contradictory. Phonon drag is consistent with screened DP scattering and no observable piezoelectric component. Energy-relaxation measurements by Fletcher *et al.* [4, 22] were inconsistent with a screened DP below ~ 1 K, the observed loss rate being considerably larger than predicted. More recent energy-loss rate data [23] have been analyzed by the combination of unscreened DP and unscreened piezoelectric scattering, but the coupling constants were not evaluated. Because phonon-drag thermopower and energy-loss rate measure different relaxation rates,

momentum in the former case and energy in the latter, the observed discrepancy between the well-behaved drag and the anomalous energy-loss rate in Si-MOSFETs could imply that they are caused by different physical mechanisms. For example, energy-loss rates involving localized excitations would not necessarily be visible in phonon drag. With the SiGe system the two relaxation rates are very consistent, indicating that the same mechanism is responsible for both and is connected with scattering by delocalized excitations, presumably phonons, in both cases.

In a more phenomenological approach, S^g can be expressed in terms of the momentum relaxation time of the carriers, which is directly related to the hole mobility due to phonon scattering, μ_{hp} by [6]

$$S_i^g = \frac{\Lambda_i v_i}{\mu_{hp,i} T} \quad (3.9)$$

where v is the sound velocity and the subscript i refers to phonon polarization. Assuming all 3 modes contribute equally to h-p scattering and using an average sound velocity of $\sim 5600\text{m/s}$, we estimate μ_{hp}/μ_t to be about 10^{-3} for our samples at 4.2K, and it decreases to about 10^{-6} at 1K. The total mobility μ_t is unaffected by phonons. The values are not significantly changed for other h-p scattering mechanisms. Clearly, the strong resistivity variation with temperature that is observed in these and similar samples is not related to phonon scattering. Nevertheless, the fact that the fundamental mechanism responsible for the unexpected temperature variation of resistivity is not known leaves open the possibility that h-p scattering might also be affected in some way.

3.5 Conclusions

The results show that the magnetic field dependence of both the longitudinal and transverse thermopower are well understood. The low-field dependence of both the oscillatory and non-oscillatory parts are well described by the Mott model and all the data agree with the predictions that drag plays no significant role in either component.

On the other hand the zero field thermopower exhibits various features that are not understood. The data in a magnetic field prove that the diffusion component at zero field deviates from the expected linear temperature dependence. We believe that this observation is connected with the nearby metal-insulator transition, though the detailed mechanism is not known.

The temperature dependence of the phonon drag contribution at zero field is also not understood. The dependence does not fully agree with screened deformation-potential scattering of holes by phonons. Two possible models can explain the data, but it is impossible to decide which is correct. The first model used an unscreened deformation-potential, hole-phonon interaction and yielded excellent agreement with experiment. However, it is not clear why screening should be so ineffective in this system. The second model using screened piezoelectric and screened deformation-potential contributions also provides a reasonable representation of the data. However in this model a large piezoelectric interaction is required, and the deformation potential coupling constant must be larger than expected. Both models are consistent with recent work on energy relaxation of holes in a similar system. Possibly the nearby metal-insulator transition plays a role, though this cannot be substantiated.

3.6 References

- [1] R. Fletcher, *Semicond. Sci. Technol.* **14**, R1 (1999).
- [2] B. Tieke, R. Fletcher, U. Zeitler, M. Henini and J. C. Maan, *Phys. Rev. B* **58**, 2017 (1998).
- [3] R. Fletcher, M. Tsaousidou, P. T. Coleridge, Z. R. Wasilewski and Y. Feng, *Physica E* **12**, 272 (2002).
- [4] R. Fletcher, V. M. Pudalov, Y. Feng, M. Tsaousidou and P. N. Butcher, *Phys. Rev. B* **56**, 12422 (1997).
- [5] O. A. Mironov, I. G. Gerleman, P. J. Phillips, E. H. C. Parker, M. Tsaousidou and P. N. Butcher, *Thin Solid Films* **294**, 182 (1997); S. Agan, O. A. Mironov, M. Tsaousidou, T. E. Whall, E. H. C. Parker, P. N. Butcher, *Microelectronic Engineering*, **51-52**, 527 (2000).
- [6] A. Miele, R. Fletcher, E. Zaremba, Y. Feng, C. T. Foxon and J. J. Harris, *Phys. Rev. B* **58**, 13181 (1998).
- [7] M. Tsaousidou, P. N. Butcher and G. P. Triberis, *Phys. Rev. B* **65**, 165304 (2001).
- [8] G. Stoger, G. Brunthaler, G. Bauer, K. Ismail, B. S. Meyerson, J. Lutz and F. Kuchar, *Phys. Rev. B* **49**, 10417 (1994); *Semicond. Sci. Technol.* **9**, 765 (1994).
- [9] Y. H. Xie, R. People, J. C. Bean, K. W. Wecht, *Appl. Phys. Lett.* **49**, 283 (1986).
- [10] G. Braithwaite, N. L. Matthey, E. H. C. Parker, T. E. Whall, G. Brunthaler and G. Bauer, *J. Appl. Phys.* **81**, 6853 (1997).

- [11] G. Ansaripour, G. Braithwaite, M. Myronov, O. A. Mironov, E. H. C. Parker and T. E. Whall, *Appl. Phys. Lett.* **76**, 1140 (2000).
- [12] R. Leturcq, D. L'Hote, R. Tourbot, V. Senz, U. Gennser, T. Ihn, K. Ensslin, G. Dehlinger and D. Grutzmacher, *Europhys. Lett.* **61**, 499 (2003).
- [13] M. D'Iorio, R. Stoner and R. Fletcher, *Solid St. Comm.* **65**, 697 (1988).
- [14] H. Havlova And L. Smrcka, *Phys. Status Solidi (b)* **137**, 331 (1986).
- [15] R. Fletcher, V. M. Pudalov and S. Cao, *Phys. Rev. B* **57**, 7174 (1998).
- [16] P. T. Coleridge, R. L. Williams, Y. Feng and P. Zawadzki, *Phys. Rev. B* **56**, R12764 (1997).
- [17] S. V. Kravchenko, G. V. Kravchenko, J. E. Furneaux, V. M. Pudalov and M. D'Iorio, *Phys. Rev. B* **50**, 8039 (1994); S. V. Kravchenko, W. E. Mason, G. E. Bowler, J. E. Furneaux, V. M. Pudalov and M. D'Iorio, *Phys. Rev. B* **51**, 7038 (1995).
- [18] R. Fletcher, V. M. Pudalov, A. D. B. Radcliffe and C. Possanzini, *Semicond. Sci. Technol.* **16**, 386 (2001).
- [19] V. V. Karavolas and P. N. Butcher, *J. Phys.: Condens. Matter* **3**, 2597 (1991); X. Zianni and P. N. Butcher, *J. Phys.: Condens. Matter* **6**, 2713 (1994).
- [20] P. T. Coleridge, R. Stoner and R. Fletcher, *Phys. Rev. B* **39**, 1120 (1989).
- [21] M. Tsaousidou, private communication; C. Possanzini, R. Fletcher, M. Tsaousidou, P. T. Coleridge, Y. Feng, R. L. Williams and J. C. Maan, *Thermopower of a p-type Si/SiGe heterostructure*, conditionally accepted for publication in *Phys. Rev. B*.
- [22] R. Fletcher, V. M. Pudalov, Y. Feng, M. Tsaousidou and P. N. Butcher, *Phys. Rev. B* **60**, 8392 (1999).
- [23] O. Prus, M. Reznikov, U. Sivan and V. Pudalov, *Phys. Rev. Lett.* **88**, 016801 (2002).

Chapter 4

Metal-insulator transitions in a Si/SiGe two-dimensional hole gas in high magnetic fields

Si/SiGe heterostructures show several localization phenomena both at zero and non-zero magnetic field, which are not fully understood. The next two Chapters are dedicated to the analysis of localization phenomena in high magnetic fields.

In Paragraph 4.1, we briefly review experiments and theoretical models for the metal and insulator behavior in two dimensions. This section can be considered as an introduction to Paragraph 4.2, where we investigate the field driven metal-insulator transitions in terms of scaling, and to Chapter 5, dealing with thermoelectric power experiments.

4.1 The metal insulator transition in 2D

4.1.1 The metallic and the insulating states in a Si/SiGe two dimensional hole gas

By definition at $T=0$ a system is metallic if the resistivity is finite, whereas it is an insulator if the resistivity is infinite. Therefore, a metal-insulator transition distinguishes two completely different ground states. At temperatures that are experimentally accessible ($T>0K$), thermal excitations allow even an insulator to carry current, therefore the former definition is no longer applicable. In practice, an insulator or a metal are distinguished on the basis of the temperature dependence of

the resistivity coefficient ρ : in the metallic state $\partial\rho/\partial T > 0$, whereas in the insulating phase $\partial\rho/\partial T < 0$.

The zero-field resistivity of a Si/SiGe 2DHG shows $\partial\rho/\partial T > 0$ at carrier densities p_h above a certain critical value p_{hc} , and $\partial\rho/\partial T < 0$ at densities below p_{hc} [1, 2]. Qualitatively similar features have been observed in other systems, like p -GaAs/AlGaAs [3, 4] and Si-MOSFET [5, 6].

In magnetic field, in addition to the normal integer quantum Hall effect, two new but possibly related insulating phases are observed. Namely, in the extreme quantum limit ($\nu < 1$), when the energy of the lowest Landau level exceeds the Fermi energy, and between filling factors $\nu=1$ and $\nu=2$.

Although there is not a clear understanding of the mechanisms responsible for the appearance of an insulating state between two integer quantum states, many experimental observations indicate that they are related to the degeneracy and crossing of Landau levels [7, 8, 9]. The particular energy level structure at $\nu=1$ with the quasi-degeneracy of the $N_L=0\downarrow$ and $N_L=1\uparrow$ [10] can be varied by tilting the sample with respect to the magnetic field. Experimental observations show that by increasing the degeneracy of these two levels the resistivity of the insulating state increases [7, 9]. The origin of the insulating state is attributed to many-body interactions in combination with this peculiar energy level structure [7, 9]. At high tilt angles or magnetic fields, the Zeeman splitting may exceed the cyclotron spacing, as shown in Fig.(4.1) and a ferromagnetically polarized state at $\nu=2$ may occur.

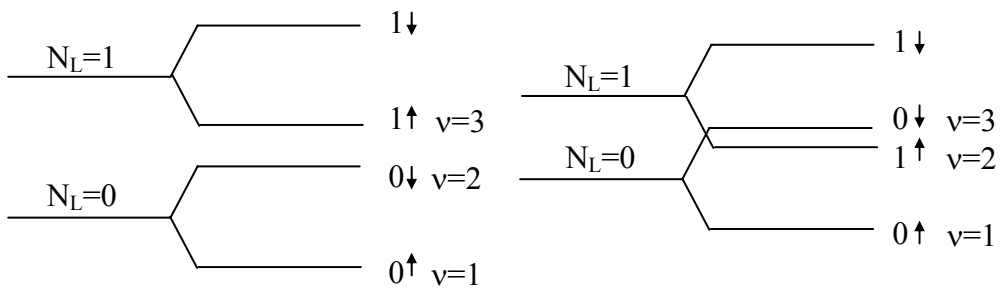


Figure 4.1: On the left the cyclotron splitting $\hbar\omega_c$ is larger than the Zeeman splitting ΔE_s ; the scheme on the right represents the situation when $\Delta E_s > \hbar\omega_c$.

4.1.2 Two mechanisms for electron localization

Carrier localization can be explained by the electron-electron (hole-hole) interaction and/or the disorder. The first effect has been introduced by Mott, the second by Anderson. Mott demonstrated that the repulsion between electrons can induce the opening of a gap and lead to an insulating state. Anderson discovered that disorder in the electrostatic potential, given by a random impurity distribution, can also lead to an insulating state even in a system of non-interacting electrons. In the presence of strong disorder, the electronic wave function is exponentially localized over a characteristic length ξ . The transition between localized and extended states is determined by the level of disorder, or equivalently by a critical value of the energy E_c , called *mobility edge*.

In the Anderson transition the conductivity in the insulating state vanishes at $T=0$, although the density of states is finite, contrary to the Mott transition where a gap appears at the Fermi energy E_F . A metal-insulator transition can occur in the Anderson model by changing the Fermi energy with respect to E_c .

It is nowadays clear that the integer quantum Hall effect is an example of quantum Hall phase transition in two dimensions and can be described in terms of Anderson transition. The scaling theory (see 4.1.3) provides a good framework to describe quantum critical phenomena.

4.1.3 One-parameter scaling theory

Scaling theory was formulated originally for a system of non-interacting electrons in the presence of disorder. The scaling theory [11] explains the behavior of the conductivity as a function of the system size L . The conductivity properties of the system are described in terms of a dimensionless conductance G . If the system is large ($L > l_m$, where l_m is the electron mean free path) the system is in the metallic state and $G = L^{d-2} \sigma$, with σ constant. If the system is in the insulating state, σ and G have to be exponentially small and $G(L) \sim e^{-L/\xi}$. The transition in the intermediate state from the metal to the insulating phase is described by the equation for the renormalization group:

$$\frac{d \ln G(L)}{d \ln L} = \beta(G)$$

where $\beta(G)$ is an unknown function independent on L . The asymptotic limits of this equation are

$G \rightarrow \infty$: in this case the system behaves as a metal, the disorder has a weak influence on the electronic states and $\beta(G) = d-2$

$G \rightarrow 0$: the electrons are localized (insulating phase) and the conductance decreases exponentially with the size L : $G = G_0 e^{-L/\xi}$.

The flux diagram of the renormalization group equation is shown in Fig. (4.2).

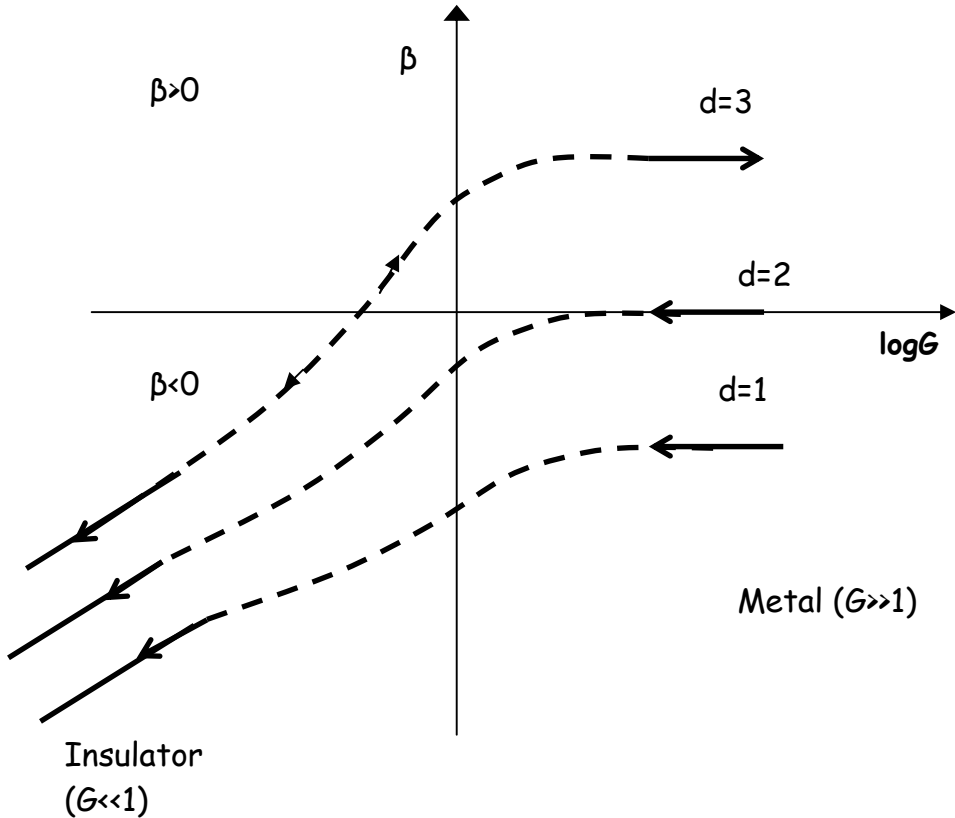


Figure 4.2: Flux diagram for the renormalization group equation.

Important conclusion can be drawn from Fig. (4.2):

For $d \leq 2$ the system evolves always to an insulator ($\beta < 0$), whatever is the level of the disorder ($G(L \rightarrow \infty) = 0$)

For $d > 2$, the states with $G_0 > G_c$ ($\beta > 0$) evolve towards a metallic behavior ($G(L \rightarrow \infty) = \infty$), whereas the states with $G_0 < G_c$ ($\beta < 0$) evolve towards an insulating behavior ($G(L \rightarrow \infty) = 0$).

Experimentally, the temperature sets the scale of the system. The theory predicts that there can be no metallic state in 2D. Subsequently, experimental observation

have supported that in fact two-dimensional systems remain metallic in the limit $T \rightarrow 0$ [5]. Finkelstein [12] and Castellani [13] consider the combined role of disorder and interaction and showed that a metallic state can be achieved in agreement with experiments [5]. As mentioned above, experimental observations in different systems confirm indeed the existence of a metal-insulator transition at $B=0$ for different densities.

4.1.4 Scaling in the quantum Hall regime: the two parameter theory

The one-parameter theory of renormalization is not sufficient to explain the quantum Hall effect, which is also characterized by the presence of extended states and two-parameter scaling is needed, namely σ_{xx} and σ_{xy} . Most of the experimental work on the transitions in quantum Hall effect can be understood in terms of quantum critical phenomena. The localization length ξ is a function of magnetic field and diverges as the magnetic field B approaches the critical field B_c . The divergence is described by the power law:

$$\xi(B) = |B - B_c|^{-\chi} \quad (4.1)$$

where χ is the localization critical exponent.

The scaling theory predicts that the resistivity is a function of the ratio L/ξ :

$$\rho_{ij} = f_{ij}\left(\frac{L}{\xi}\right) \quad (4.2)$$

At finite temperature, the effective length is given by the inelastic scattering size l_{in} , which is determined by the temperature according to $l_{in} \propto T^{-1/z}$, where z is the ‘‘dynamical exponent’’. The scaling exponent is $\kappa = (\chi z)^{-1}$, which is a combination between the localization exponent and the dynamical exponent.

Combining the equations (4.1) and (4.2), we obtain that the resistivity $\sigma_{ij}(B, T)$ behaves in two dimensions as

$$\rho_{ij}(B, T) = g_{ij}((B - B_c)T^{-\kappa})$$

where $\kappa = (\chi z)^{-1}$

The scaling theory for the transitions between integer quantum Hall plateaus predicts that the half-width for ρ_{xx} $\Delta B = |B - B_c|$ vanishes upon decreasing the temperature like T^κ , whereas the maximum slope of the Hall resistivity between neighboring Hall plateaus $(\partial\rho_{xy}(T)/\partial B)_{max}$ diverges with the power law $T^{-\kappa}$. It has been shown [14] that at $B=B_c$ if the n^{th} order derivative of the resistivity ρ has extrema in B_c , the magnitude of the extrema in all spin-split Landau levels diverges like $T^{-n\kappa}$. Similar behavior has been experimentally observed in InGaAs/InP heterostructures [14] and in the p -type Si/SiGe heterostructures [15] studied here.

4.1.5 An overview of the experiments and issues in the scaling in quantum Hall regime

The most complete analysis of the temperature scaling in the quantum Hall plateau has been carried out in a fairly low mobility ($\mu=3.4 \text{ m}^2\text{V}^{-1}\text{s}^{-1}$) InGaAs/InP two-dimensional electron gas (the electrons are in InGaAs) [16]. The low mobility assures that scattering on short-range potential fluctuations dominates transport properties and therefore only IQHE is observed in this structure. The InGaAs/InP shows scaling for different resolved Landau levels ($0\downarrow$, $1\downarrow$, and $1\uparrow$) in the very wide temperature range 0.1K-4.2K with a critical exponent $\kappa=0.42\pm 0.04$ [16]. It was also shown that the first and the second order derivative of the resistivity ρ_{ij} scale with the same exponent $\kappa=0.42\pm 0.04$ [14], confirming the theoretical prediction. One of the predictions of scaling theory is that the transition between two adjacent quantum Hall plateaus (PP transition) and the transition between the lowest Landau level and the insulator at $\nu < 1$ (PI transition) can be all described as quantum critical phenomena [17]. Experimental observations show that for the conductivity of InGaAs/InP 2DEG in the PI transition $\Delta B \propto T^\kappa$ with a critical exponent $\kappa=0.46\pm 0.05$, and in the PP transition $(\partial\sigma_{xy}(T)/\partial B)_{\min} \propto T^\kappa$ with $\kappa=0.43\pm 0.05$ and the half-width $\Delta B \propto T^\kappa$ has a critical exponent $\kappa=0.42\pm 0.05$ [18]. The resulting exponents for the conductivity are therefore all the same within the experimental error indicating that the PP and PI transitions belong to the same universality class [18]

In order to observe scaling behavior over a wide range of temperatures it is essential to have low mobility structures with short-range potential scattering. In this respect, the InGaAs/InP is a perfect material for scaling analysis. In fact, despite the theoretical predictions of the universality of the scaling behavior, such a behavior has been observed only in a few experiments, in InGaAs/InP. However the Si/SiGe is also low mobility structure with a short-range potential scattering and it is expected to exhibit scaling behavior over a wide range of temperatures, which would generalize the experimental observation of scaling beyond a single material.

Scaling theory predicts a universal value of the temperature exponent κ . InGaAs/InP low mobility samples give indeed a universal exponent independent on the Landau level index. However, in corresponding low-mobility GaAs/AlGaAs, the scaling is much poorer with values of κ , which clearly depend on Landau level index at temperatures above 200mK [19]. The difference in the temperature scaling behavior has been attributed to the different scattering processes of the AlGaAs/GaAs, characterized by long range scattering arising from the remote ionized impurities, compared to alloy scattering in InGaAs/InP. The value of κ at finite temperatures depends on the temperature dependence of inelastic scattering $I_{in} \propto T^{p/2}$. The universal critical exponent κ is the ratio between two exponents: $\kappa=p/2\chi$, where χ is a universal value, but the value on the inelastic scattering is sample dependent, according to the dominant inelastic scattering process. For instance, in GaAs/AlGaAs, it was found that κ increases as the mobility of the

sample decreases [20]. Other experiments [21] tried to measure directly the localization length exponent χ using samples of different sizes.

A great deal of experimental work carried out to prove the validity of the scaling theory shows that, despite the theoretical predictions of the universality of the scaling behavior, such a behavior has been observed only in a few experiments.

In this chapter, we report magnetotransport measurements of a low mobility strained p -type $\text{Si}_{0.88}\text{Ge}_{0.12}/\text{Si}$ heterostructure [4], which has the same short range scattering potential as $\text{In}_{0.53}\text{Ga}_{0.47}\text{As}/\text{InP}$, but a completely different energy level structure. This sample shows not only a Hall-insulator transition in the quantum limit ($\nu < 1$) but also an insulating phase around $\nu = 1.5$, not seen in $\text{In}_{0.53}\text{Ga}_{0.47}\text{As}/\text{InP}$. The scaling theory is used to understand if the transition at $\nu = 1.5$ is driven by similar mechanism as the transition at $\nu < 1$.

4.2 Scaling of the magnetic field induced metal-insulator transitions

Si/SiGe two-dimensional hole gases exhibit a re-entrant metal-insulator transition at $\nu = 1.5$, where an insulating phase appears between two integer quantum hall states. In Fig. (4.3a) the longitudinal magnetoresistivity is plotted at different temperatures. There are three values of the field (B_c' , B_c , and B_c'') where the resistivity does not depend on temperature: these three fields, called critical fields, separate the Hall states ($B < B_c'$, $B_c' < B < B_c''$) from the insulating phases ($B_c' < B < B_c$, $B > B_c''$). In order to study the temperature scaling of the two insulating transitions, we converted the ρ_{xx} and ρ_{xy} into the longitudinal (σ_{xx}) and the Hall (σ_{xy}) conductivity, through inversion of the transport matrix. Fig. (4.3b) shows σ_{xx} calculated for $p_h = 2.42 \cdot 10^{15} \text{m}^{-2}$ between filling factors 2 and 1: σ_{xx} vanishes in both the insulating and in the Hall states and reaches its maximum value at the critical field B_c and B_c' . The analysis of the conductivity, which is always finite in the metal-insulator transition, proves to be more accurate than the analysis of the resistance, which diverges in the insulating state. This fact might explain the different values of the exponents reported in earlier scaling analysis [22, 23], obtained by overlapping the resistance curves. In this paper, we analyze the conductivity measurements over a wide temperature range for both the longitudinal and the Hall conductivity in terms of scaling and we obtain the same critical exponent for the two Hall insulating transitions.

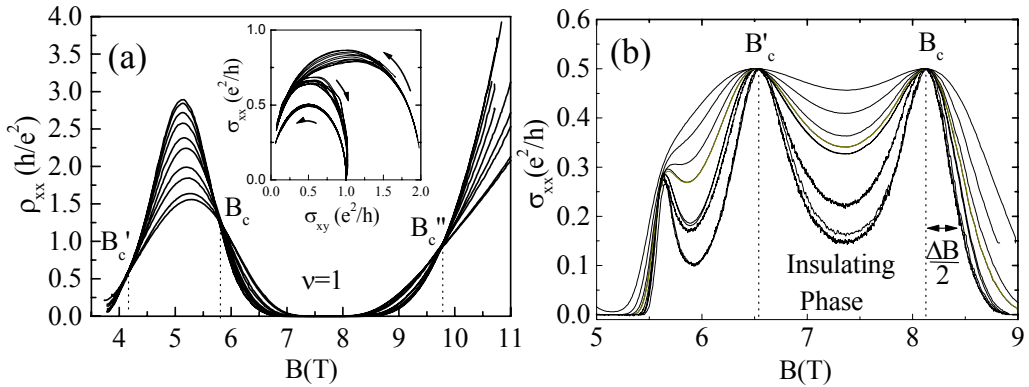


Figure 4.3.(a) Longitudinal magnetoresistivity at different temperatures ($0.3\text{K} < T < 1.2\text{K}$) for a carrier density $p_h = 1.76 \cdot 10^{15} \text{m}^{-2}$. The inset shows σ_{xx} as a function of σ_{xy} and demonstrates how the conductivity enters and leaves the insulating state at $\nu = 1.5$ for different temperatures. (b) The longitudinal conductivity σ_{xx} for the insulator transition at filling $\nu = 1.5$ in the temperature range $70\text{mK} - 850\text{mK}$ ($p_h = 2.42 \cdot 10^{15} \text{m}^{-2}$).

In our measurements, different cooling procedures allow experiments at different carrier density ($p_h = 1.76 \cdot 10^{15} \text{m}^{-2}$ and $p_h = 2.42 \cdot 10^{15} \text{m}^{-2}$) with the same sample. Fig.(1a) shows the magnetoresistance curves for $p_h = 1.76 \cdot 10^{15} \text{m}^{-2}$ in magnetic field up to 12T and in the temperature range $300\text{mK} - 1.2\text{K}$. The flow diagram in the inset of Fig.(1a) shows the transition from $\nu = 2$ to insulating state where $\sigma_{xx} \rightarrow 0$ (as the field increases), the insulating state goes to a Hall state at $\nu = 1$ at higher fields, and, in the end, there is the insulating transition in the quantum limit ($\nu < 1$).

The scaling theory predicts that the width of the conductivity ΔB (defined as in Fig.(4.3b)) vanishes with temperature with a power law T^κ . Moreover, the same theory predicts that the slope of the Hall conductivity $(\partial\sigma_{xy}/\partial B)_{B=B_c}$ diverges at $T=0$ with the same critical exponent. In our measurements, the analysis of the longitudinal conductivity σ_{xx} allows to calculate the high field halfwidth of the conductivity $(\Delta B/2)$ for the IP transition centered around the critical field B_c , which is not influenced by the proximity of the critical field B_c' of the PI transition (Fig.(4.3b)).

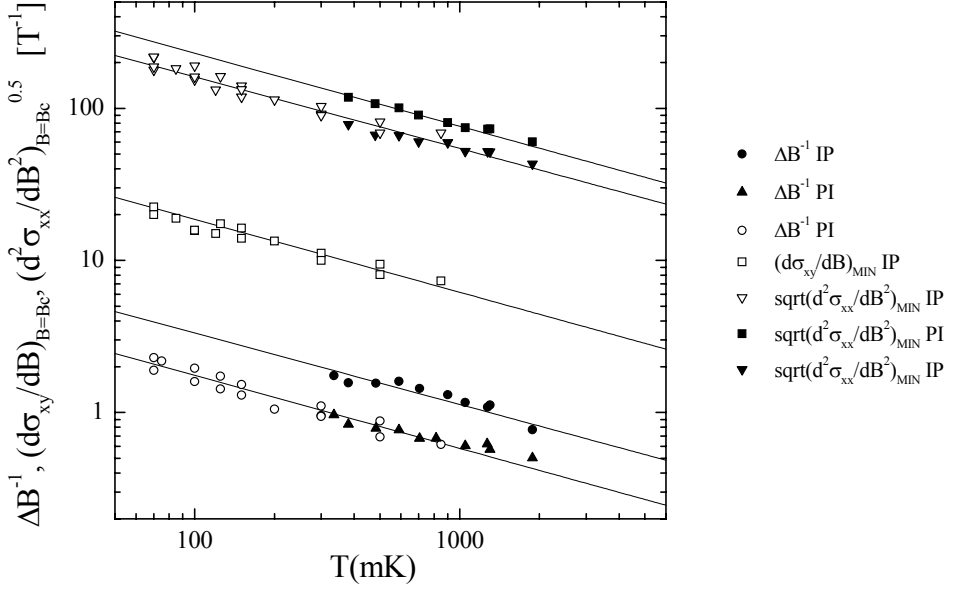


Figure 4.4. The temperature scaling of $1/\Delta B$, $(\partial\sigma_{xy}/\partial B)_{B=Bc}$, and square root of $(\partial^2\sigma_{xx}/\partial B^2)_{B=Bc}$ in a $\text{Si}_{0.88}\text{Ge}_{0.12}/\text{Si}$ heterostructure for both the high field plateau-insulator (PI) at $\nu < 1$ and the reentrant insulator-plateau (IP) transitions at $\nu = 1.5$. The solid symbols are data taken for a hole density $p_h = 1.76 \cdot 10^{15} \text{m}^{-2}$, while the open symbols are measurements at $p_h = 2.42 \cdot 10^{15} \text{m}^{-2}$. The slope of the straight line gives critical exponent: $\kappa = 0.45 \pm 0.05$.

The temperature dependence of the width of the conductivity ΔB is the same for IP and PI transitions and the critical exponent κ in both the cases $\kappa = 0.45 \pm 0.05$ (Fig.(4.4)). The value of the critical exponent κ in the IP transition is $\kappa = 0.45 \pm 0.05$ for both the densities. The analysis of the slope of the Hall conductivity $(\partial\sigma_{xy}/\partial B)_{B=Bc}$ for $p_h = 2.42 \cdot 10^{15} \text{m}^{-2}$ (Fig.(2)) shows that $(\partial\sigma_{xy}/\partial B)_{B=Bc} \propto T^\kappa$, with $\kappa = 0.45 \pm 0.05$.

According to the scaling theory, if the width of the conductivity ΔB exhibits a scaling behavior in temperature with an exponent κ , the second derivative calculated at the critical field should diverge approaching $T=0$ with the power law $T^{-2\kappa}$. In our measurements, the calculation of the second derivative of the longitudinal conductivity $(\partial^2\sigma_{xx}/\partial B^2)_{B=Bc} \propto T^{-2\kappa}$ for both the PI and IP transitions confirms the value of the critical exponent already found for ΔB : $\kappa = 0.45 \pm 0.05$. Fig. (4.4) summarizes all

the results for the exponents of different transitions and densities, obtained by the analysis of experimental curves at different temperatures. It can be seen that the transition to the insulating state and the reentrant insulating phase transition all exhibit the same scaling behavior, with the same critical exponent: $\kappa = 0.45 \pm 0.05$. The critical exponents of the σ_{xx} width, the slope of σ_{xy} and the second derivative of σ_{xx} are the same and, within the experimental error, in agreement with the critical exponents previously observed in InGaAs/InP heterostructures [14, 16, 18].

In summary, through an accurate scaling analysis over a wide temperature region, we observed scaling properties for both the reentrant Hall insulator transition at $\nu=1.5$ and the high field insulating phase transition, at two different densities. Our analysis is based not only on the value of σ_{xx} width but also on the first and second derivatives of the conductivity. Since the two transitions show the same scaling behavior, with the same critical exponent, they belong to the same universality class.

4.3 References

- [1] P.T.Coleridge, R.L.Williams, Y.Feng and P.Zawadzki, Phys. Rev B **56**, R12764 (1997). The present sample is from the growth CVD191 in this paper.
- [2] J.Lam, Phys. Rev B **56**, R12741 (1997).
- [3] Y.Hanein, U.Meirav, D.Shahar, C.C.Li, D.C.Tsui, H.Shtrikman, Phys. Rev. Lett. **80**, 1288 (1998).
- [4] M.Y.Simmons, A.R.Hamilton, M.Pepper, E.H.Linfield, P.D.Rose, D.A.Ritchie, A.K.Savchenko, and T.G.Griffiths, Phys. Rev. Lett. **80**, 1292 (1998).
- [5] S.V.Kravchenko, D.Simonian, M.P.Sarachik, W.Mason, and J.E.Furneaux, Phys. Rev. Lett. **77**, 4938 (1996).
- [6] R.Fletcher, V.M.Pudalov, A.D.B.Radcliffe, and C.Possanzini, Semicond. Sci. Technol. **16**, 386 (2001).
- [7] R.B.Dunford *et al.*, J.Phys.:Condens. Matter **9**, 1565 (1997).
- [8] T.J.Lin, M.S.Tsai, Y.F.Chen, F.F.Fang, J.Phys.:Condens. Matter **10**, 9691 (1998).
- [9] P.T.Coleridge, A.S.Sachrajda, P.Zawadzki, R.L.Williams, H.Lafontaine, Solid State Communications **102**, 755 (1997).
- [10] F.F.Fang, P.J.Wang, B.S.Meyerson, J.J.Nocera, and K.E.Ismail, Surface Science **263**, 175 (1992)
- [11] E.Abrahams, P.W.Anderson, D.C.Licciardello, and T.V.Ramakrishnan, Phys.Rev.Lett. **42**, 673 (1979).
- [12] A.M.Finkelstein, Z.Phys.B: Condens. Matter **56**, 189 (1984)
- [13] C.Castellani, C.Di Castro, P.A.Lee, and M.Ma, Phys.Rev.Lett. **30**, 527 (1984).

- [14] H.P.Wei, S.W.Hwang, D.C.Tsui, and A.M.M.Pruisken, *Surface Science* **229**, 34 (1990).
- [15] C.Possanzini, L.Ponomarenko, D.de Lang, A.de Visser, S.M.Olsthoom, R.Fletcher, Y.Feng, P.T.Coleridge, R.L.Williams, and J.C.Maan, *Physica E* **12**, 600 (2002).
- [16] H.P.Wei, D.C.Tsui, M.Paalanen and A.M.M.Pruisken, *Phys.Rev.Lett.* **61**, 1294 (1988).
- [17] A.M.M.Pruisken, *Phys. Rev. Lett.* **61**, 1297 (1988); A.M.M.Pruisken and M.A.Baranov, *Europhys. Lett.* **31**, 543 (1995).
- [18] R.T.F. van Schaijk, A. de Visser, S.M.Olsthoom, H.P.Wei, A.M.M.Pruisken, *Phys.Rev.Lett.* **84**,1567 (2000).
- [19] S.Koch, R.J.Haug, K.von Klitzing, and K.Ploog, *Phys.Rev.B* **46**,1596 (1992); *Mod.Phys.Lett.* **6**,1 (1992).
- [20] S.Koch, R.J.Haug, K.von Klitzing, and K.Ploog, *Phys.Rev.B.* **43**, 6828 (1991).
- [21] S.Koch, R.J.Haug, K.von Klitzing, and K.Ploog, *Phys.Rev.Lett.* **67**,883 (1991).
- [22] R.B.Dunford, N.Griffin, M.Pepper, P.J.Phillips and T.E.Whall, *Physica E* **6**, 297 (2000); R.B. Dunford, N.Griffin, P.J.Phillips, T.E.Whall, *Physica B* **298**, 496 (2001).
- [23] P.T.Coleridge P.Zawadzki, A.S.Sachrajda, R.L.Williams, Y.Feng, *Physica E* **6**, 268 (2000).

Chapter 5

Diffusion thermopower of a two-dimensional hole gas in SiGe in a quantum Hall insulating state

The origin of the insulating state occurring between the first two Landau levels and investigated in Chapter 4 is still controversial. In this Chapter, we measure resistivity and thermoelectric power of the insulating state at filling factor $\nu=1.5$. Both show a re-entrant metal-insulator transition at filling factor $\nu = 1.5$, but with strikingly different behavior of the two coefficients. As the temperature is decreased in the insulating state, the resistivity diverges exponentially while the thermopower decreases rapidly, suggesting that the insulating state is due to the presence of a mobility edge rather than a gap at the Fermi energy.

5.1 Introduction

In a perpendicular magnetic field, two-dimensional systems characterized by short-range carrier scattering frequently exhibit a re-entrant metal-insulator transition (MIT) where an insulating phase appears between two integer quantum Hall states [1–3]. Such insulating states have been observed in p -type Si/SiGe heterostructures [1] and in Si metal-oxide semiconductor field-effect transistors (Si-MOSFETs) [4], while in GaAs heterostructures, characterized by long-range scattering, an insulating phase appears only between fractional Hall states [5].

In *p*-type Si/SiGe, this re-entrant MIT at a filling factor $\nu = 1.5$ is followed at higher field by a second MIT, which occurs in the quantum Hall limit ($\nu < 1$) where the Fermi energy, E_F , lies within the lowest Landau level [1–3, 6, 7]. The origin of the MIT at $\nu = 1.5$, i.e., an insulating phase in the presence of extended states below E_F , is not understood. Recently, a scaling analysis of the magnetoconductivity measurements [1, 2, 6] demonstrated that the MITs at $\nu = 1.5$ and in the quantum limit both scale with the same critical exponent (see also Chapter 4), supporting the idea that both MITs are driven by the same mechanism. However, although scaling is a signature of a phase transition, it does not reveal the origin of the insulating state at $\nu = 1.5$.

In this chapter, we report thermoelectric power (TEP) measurements on a two-dimensional hole gas in a Si/SiGe heterostructure as a function of temperature and magnetic field near the field-induced insulating state at $\nu = 1.5$. At low temperatures, TEP is mainly due to diffusion which probes the energy distribution of the carriers. Diffusion TEP is expected to provide more information on the behavior of the density of states around E_F . In particular, TEP is expected to answer the question whether the field-driven insulating phase is the result of an opening of an energy gap at E_F or if it is due to the presence of a disorder-induced mobility gap. In both cases, on decreasing the temperature the resistivity diverges in the insulating state, while the TEP is expected to diverge in the former [8] and to vanish or approach a constant value in the latter [9]. Therefore TEP can distinguish between the two possibilities. In our measurements, TEP does not diverge but tends to a constant at $\nu = 1.5$ showing that the insulating phase is due to a mobility gap. This observation may be related to the peculiar many-level structure of a *p*-type Si/SiGe heterostructure in a magnetic field, when the Zeeman splitting may exceed the cyclotron energy and the state at $\nu = 2$ therefore becomes ferromagnetically polarized. The degeneracy and crossing of Landau levels has been indicated as one of the reasons for the appearance of the insulating state at $\nu = 1.5$ [1, 3, 10]. The present experiments were performed on a strained, asymmetrically-doped Si/Si_{0.88}Ge_{0.12} quantum well in which the carriers were confined in a triangular potential well (the sample used in this chapter was fabricated from the same wafer as CVD191 in Ref.[11]). By applying a substrate bias, measurements could be made at two different densities: $p = 1.9 \times 10^{15} \text{m}^{-2}$ and $p = 2.4 \times 10^{15} \text{m}^{-2}$. The mobilities were strongly temperature dependent [12] and at 1K they were 1.3 and 1.5 m^2/Vs , respectively. Conductivity and TEP measurements at zero field show that at the sample densities used here there is no sign of localization (seen for $p < 1.0 \times 10^{15} \text{m}^{-2}$ [11]) and metallic conductivity prevails down to the lowest temperature.

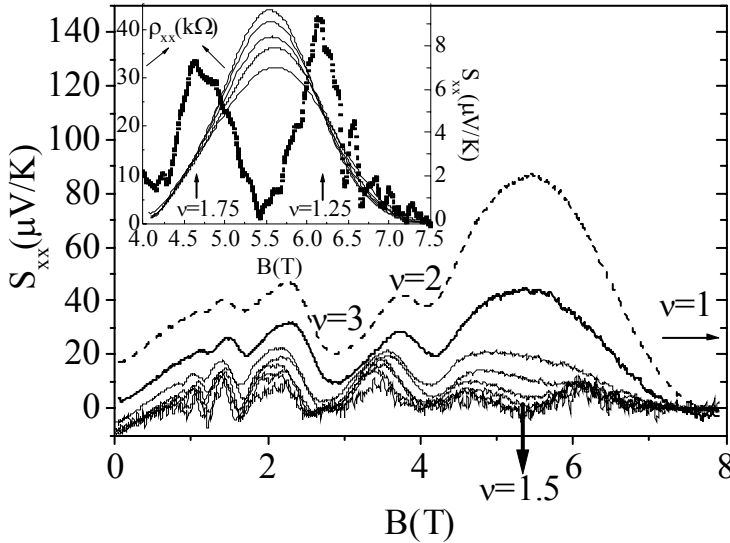


Figure 5.1: The thermopower, S_{xx} , as a function of magnetic field at temperatures of 0.32, 0.43, 0.50, 0.63, 0.76, 0.89, 1.07 and 1.23 K. The dashed line is S_{xx} at the highest temperature (1.23K). The insert shows resistivity measurements (solid line) at 0.3, 0.4, 0.5, 0.6 and 0.8 K, and thermopower (dotted line which is a smoothed version of the curve of S_{xx} at 0.3K shown in the main panel) as a function of magnetic field around $\nu = 1.5$. The sample density is $\rho = 1.9 \times 10^{15} \text{ m}^{-2}$.

5.2 Experimental setup

The TEP was measured between two contacts diffused into the ends of the Hall bar which also served as current contacts for resistivity measurements. Measurements of TEP in the insulating state as a function of temperature were made with a Keithley 182 dc voltmeter which provides a good compromise between input impedance, input bias current and noise. In order to eliminate any spurious voltage caused by the bias current, the signal was measured both with and without temperature gradient, keeping the average temperature of the sample constant [13, 14]. Data in swept magnetic fields were obtained with an ac lock-in technique

detecting at 4 Hz [15]. The factor used to convert the ac data to absolute thermopower was determined by comparing ac and dc measurements at zero field. An analysis of both the temperature dependence of TEP at zero field and the temperature and field dependence of the quantum oscillations in the TEP at low fields [12] shows that phonon drag becomes negligible below 0.7K leaving diffusion as the dominant driving mechanism at low temperatures. In this chapter we focus on the behavior at higher fields, especially in the field-induced insulating phase around $\nu = 1.5$.

5.3 Magnetothermopower measurements

Figure (5.1) shows the TEP, S_{xx} , as a function of magnetic field at various fixed temperatures. In general, previous work on the TEP of many systems in the integer quantum Hall regime leads us to expect that S_{xx} will vanish at integer filling factors and show maxima at half-integer filling factors, analogous to the resistivity [16]. This pattern is followed in the present sample except around $\nu = 1.5$. Here S_{xx} shows a double peak structure at low temperatures and, at $\nu = 1.5$, its magnitude decreases to very small values at the lowest temperatures. For comparison, at the same point the resistivity, ρ_{xx} , increases as the temperature decreases indicating an insulating phase.

Figure (5.2) shows the detailed temperature dependences of S_{xx} and ρ_{xx} at $\nu = 1.5$ for two different densities: $p = 1.9 \times 10^{15} \text{ m}^{-2}$ and $p = 2.4 \times 10^{15} \text{ m}^{-2}$. The graph clearly shows that in the insulating state the resistivity diverges at low temperatures, while the TEP appears to vanish. The low temperature peaks in S_{xx} around $\nu = 1.5$ shown in Fig. (1) at approximately 4.7T and 6.2T occur at $\nu = 1.25$ and 1.75 and correspond to the “critical magnetic fields”, where ρ_{xx} is temperature-independent. They separate the metallic phases ($\nu < 1.25$ and $\nu > 1.75$) from the insulating phase ($1.25 < \nu < 1.75$) [6]. In the resistivity shown in the inset to Fig. (5.1), this is particularly clear at $\nu = 1.25$, but at $\nu = 1.75$ it is blurred by the proximity of a separate integer quantum Hall effect transition [1, 6] and a sharp crossing point can be resolved only at lower temperatures. Thus, the transition from the metal to the insulating state is directly seen in S_{xx} , but in a completely different manner from ρ_{xx} .

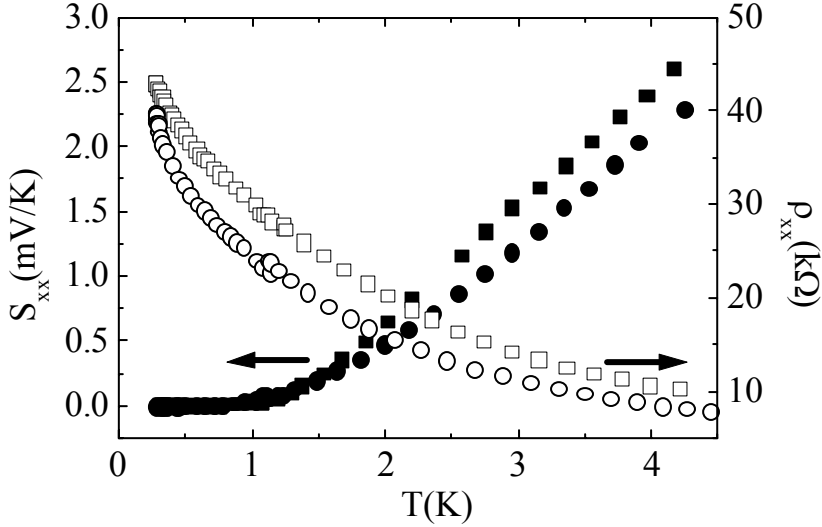


Figure 5.2: The temperature dependence of the resistivity (open symbols) and thermopower (solid symbols) at $\nu = 1.5$ for two different densities: $p = 1.9 \times 10^{15} \text{ m}^{-2}$ (\square) and $p = 2.4 \times 10^{15} \text{ m}^{-2}$ (\circ).

To illustrate the difference in behavior between TEP in the various states, in Fig. (5.3) we plot S_{xx} as a function of temperature for four different filling factors, $\nu = 2.5$ (metallic), $\nu = 1.25$ and 1.75 (critical), and $\nu = 1.5$ (insulating). At low temperatures S_{xx} clearly decreases more rapidly in the insulating state than in the other states. At higher temperatures the rise of S_{xx} is undoubtedly due to phonon drag, S_{xx}^g . However, here we concentrate on the behavior of S_{xx} at low temperatures where diffusion dominates.

For metallic samples, when the cyclotron energy $\hbar\omega_c$ exceeds the broadening of the Landau level Γ (low disorder), S_{xx}^d is directly related to the entropy of the partially filled Landau levels. When the spin splitting is resolved, S_{xx}^d is determined by the entropy $S = k_B \ln W$ where $W = N!/(fN)!(N-fN)!$ with N the number of states in a spin-resolved level and f the fractional filling of the last level. The total charge is Nve and, e.g., at half filling where $k_B \ln W = k_B N \ln 2$, the TEP is maximum and is given by the entropy per unit of charge, i.e., $S_{xx}^d = k_B \ln 2 / ve$ [17].

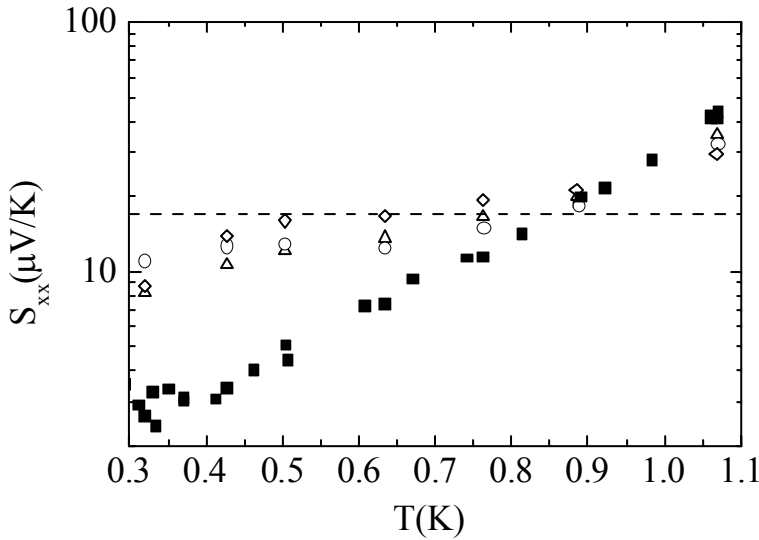


Figure 5.3: Temperature dependence of S_{xx} in the insulating phase at $\nu = 1.5$ (■), in the critical states at $\nu = 1.75$ (Δ) and $\nu = 1.25$ (\circ), and in the metal state at $\nu = 2.5$ (\diamond). The dashed line is the theoretical entropy limit at $\nu = 2.5$.

When $k_B T < \Gamma$ the expected values become a function of $k_B T/\Gamma$ and decrease with decreasing temperature [18]. The measured quantum mobility of this sample at low magnetic fields is found to be $1.4 \text{ m}^2/\text{Vs}$ at $2.4 \times 10^{15} \text{ m}^{-2}$ [11], giving $k_B T = \Gamma$ at $T \approx 1.65 \text{ K}$, and reducing the calculated values of the maxima of S_{xx} by a factor of about 0.7 at 0.3 K. However, Γ is known to increase as $B^{1/2}$ at high fields so that this reduction factor will be an underestimate. On the basis of these arguments we estimate S_{xx} at $\nu = 1.25$, 1.75 and 2.5 to be 27, 19 and $17 \mu\text{V/K}$ respectively, which are consistent with the observed values in Fig. (5.3) of about $10 \mu\text{V/K}$ at 0.3K. The previous argument is not appropriate for the insulating phase at $\nu = 1.5$, and indeed the experimental value of S_{xx} at low temperature is $2\text{-}3 \mu\text{V/K}$, an order of magnitude smaller than the estimated value of $S_{xx} = 28 \mu\text{V/K}$ based on the entropy result.

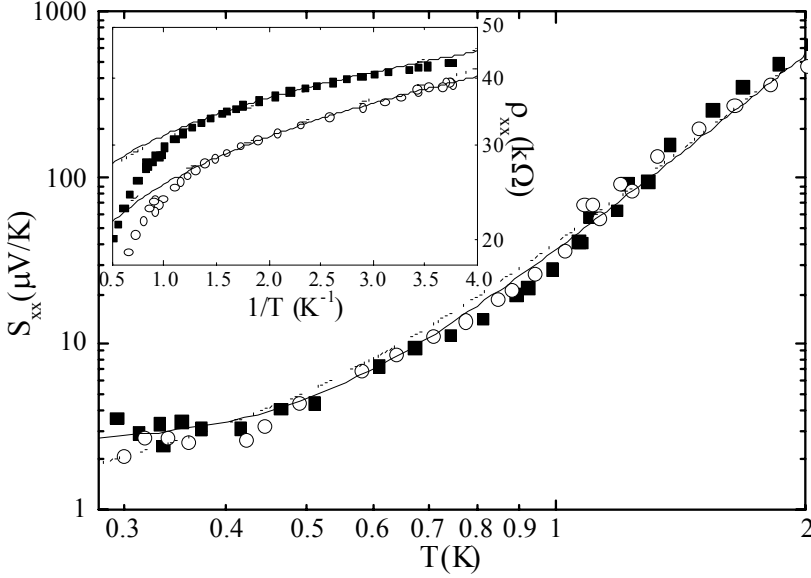


Figure 5.4: The thermopower measured at $\nu = 1.5$ as a function of temperature for two different densities: $p = 1.9 \times 10^{15} \text{m}^{-2}$ (\blacksquare) and $p = 2.4 \times 10^{15} \text{m}^{-2}$ (\circ). The dotted line is the fit $S_{xx} = \alpha T^{1/3} + \eta T^4$ (Mott VRH), and the solid line is the fit $S_{xx} = \gamma + \eta T^4$ (Efros-Shklovskii VRH). Resistivity measurements are shown for the same two densities (same symbols as for TEP) in the insert. The solid line is the fit to the Efros-Shklovskii model and the dotted line the fit to the Mott model.

5.4 The TEP in the insulating state

Previous work has been inconclusive about whether the MIT at $\nu = 1.5$ should be attributed to an opening of a many body gap at E_F , or to E_F being located in localized states below a mobility edge. At zero magnetic field it is known that S^d can distinguish these two cases, and we believe that the results remain valid in arbitrary fields as long as $\rho_{xx} \gg \rho_{yx}$ as here [1]. When E_F is located in a gap, $S^d \sim T^{-1}$ and S^d should therefore diverge at low temperatures. Such behavior has previously been seen in p-type GaAs heterostructures [19, 20] and in Pd and Pd-Au films [9]. However, our experimental results clearly show that S_{xx} becomes very small as $T \rightarrow 0$, contrary to the expected behavior due to the opening of a gap.

On the other hand, a finite S^d at low temperatures is expected when carriers conduct by hopping between localized states below a mobility edge. For variable range hopping (VRH) theory predicts an activated behavior of the resistivity $\rho_{xx}(T) = \rho_c \exp(T_0/T)^n$, where $n = 1/3$ if the density of states is finite at E_F (Mott VRH) and $n = 1/2$ if a soft Coulomb gap opens up at E_F (Efros-Shklovskii VRH) [21]. The corresponding results for TEP are $S^d \sim T^{1/3}$ for the Mott model and S^d becomes constant with a Coulomb gap [9,22].

We now focus on a more detailed analysis of our data in the insulating state. In Fig. (4) we show S_{xx} as a function of temperature at $\nu = 1.5$ for the same two densities as in Fig. (3). The temperature dependence can be described by either $S_{xx} = \alpha T^{1/3} + \eta T^4$ (Mott VRH shown as the dotted line in Fig. (4)) or $S_{xx} = \gamma + \eta T^4$ (Efros-Shklovskii VRH, solid line in Fig. (5.4)), with $\alpha = 18 \mu\text{V/K}^{4/3}$ and $\gamma = 2.5 \mu\text{V/K}$.

The term T^4 , with $\eta = 35 \mu\text{V/K}^5$, describes the residual contribution of the phonon drag, dominant at higher temperatures ($T > 0.6$ K). At low temperatures when carriers are localized, theory predicts S^g to be zero because drag requires the conservation of crystal momentum which cannot hold for electron scattering by phonons between localized states [19, 22]. Andreev *et al.* [23] recently reported that S^g vanished in a bulk doped Ge sample at zero field in the hopping regime. Therefore, regardless of the particular model for the MIT in the present case, we might have anticipated a rapid drop in S^g_{xx} in the insulating phase as the temperature decreases. Drag would still be possible via carriers excited above the mobility gap but this would presumably show activated behavior. We see no strong evidence for this, the weaker T^4 dependence apparently being followed to the lowest temperatures.

In the localization regime, the calculated magnitudes of S^d [9] for both the Efros-Shklovskii (γ) and Mott (α) VRH models depend linearly on the asymmetry of the density of states, $D(E)$ at E_F , i.e., on the factor $[\partial \ln D(E)/\partial E]_{EF}$. Using Γ as the energy scale, we have $[\partial \ln D(E)/\partial E]_{EF} \sim 1/\Gamma$ which leads to the estimates $\alpha = 32 \mu\text{V/K}^{4/3}$ and $\gamma = 2.2 \mu\text{V/K}$ in keeping with the experimental values of $18 \mu\text{V/K}^{4/3}$ and $2.5 \mu\text{V/K}$, respectively.

In conclusion, we have measured the thermopower of a *p*-type Si/SiGe heterostructure as a function of magnetic field and temperature. The thermopower reflects the metal-insulator transition previously probed by magnetoresistance measurements [1–3, 5–7] but in a totally different manner. The combined data on the resistivity and thermopower at $\nu = 1.5$ suggest that the insulating state is not due to an opening of an energy gap at the Fermi energy, but it is caused by a mobility gap.

5.5 References

- [1] P.T. Coleridge, A.S. Sachrajda, P. Zawadski, R.L. Williams, and H. Lafontaine, *Solid State Commun.* **102**, 755 (1997); P.T. Coleridge, P. Zawadski, A.S. Sachrajda, R.L. Williams, Y. Feng, *Physica* **6E**, 268 (2000).
- [2] R.B. Dunford *et al.*, *J.Phys.: Condens. Matter* **9**, 1565 (1997); R.B. Dunford, N. Griffin, M. Pepper, C.J. Emeleus, P.J. Phillips, and T.E. Whall, *Physica (Amsterdam)* **6E**, 297 (2000).
- [3] M.R. Sakr, M. Rahimi, S.V. Kravchenko, P.T. Coleridge, R.L. Williams, and J. Lapointe, *Phys. Rev. B* **64**, 161308(R) (2001).
- [4] S.V. Kravchenko, J.A.A.J. Perenboom, and V.M. Pudalov, *Phys. Rev. B* **44**, 13513 (1985).
- [5] T. Sajoto, Y.P. Li, L.W. Engel, D.C. Tsui, and M. Shayegan, *Phys. Rev. Lett.* **70**, 2321 (1993).
- [6] C. Possanzini, L. Ponomarenko, D. de Lang, A. de Visser, S.M. Olsthoorn, R. Fletcher, Y. Feng, P.T. Coleridge, R.L. Williams and J.C. Maan, *Physica* **12E**, 600 (2002).
- [7] M. Hilke, D. Shahar, S.H. Song, D.C. Tsui, Y.H. Xie, and D. Monroe, *Nature* **395**, 675 (1998).
- [8] B.L. Gallagher and P.N. Butcher, in *Handbook on Semiconductors*, edited by P.T. Landsberg (Elsevier, Amsterdam, 1992), vol.1, p.817.
- [9] M.J. Burns and P.M. Chaikin, *Phys. Rev. B* **27**, 5924 (1983); M.J. Burns, *Phys. Rev. B* **40**, 5473 (1989).
- [10] F.F. Fang, P.J. Wang, B.S. Meyerson, J.J. Nocera, and K.E. Ismail, *Surf. Sci.* **263**, 175 (1992).
- [11] P.T. Coleridge, R.L. Williams, Y. Feng and P. Zawadzki, *Phys. Rev. B* **56**, R12764 (1997).
- [12] C. Possanzini, R. Fletcher, M. Tsaousidou, P.T. Coleridge, R.L. Williams, Y. Feng, and J.C. Maan, conditionally accepted for publication in *Phys. Rev. B*.
- [13] R. Fletcher, V.M. Pudalov, A.D.B. Radcliffe, and C. Possanzini, *Semicond. Sci. and Technol.* **16**, 386 (2001).
- [14] R. Fletcher, P.T. Coleridge, and Y. Feng, *Phys. Rev. B* **52**, 2823 (1995).
- [15] B. Tieke, R. Fletcher, U. Zeitler, M. Henini, J.C. Maan, *Phys. Rev. B* **58**, 2017 (1998).
- [16] In general E_F is always located in localized states at integer filling factors. However, although S^d and S^g do appear to go to zero at these points, because $\rho_{xx} \gg \rho_{yx}$ the situation is not the same as in the usual case at zero magnetic field or in the present case.
- [17] H. Oji, *Phy. Rev. B* **29**, 3148 (1984).
- [18] W. Zawadski and R. Lassnig, *Surf. Sci.* **142**, 225 (1984).
- [19] V. Bayot, X. Ying, M.B. Santos, and M. Shayegan, *Europhys. Lett.* **25**, 613 (1994).

- [20] V. Bayot, E. Grivei, H.C. Manoharan, X. Ying, and M. Shayegan, *Phy.Rev.B* **52**, R8621 (1995).
- [21] D.G. Polyakov and B.I. Shklovskii, *Phys. Rev. B* **48**, 11167 (1993); *Phys. Rev. Lett.* **70**, 3796 (1993).
- [22] I.P. Zvyagin in *Hopping transport in Solids* edited by M. Pollak and B. Shklovskii (North-Holland, Amsterdam, 1991).
- [23] A.G. Andreev, A.G. Zabrodskii, S.V. Egorov, I.P. Zvyagin, *Sov. Phys. Semiconductors*, **31**, 1008 (1997).

Chapter 6

Probing the two-dimensional gas with short non-equilibrium phonon pulses

Thermoelectric power measurements provide information about the thermodynamic of the electron system (diffusion thermopower) and about the electron-phonon interactions (phonon drag), which are impossible to detect with resistivity measurements characterized by impurity scattering. In thermopower experiments, a constant heating is applied at one side of the sample and the response of the carriers in this fixed thermal gradient is measured as a function of temperature and magnetic field. In this Chapter, we explore the possibility to extend the thermopower technique to probe the response of the two-dimensional electron gas (2DEG) to a short-pulsed heat excitation.

6.1 Introduction

The scope of this experiment is to detect how local is the electron-phonon coupling and, in the fractional quantum Hall regime, the phonon-“Composite Fermions” interaction. Previous experiments on our GaAs/GaAlAs heterostructure demonstrate that the sample shows fractional quantum Hall effect [1] and that the phonon mean free path is limited by sample boundary scattering [1], which means that phonons propagate ballistically through the substrate.

When a heat pulse is produced by a source (heater), the heat propagates in the solid along preferential channels [2]. This effect is called “phonon focusing” and has been studied in the past in different substrates [2, 3]. The generation of a short burst of non-equilibrium phonons at one surface of the substrate, the propagation along the crystal and the detection on the other surface of the substrate has been observed in the past in different substrates, such as quartz, Ge, LiF, and GaAs (a good review is

given in Ref. [2] and [3] and references therein). In these experiments, the phonons were detected with a bolometer (typically a superconductive film) on the surface opposite to the generator. Fig. (6.1) (modified from Ref. [2]) shows a typical setup for pulsed phonon excitation. Heat pulses are generated by exciting with a focused laser beam a metal film deposited on the surface. On the opposite side of the crystal a strip of aluminum (detector) is evaporated. The phonon pulses, created by the heater, are transmitted in the medium and propagate with a velocity, which in an anisotropic solid is different for each of the three phonon polarizations (longitudinal, fast and slow transversal). The phonon modes can be resolved on basis of their different “time-of-flight”, if the detector has a small heat capacitance and therefore a fast response-time (Fig. 6.1). Phonons that do not propagate ballistically but are scattered in the bulk of the substrate are expected to arrive after the “time-of-flight” to the detector giving a long diffusive tail in the signal.

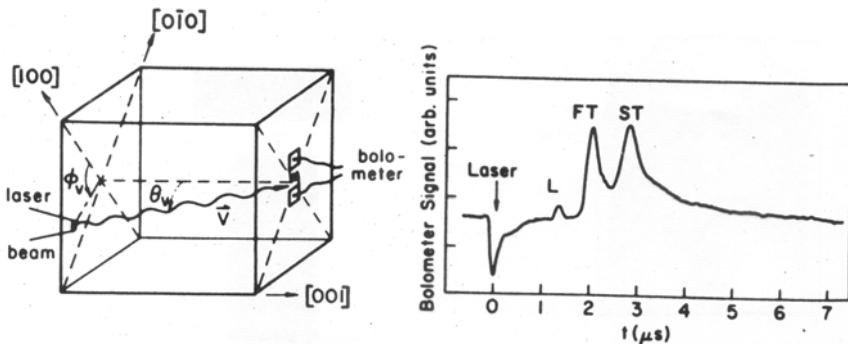


Figure 6.1: Sample geometry used in the first phonon imaging experiment (left) and bolometer signal (right) showing the arrival of longitudinal (L), fast (FT) and slow (ST) transversal phonons. Picture adapted from Ref. [2].

Beams of non-equilibrium phonons have been used to study the absorption of ballistic phonons in two-dimensional electron systems in fractional and integer quantum Hall regime [4,5]. In these experiments the interaction between phonons and the 2DEG has been deduced by the changes in resistivity of the 2DEG due to the absorption of phonons by the 2DEG:

In this chapter, we explore the possibility of detecting the response of a 2DEG to a pulsed non-equilibrium phonon excitation. In order to detect time resolved the response of the electrons, the phonon wave should not warm up the entire 2DEG (like in Ref. [4, 5]), it has to propagate as a single wave along the sample and its width should be less than the smallest contact distance available (1mm which

corresponds in GaAs to around 200ns). In these conditions, it is possible to measure the electronic response between two longitudinal contacts with time resolved measurements before, during, and after the passage of the pulse (Fig. (6.2)).

In order to be able to probe the local interaction between the electrons of the 2DEG and the phonons of the three-dimensional substrate by time resolved measurements, the signal between two contacts has to be measured. Therefore the spatial width of the pulse has to be much less than the separation between two adjacent contacts, which is 1mm (Fig. (6.2)). Considering the longitudinal sound velocity in GaAs (5000m/s), the phonon pulse should be shorter than 200ns.

6.2 Experimental technique

6.2.1 The sample

The 2DEG-sample was a GaAs/Ga_{1-x}Al_xAs heterostructure MBE-grown at the University of Nottingham and etched in a mesa on a semi-insulating GaAs substrate. The length and the width of the 2DEG channel are 4mm and 300 μ m, respectively. The substrate is 4mm wide and 0.4mm thick. The distance between two adjacent contacts of the mesa is 1mm and the distance between the two more far apart contacts is 4mm. Figure (6.2) shows a schematic view of the sample and the mesa.

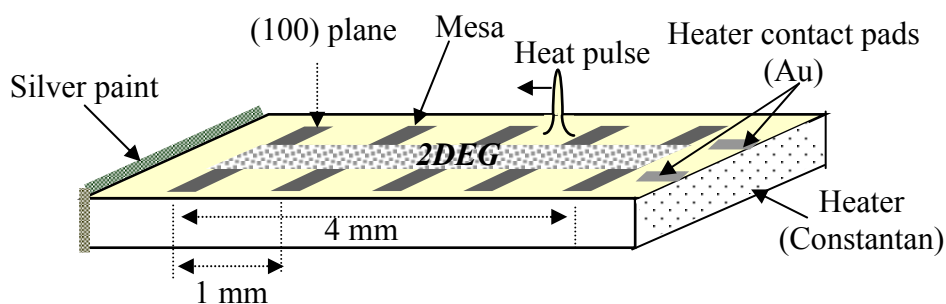


Figure 6.2: Schematic representation of the sample for pulsed thermopower experiments

In order to be able to transfer a short pulse from the heater to the substrate, it is necessary to have a very good contact between them. For this reason a thin heater of constantan was evaporated on the edge of the sample (Fig. (6.2)). During the evaporation, the thickness of the evaporated layer was measured as well as the resistance of the film. The evaporation was stopped when the constantan film had a resistance of 55Ω , corresponding to a nominal resistance of 50Ω at low temperatures, which provides a good impedance matching to the electrical circuit (pulse generator and coaxial cables) with 50Ω characteristic impedance. In order to avoid diffusion of constantan into the GaAs with the consequent increase of its resistance and mismatch with the electronics, a layer of 30\AA of titanium was evaporated between the substrate and the constantan. The contacts on the heater were realized by evaporating chromium and gold on the sample. Special masks were developed in order to protect the 2DEG during the evaporations.

Typical parameters for the evaporated materials are reported in table I. An important parameter is the deposition rate, which was controlled mainly to prevent the excessive heating of the sample during the evaporation:

Table I.

Material	Thickness (\AA)	Deposition rate ($\text{\AA}/\text{s}$)	Evaporation pressure (mbar)
Au	~ 1000	10-15	$2 \cdot 10^{-6}$
Cr	100	0.5-1.0	$2 \cdot 10^{-6}$
Constantan	~ 700	0.5-1.0	$1 \cdot 10^{-6}$
Ti	30	0.4-0.5	$2 \cdot 10^{-6}$

To increase the mean free path of the phonons, which have to propagate ballistically in the substrate, the back surface of the substrate was optically polished.

The sample was glued with silver paint on a printplate, which was soldered to the cold finger of the cryostat. Aluminum wires were bonded from the contact pads of the sample to the printplate. Between the printplate and the top of the cryostat, the RF pulses were generated and detected by using 50Ω miniaturized non-magnetic semi-rigid cryogenic coaxial cables [6].

The electron density of the sample could be varied between $n_e = 1.0 \cdot 10^{15} \text{ m}^{-2}$ and $1.5 \cdot 10^{15} \text{ m}^{-2}$ by illuminating with an infrared emitting diode. The mobility was between 60 and $100 \text{ m}^2/\text{Vs}$. The sample is known to exhibit integer and fractional quantum Hall effect at low temperatures and high magnetic fields [1], as shown in Fig. (6.3) where the longitudinal resistance of the sample is reported as a function of magnetic field at $T=0.3\text{K}$.

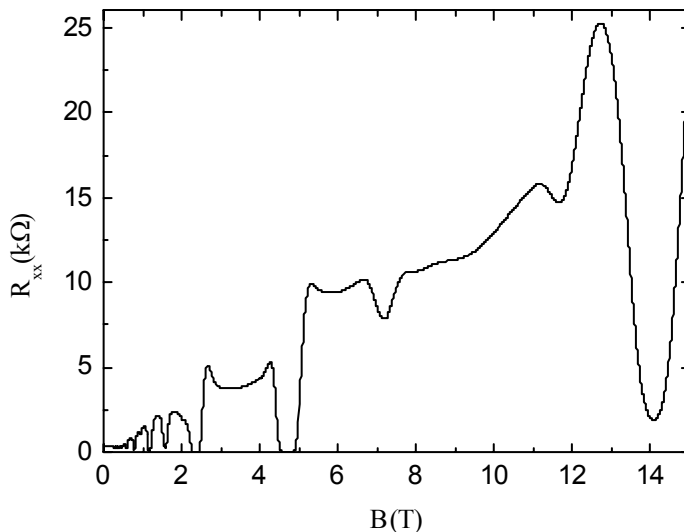


Figure 6.3: Longitudinal resistance of our 2DEG as a function of magnetic field at the base ^3He temperature ($T=300\text{mK}$).

6.2.2 Electronic system for pulse generation and detection

The voltage pulses were supplied to the constantan heater by a pulse generator [7], which could generate pulses in the range 1ms - 1ns with a delay time t_d with respect to the trigger. The repetition rate was either 100Hz or 1kHz , depending on the length of the pulse and the allowed energy dissipation. The pulse amplitudes were between 0.1V and 1.0V over a 50Ω heater, connected to the electronic equipment with a 50Ω miniature cryogenic coaxial cable.

The signal between the 2DEG contacts was amplified with a low noise, wide band, RF-preamplifier [8] and acquired with a fast digital oscilloscope [9], able to average up to 256 traces.

Since at high magnetic fields the resistance of the GaAs/AlGaAs heterostructure may become very high (20 - $30\text{k}\Omega$, as shown in Fig. (6.3)), it was necessary to transform the impedance in situ to 50Ω . A cryogenic impedance transformer working down to 300mK was therefore built *ad hoc*. The scheme of the transformer circuit is

shown in Figure 6.4. The first stage of the transformer, placed close to the sample, in the cold, works as a transconductance amplifier, which outputs a current proportional to the input voltage. It uses as active device a GaAs metal-semiconductor field-effect transistor (MESFET), which operates at He temperature without carrier freeze-out [10]. The cryogenic stage of the transformer was connected in cascade to a FET operating at room temperatures through a 50Ω coaxial line. This second stage works as a transimpedance amplifier, which converts the output current of the first stage into voltage and provides a 10 times amplification of the signal. With a typical bias of 0.5mA (the lower possible for a correct functioning of the FET) the drain source voltage of 2V, the power dissipation was around 1mW. To prevent the warming up of the sample and the evaporation of ³He, we thermally disconnected the transformer from the ³He connecting it directly to the ⁴He bath (see next section, Fig. (6.6)), and we reduced the operational time of the transformer to 1% of the duty cycle. The MESFET was therefore active only for $t_{FET}=10\mu s$ every duty cycle (of 10ms).

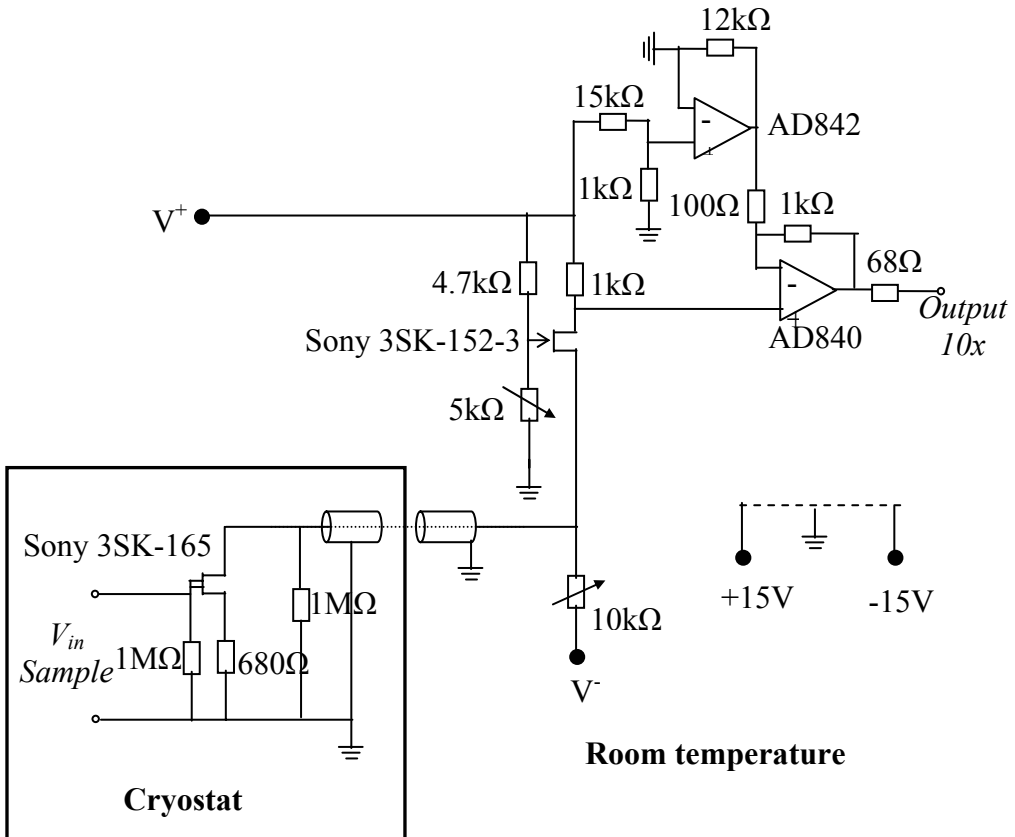


Figure 6.4. Impedance transformer schematic.

The signals of the pulse generator and the detection system were coordinated as described in Fig. (6.5).

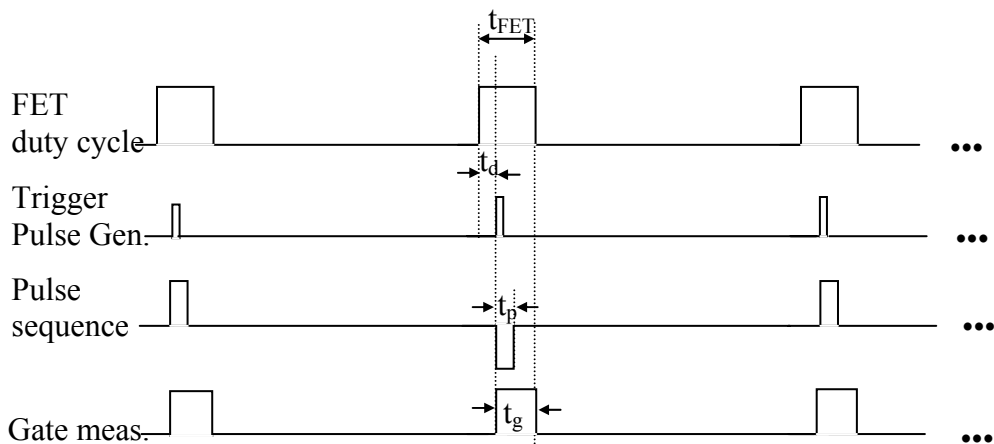


Figure 6.5: Time scheme for the generation and detection system in pulse experiments. The figure is not in scale. The duty cycle was typically 10ms (100Hz) and the cryogenic FET was active only for $t_{FET}=10\mu s$ (see text). The delay time of the pulse is indicated with t_d , the duration of the pulse with t_p , and the measuring time with t_g .

Since the heat pulse propagated with the sound velocity of GaAs (5000m/s) through the substrate, the response of the 2DEG is expected between 200ns and 400ns after the beginning of the pulse. Any spurious electronic signal had to be eliminated during the detection time of the pulse. The delay time t_d allowed to shift the beginning of the pulse in the region where the FET was stable, typically $t_d=2\mu s$. The duration of the pulse is limited by two conditions. The pulse should be a local excitation and therefore should not heat up the entire sample. Moreover, in order to perform time resolved measurements, the heat pulse should be not be broader than the most distant contacts (4mm), which determines the maximum duration of the pulse being $t_p \leq 800ns$.

Since the pick-up depends on the sign of the voltage on the heater while the thermal response of the sample does not, the effect of the cross-talk of the generated pulse on the detected signal has been minimized by inverting the sign of the pulse every cycle and averaging the detected signal up to 64 times with the oscilloscope [9].

6.2.3 Cryogenic system

Since the sample has to be mounted adiabatically *in vacuum*, a ^3He system was designed and home-built. In this system the mixture is condensed in a “ ^3He chamber” above the space where the sample is placed. The sample is therefore situated *in vacuum*, and thermally connected to the ^3He through a cold finger. Fig. (6.6) gives a schematic drawing of the sample chamber in the ^3He system, and it shows the position of the sample and the MESFET.

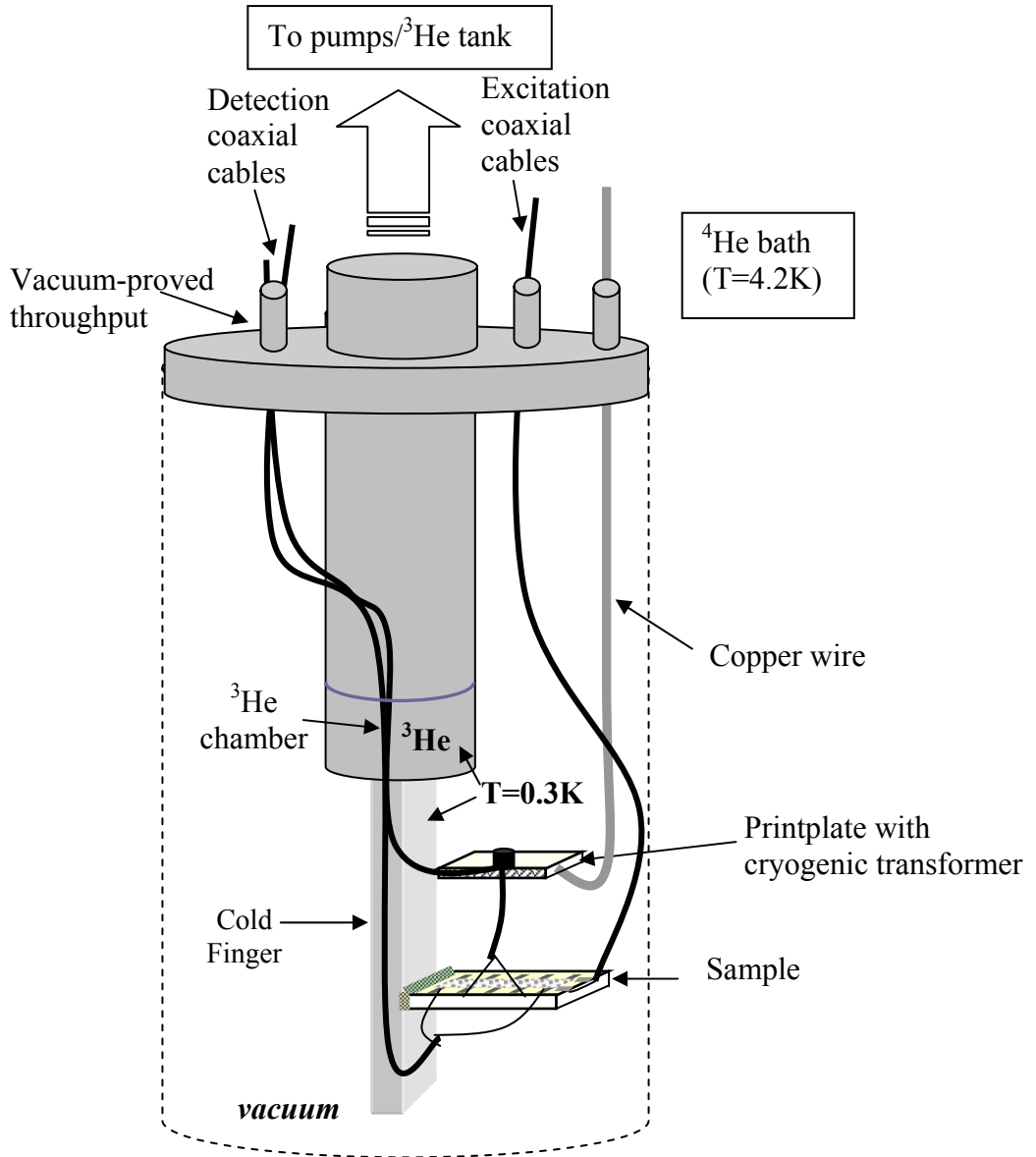


Figure 6.6: Schematic drawing of the ^3He system (not in scale). The position of the sample and of the cryogenic transformer (MESFET) is indicated. In the real setup the sample is mounted on a printplate, but for clarity the printplate was not drawn.

6.3 Measurements

The good thermal contact between the heater and the sample was checked by sending pulses and recording with a standard AC Lock-in technique the magnetoresistance curves. The resistivity measurements reported in Fig. (6.7) show an increase of the average temperature of the sample.

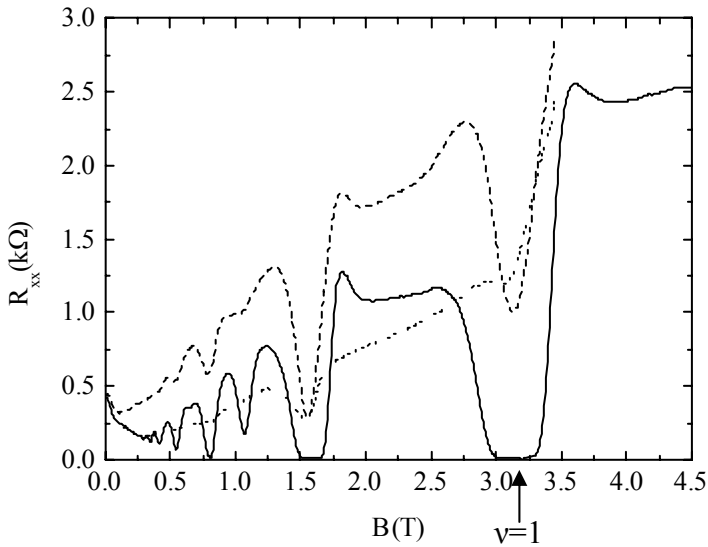


Fig. 6.7: The longitudinal resistivity measurements show that the Constantan heater transfers the heat to the substrate and increase its temperature from 0.4K (solid line), to 0.8K (dashed line) and 1.5K (dot line).

During these measurements the cryogenic transformer was not present and the sample was connected directly to a Lock-in.

The present configuration with the sample mounted on a printplate is suitable for short pulses, but not for low frequency thermopower (longer pulses), which is thermally equivalent to DC thermopower. The sample was cooled down only by the thermal contact with the printplate realized with silver paint. The effect of a DC signal on the heater was therefore translated into an average increase of temperature of the sample rather than in a temperature gradient. For this reason, low frequency or

DC thermopower could not be measured on the sample and in the magnetoresistance curves (Fig. (6.7)), there is not any thermopower voltage superimposed to the resistance.

As shown in Fig. (6.7), the resistivity at $\nu=1$ depends strongly on temperature, i.e. it is zero at 0.4K and 1 k Ω at 0.8K. Therefore heat pulses were generated with the pulse generator at filling factor $\nu\sim 1$. The changes in resistance of the 2DEG could be detected by applying a DC current and detecting the change in resistance of the 2DEG with a Lock-In, where the integration time constant was comparable with the duration of the pulse t_p . The shortest pulses we could detect in this way were 50 μ s long. Fig. (6.8) shows a pulse of 500 μ s (the integration time constant of the Lock-In was 1ms in order to follow the rise and decay of the pulse) and a repetition rate of 20Hz.

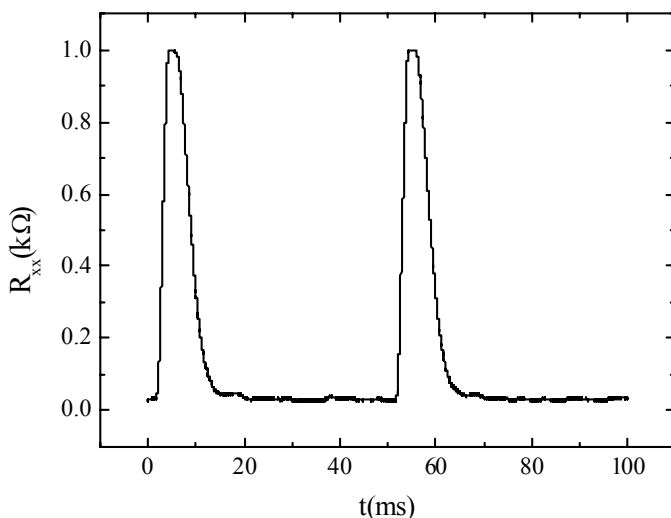


Figure 6.8: Response in the resistivity of the 2DEG to a pulsed heat excitation of 500 μ s (see text).

Fig. (6.9) and (6.10) show the change in resistance of the 2DEG at filling factor $\nu=1$ at different values of the repetition rate (Fig. (6.9)) for a fixed pulse excitation (100 μ s), and of the heat pulse duration (Fig. (6.10)) at a fixed repetition frequency (20Hz). These measurements show that with a repetition rate of 100Hz the system can still get rid of the heat pumped by the heater into the sample.

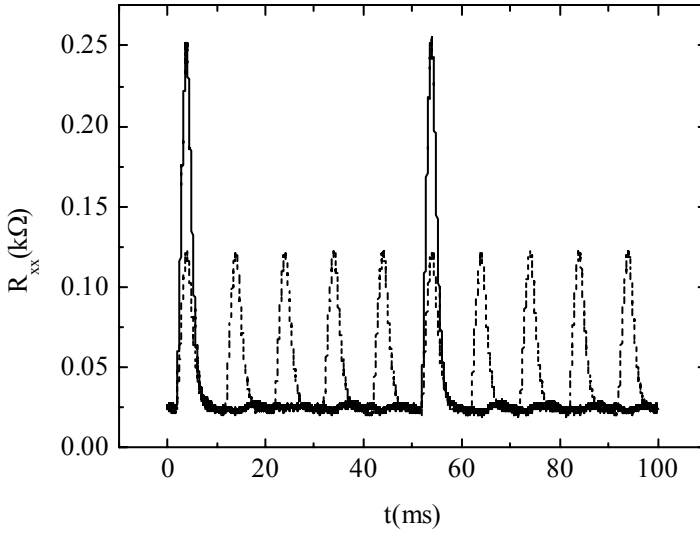


Figure 6.9: Change in resistivity of the sample with a pulsed excitation of $100\mu\text{s}$ at the frequency of 20Hz (solid line) and 100Hz (dot line).

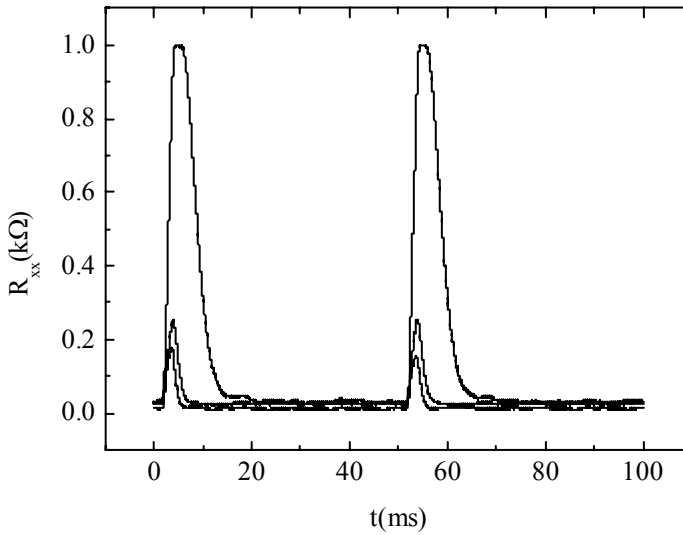


Figure 6.10: Detected resistivity changes in the 2DEG by applying heat pulses with a frequency of 20Hz and duration $t_p=500\mu\text{s}$, $100\mu\text{s}$, and $50\mu\text{s}$.

The shortest detected pulse was around $20\mu\text{s}$, which corresponds to a width of 1cm . In this regime, the phonon pulse is longer in length than the sample. With shorter pulses ($<1\mu\text{s}$), high intensity phonons can be generated locally resulting in a lower thermal load and therefore a shorter thermal time constant for the detected heat pulse. At these frequencies, the signal has to be properly matched to the electronics. For this reason, we used the impedance transformer described in Section 6.3.2.

Even if the cryogenic transformer works properly at He temperatures, and the crosstalk was clearly removed in the detected signal by averaging 64 times with positive and negative excitation pulses on the heater, we could not detect any response neither in resistivity nor in thermopower of the 2DEG to a shorter pulse excitation. This is due to the high level of pickup, comparable with the expected amplitude of the pulses. Fig. (6.8) and (6.9) show that the amplitude of resistivity pulses is maximum $1\text{k}\Omega$. The expected pulse voltage with a current in the range of $10\text{-}100\text{nA}$ is therefore $10\text{-}100\mu\text{V}$. As regards the thermopower pulses, the applied voltages on the heater should correspond to a temperature increase of the heater of the order of $1\text{-}4\text{K}$. A local temperature gradient of $1\text{-}4\text{K/mm}$ corresponds to a thermopower voltage of the order of $100\text{-}500\mu\text{V}$ if it is measured in magnetic field between integer filling factors [1], where the TEP has the strongest dependence on temperature [1]. A voltage amplitude of $100\mu\text{V}$ amplified 10 times in the order of the measured pickup voltage of the detection line, which is 5mV . Therefore the signal is overwhelmed by the pickup noise of the detection system.

Unfortunately, we could not understand the origin of this high pickup voltage, which is far above the voltage noise of $10\text{-}100\mu\text{V}$ expected for the cryogenic preamplifier [10]. The elimination of the pick-up signal is a *conditio sine qua non* to measure the pulses, at least in resistivity. In order to detect thermopower pulses, and therefore to probe the local phonon-electron interaction, another condition has to be satisfied: the heat pulse must propagate coherently as a wave along the substrate in the longitudinal direction. If this condition is not accomplished, the phonon pulse spreads out, giving rise to an average increase of temperature in a large part of the system rather than a local non-equilibrium heat excitation.

6.4 Conclusions

This Chapter was devoted to the description of the experimental setup for pulsed thermopower measurements. The response of the 2DEG to heat pulses has been detected for pulse duration above $20\mu\text{s}$, which still warms up the entire sample. Shorter pulses ($<1\mu\text{s}$) need the use of an impedance transformer between the sample (with a resistivity of $20\text{k}\Omega$) and the electronics (50Ω). The transformer built for the purpose and working at He temperatures exhibits a pickup voltage of 10mV , which is much higher than the expected noise figure of such a device and well above the expected pulsed thermopower or resistivity amplitude of the 2DEG. The origin of such a voltage has not yet been understood. In this case, it should be possible to

detect the change in the resistivity of the 2DEG caused by short phonon pulses. However, a time resolved response of the 2DEG to a non-equilibrium phonon excitation will only be detected if the pulse does not broaden during its propagation in the substrate and it is able to propagate coherently along the substrate in the longitudinal direction.

6.5 References

- [1] B.Tieke, *Thermoelectric Power of Two- and Three-Dimensional Metallic Semiconductors in High Magnetic Fields*, Ph.D. Thesis, University of Nijmegen, 1997 and References therein.
- [2] G.A. Northrop and J.P.Wolfe, in *Nonequilibrium Phonon Dynamics*, Ed. W.E.Bron (Plenum, New York, 1984).
- [3] R.J. von Gutfeld, *Physical Acoustic Vol. V-6*, Ed. W.P.Mason, p.233.
- [4] U. Zeitler, A.M. Devitt, J.E. Digby, C.J.Mellor, A.J.Kent, K.A.Benedict, and T.Cheng, *Physica B* **249-251**, 49 (1998).
- [5] F.Schulze-Wischeler, U.Zeitler, F.Hohls, R.J.Haug, D.Reuter, and A.D.Wiek, *Physica B* **12**, 474 (2002).
- [6] Semirigid Coaxial Cables, Type SR, Lakeshore.
- [7] Digital Delay/Pulse Generator, DG535, Stanford Research Systems.
- [8] Wideband voltage amplifier, DHPVA-200, Femto.
- [9] Digital Phosphor Oscilloscope, TDS-3052, Tektronix.
- [10] Adrian Tae-Jin Lee, *Rev. Sci. Inst.* **64**, 2373 (1993).

Summary

The two-dimensional hole gas in a strained $\text{Si}_{0.88}\text{Ge}_{0.12}$ channel is an unusual system, characterized by the confinement of the holes in a simple parabolic heavy hole valence band, a high effective mass, a large effective g-factor and a short-ranged scattering potential. This system is therefore interesting to study new localization phenomena in both conduction and thermoelectric power. This thesis focuses on the transport properties of a Si/SiGe two dimensional hole gas at low temperatures ($T < 4\text{K}$) and high magnetic field. In particular, we measured resistivity and thermoelectric power.

The thermoelectric power consists of two additive contributions: *phonon drag*, related to the carrier-phonon interactions, and *diffusion*, related to the thermodynamic properties of the system. Previous experiments on AlGaAs/GaAs heterostructures showed that phonon drag is dominant down to very low temperatures, making diffusion difficult to probe. As explained in detail in Chapter 3, the predominance of phonon drag is due to the presence of a piezoelectric potential scattering besides the deformation potential scattering. A Si/SiGe heterostructure is expected to be a non-piezoelectrically active material and therefore a very good candidate to measure diffusion thermopower at low temperatures. Chapter 3 shows the thermopower measurements at zero field and at low magnetic fields. Although phonon drag is found to be anomalous, it is small enough to enable us to study the diffusion in details. In magnetic field, the transverse and longitudinal components of the diffusion thermopower are well described by the Mott theory, including the quantum oscillations which show, as expected, a phase shift of $\pi/2$ in respect to the Shubnikov-de Haas oscillations of the resistivity. However the diffusion shows deviations from the linear behavior expected at zero field, probably connected to the

nearby metal-insulator transition at low fields. Surprisingly, the phonon drag data suggest either the presence of a piezoelectric coupling or an unscreened deformation potential. Although it is not clear why the piezoelectric potential should be so large or the screening so ineffective in this system, the data are consistent with other recent work on energy relaxation of holes in similar structures.

Besides the integer quantum Hall effect, Si/SiGe systems exhibit other interesting localization phenomena: in zero magnetic field, a metal-insulator transition is observed by decreasing the carrier density, in high magnetic field two consecutive metal insulator transition are observed, one at $\nu=1.5$ and the other in the extreme quantum limit. Although similar localization effects have been observed in other systems, the mechanisms that lead to an insulating state in between two integer quantum Hall states are not understood yet. Many experimental observations suggest that the appearance of an insulating phase at $\nu=1.5$ is related to the peculiar energy level distribution (due a large g -factor) which leads in high magnetic field to the degeneracy and the crossing of Landau levels.

In Chapter 4 we analyzed the metal-insulator transition at $\nu=1.5$ and at $\nu<1$ as quantum critical phenomena. According to the scaling theory, in samples characterized by a short range scattering potential, the transitions between two adjacent plateaus (PP transitions) and between the lowest Landau level and the insulating state in the extreme quantum limit (PI transition) can be described as quantum critical phenomena. The comparison between the critical behavior of the metal-insulator transition at $\nu=1.5$, which arises from the peculiar energy level structure of Si/SiGe, and the metal insulator transition in the extreme quantum limit ($\nu<1$) shows that the two transitions belong to the same universality class. They are therefore driven by similar mechanisms.

Although scaling behavior is a signature of a phase transition, it does not reveal the origin of the insulating state at $\nu=1.5$. In Chapter 5, we measure the resistivity and the thermoelectric power of the insulating state at filling factor $\nu=1.5$. Diffusion thermopower gives information about the carrier distribution and therefore it can answer the question whether the field-driven insulating phase is the result of an opening of an energy gap at E_F or if it is due to the presence of a disorder-induced mobility gap. In both cases, on decreasing the temperature the resistivity diverges in the insulating state, whereas the TEP is expected to diverge in the former and to vanish or approach a constant value in the latter. Therefore TEP can distinguish between the two possibilities. In our measurements, the temperature dependence of both resistivity and thermopower of a two-dimensional hole gas in SiGe show a re-entrant metal-insulator transition at filling factor $\nu = 1.5$, but with strikingly different behavior of the two coefficients. As the temperature is decreased in the insulating state, the resistivity diverges exponentially while the thermopower decreases rapidly, suggesting that the insulating state is due to the presence of a mobility edge rather than a gap at the Fermi energy.

Chapter 6 describes the experimental setup for pulsed thermopower measurements, which would enable to probe how local is the electron-phonon interaction. The basic idea is to produce a pulsed phonon excitation in the heater, and to detect the response of the carriers to a non-equilibrium heat excitation. The Chapter describes the technical issues that have been solved and those that still need to be addressed to perform pulsed time resolved measurements.

Samenvatting

Het twee-dimensionele gaten gas in een onder mechanische spanning staand $\text{Si}_{0.88}\text{Ge}_{0.12}$ kanaal is een ongebruikelijk systeem, dat wordt gekarakteriseerd door de uitsluitende aanwezigheid van gaten in de valentieband, een hoge effectieve massa, een grote effectieve g -factor en een kort-reikende verstrooiingspotentiala. Dit maakt het een interessant systeem om nieuwe lokalisatiefenomenen, zowel in de geleiding als het thermoelectrische effect, te bestuderen. Dit proefschrift concentreert zich op de transport eigenschappen van een Si/SiGe twee-dimensioneel gaten gas bij lage temperaturen ($T < 4\text{K}$) en hoog magneet veld. Met name de weerstand en thermospanning hebben we gemeten.

De thermospanning bestaat uit twee bijdragen: *phonon drag*, gerelateerd aan de ladingsdrager-phonon interacties, en *diffusie*, geassocieerd met de thermodynamische eigenschappen van het systeem. Eerdere experimenten aan AlGaAs/GaAs heterostructuren toonden aan dat tot erg lage temperaturen phonon drag dominant is, waardoor het erg moeilijk is om diffusie te onderzoeken. Zoals in detail uitgelegd in Hoofdstuk 3, is de dominantie van phonon drag boven diffusie het gevolg van de aanwezigheid van een piezoelectrische verstrooiing naast de vervormingspotentiala verstrooiing. Omdat van een Si/SiGe heterostructuur wordt gedacht dat het een niet-piezoelectrisch actief materiaal is, vormt het een erg goede kandidaat voor het meten van diffusie thermospanning bij lage temperaturen. Hoofdstuk 3 toont de thermospanningsmetingen zonder magneetveld en bij een laag magneetveld. Ofschoon de gevonden phonon drag afwijkend is, is deze klein genoeg om ons in staat te stellen de diffusie in detail te bestuderen. De transversale en

longitudinale componenten van de diffusie thermospanning in een magneetveld worden goed beschreven door de Mott theorie, evenals de quantum oscillaties die, zoals verwacht, een fase verschuiving van een $\pi/2$ vertonen ten opzichte van de Shubnikov-de Haas oscillaties in de weerstand. Echter, de diffusie vertoont afwijkingen van het verwachte lineaire gedrag bij de afwezigheid van een magneetveld. Waarschijnlijk houdt dit verband met de nabijheid van een metaal-isolator overgang bij laag magneetveld. Verrassenderwijs suggereren de phonon drag data de aanwezigheid van of een piezoelectrische koppeling dan wel een niet-afgeschermd vervormingspotentiaal. Ofschoon het niet geheel duidelijk is waarom de piezoelectrische potentiaal zo groot, of de afscherming zo ineffectief zou zijn in dit systeem, komen de data overeen met andere recente studies aan energie relaxatie van gaten in vergelijkbare structuren.

Naast het integer quantum Hall effect vertonen Si/SiGe systemen ook andere interessante lokalisatie fenomenen: in de afwezigheid van een magneetveld wordt een metaal-isolator overgang gezien door het verlagen van de ladingsdragersdichtheid, terwijl in een magneetveld twee opeenvolgende metaal-isolator overgangen worden waargenomen, één bij $\nu=1.5$ en de ander in de extreme quantum limiet. Ofschoon vergelijkbare lokalisatie effecten zijn gevonden in andere systemen, zijn de mechanismen die ten grondslag liggen aan een isolerende toestand tussen twee integer quantum Hall states nog onbekend. Veel experimentele waarnemingen suggereren dat het verschijnen van een isolerende fase bij $\nu=1.5$ samenhangt met de vreemde energie niveau structuur (als het gevolg van een grote g -factor), die in hoge magneetvelden leidt tot de bijna ontaarding en het kruisen van Landau niveau's.

In hoofdstuk 4 hebben we de metaal-isolator overgang bij $\nu=1.5$ en bij $\nu<1$ als quantum kritische fenomenen geanalyseerd. In monsters met een kort-reikende verstrooiingspotentiaal kunnen de overgangen tussen twee opeenvolgende niveau's (PP-overgangen) en tussen het laagste Landau niveau en de isolerende toestand in het extreme quantum limiet (PI-overgang), volgens de schaling theorie, worden beschreven als quantum kritische fenomenen. De vergelijking tussen het kritische gedrag van de metaal-isolator overgang bij $\nu=1.5$, die ontstaat uit de vreemde energie niveau structuur van Si/SiGe en de metaal-isolator overgang in de extreme quantum limiet ($\nu<1$), laat zien dat beide overgangen tot dezelfde universele klasse behoren. Ze worden dan ook veroorzaakt door vergelijkbare mechanismen.

Ofschoon het schalingsgedrag een kenmerk is van een fase overgang, kan het niet de oorsprong van de isolerende fase bij $\nu=1.5$ verklaren. In hoofdstuk 5, hebben we de weerstand en de thermospanning van de isolerende toestand bij vulfactor $\nu=1.5$ bestudeerd. Diffusie thermospanning geeft informatie over de ladingsdragersverdeling en kan daarom de vraag beantwoorden of de veld-geïnduceerde isolerende toestand het resultaat is van de opening van een energiekloof bij the Fermi energie E_F , of dat dit het gevolg is van de aanwezigheid van een door verstrooiing-geïnduceerde mobiliteits bandafstand. In beide bovenstaande gevallen, gaat de weerstand naar oneindig in de isolerende fase bij

verlaging van de temperatuur, terwijl verwacht wordt dat de thermospanning in het eerste geval naar oneindig gaat, en verdwijnt of constant wordt in het laatste geval. Daarom kan de thermospanning deze twee mogelijkheden onderscheiden. In onze metingen vertonen de temperatuur afhankelijkheid van zowel weerstand als thermospanning een herintredende metaal-isolator overgang bij vulfactor $\nu=1.5$, maar met een opmerkelijk verschillend gedrag van de twee coëfficiënten. Als de temperatuur verlaagd wordt in de isolerende toestand neemt de weerstand exponentieel toe, terwijl de thermospanning snel afneemt. Dit suggereert dat de isolerende toestand het gevolg is van de aanwezigheid van een mobiliteits bandafstand in plaats van een energiekloof bij de Fermi energie.

Hoofdstuk 6 beschrijft de experimentele opzet voor gepulseerde thermospanning metingen, die het mogelijk zou moeten maken lokaal de elektron-phonon interactie te onderzoeken. De grondgedachte is om in de stoker een gepulste phonon excitatie te creëren en vervolgens de reactie van de ladingsdragers op deze lokale temperatuurgradient te meten. Het hoofdstuk beschrijft de technische problemen die zijn opgelost en de kwesties die nog aandacht verdienen om gepulseerde tijdsopgeloste metingen mogelijk te maken.

List of Publications

E.Silva, R.Fastampa, M.Giura, R.Marcon, C.Possanzini, S.Sarti, E.L.Wolf, *Microwave surface resistance in BSCCO crystal: magnetic field and angular measurement*, Physica C **282**, 1985 (1997).

R.Fletcher, V.M.Pudalov, A.D.B.Radcliffe and C.Possanzini, *Critical behavior of thermopower and conductivity at the metal-insulator transition in high-mobility Si-MOSFETs*, Semicond. Sci. and Technol. **16**, 386 (2001).

C. Possanzini , L. Ponomarenko , D. de Lang , A. de Visser , S.M. Olsthoorn , R. Fletcher , Y. Feng , P.T. Coleridge , R.L. Williams and J.C. Maan , *Scaling behavior of metal-insulator transitions in a Si/SiGe two dimensional hole gas*, Physica E **12**, 600 (2002).

D.T.N. de Lang , L. Ponomarenko , A. de Visser , C. Possanzini , S.M. Olsthoorn and A.M.M. Pruisken , *Evidence for a quantum Hall insulator in an InGaAs/InP heterostructure*, Physica E **12**, 666 (2002).

J. de Jonge, C. Possanzini, S.M. Olsthoorn, J.C. Maan, G.M. Mikhailov, L.I. Aparshina, A.V. Chernykh, I.V. Malikov and V.Y. Vinnichenko, *Angular dependence of longitudinal magnetoresistance in rough metal waveguides*, Proceedings of 15th Int. Conf. on High Magnetic Fields in Semiconductor Physics Semimag 15, 5 - 8 augustus 2002, Oxford, Great Britain.

C. Possanzini, R. Fletcher, P.T. Coleridge, Y. Feng, R.L. Williams and J.C. Maan, *Thermoelectric power of a magnetic field induced metal-insulator transition in a two-dimensional SiGe hole gas*, Proceedings of 15th Int. Conf. on High Magnetic Fields in Semiconductor Physics Semimag 15, 5 - 8 augustus 2002, Oxford, Great Britain.

List of Publications

C. Possanzini, R. Fletcher, P.T. Coleridge, Y. Feng, R.L. Williams and J.C. Maan, *Diffusion thermopower of a two-dimensional hole gas in SiGe in a quantum Hall insulating state*, Phys. Rev. Lett. **90**, 176601 (2003).

C. Possanzini, R. Fletcher, M.Tsaousidou, P.T. Coleridge, Y. Feng, R.L. Williams and J.C. Maan, *Thermopower of a p-type Si/SiGe heterostructure*, Phys. Rev. B, 2004 (in press).

Curriculum Vitae

Cecilia Possanzini was born the 3rd of December 1971 in Rome, Italy. She obtained the *maturità* in July 1990 at the *Liceo Classico "Orazio"* in Rome. Then, she studied physics at the University of Rome "*La Sapienza*", where she specialized in Solid State Physics. In 1997, she graduated with Prof. M. Giura with an experimental thesis on microwave surface resistance measurements on high critical temperature superconductors in magnetic field.

After her graduation, Cecilia moved to the Netherlands, where she worked with Prof. Dr. J. C. Maan at the High Field Magnet Laboratory of the University of Nijmegen as *onderzoeker in opleiding*. In this period, she accomplished her Ph.D. research, which is presented in this thesis.

Since October 2002, Cecilia is working in the RF electronic group of Magnetic Resonance development in Philips Medical Systems, Best (The Netherlands).

